

Conduction Heat Transfer*

A. AZIZ

Department of Mechanical Engineering
Gonzaga University
Spokane, Washington

- 3.1 Introduction
- 3.2 Basic equations
 - 3.2.1 Fourier's law
 - 3.2.2 General heat conduction equations
 - 3.2.3 Boundary and initial conditions
- 3.3 Special functions
 - 3.3.1 Error functions
 - 3.3.2 Gamma function
 - 3.3.3 Beta functions
 - 3.3.4 Exponential integral function
 - 3.3.5 Bessel functions
 - 3.3.6 Legendre functions
- 3.4 Steady one-dimensional conduction
 - 3.4.1 Plane wall
 - 3.4.2 Hollow cylinder
 - 3.4.3 Hollow sphere
 - 3.4.4 Thermal resistance
 - 3.4.5 Composite systems
 - Composite plane wall
 - Composite hollow cylinder
 - Composite hollow sphere
 - 3.4.6 Contact conductance
 - 3.4.7 Critical thickness of insulation
 - 3.4.8 Effect of uniform internal energy generation
 - Plane wall
 - Hollow cylinder
 - Solid cylinder
 - Hollow sphere
 - Solid sphere
- 3.5 More advanced steady one-dimensional conduction
 - 3.5.1 Location-dependent thermal conductivity

*The author dedicates this chapter to little Senaan Asil Aziz whose sparkling smile “makes my day.”

- Plane wall
- Hollow cylinder
- 3.5.2 Temperature-dependent thermal conductivity
 - Plane wall
 - Hollow cylinder
 - Hollow sphere
- 3.5.3 Location-dependent energy generation
 - Plane wall
 - Solid cylinder
- 3.5.4 Temperature-dependent energy generation
 - Plane wall
 - Solid cylinder
 - Solid sphere
- 3.5.5 Radiative–convective cooling of solids with uniform energy generation
- 3.6 Extended surfaces
 - 3.6.1 Longitudinal convecting fins
 - Rectangular fin
 - Trapezoidal fin
 - Triangular fin
 - Concave parabolic fin
 - Convex parabolic fin
 - 3.6.2 Radial convecting fins
 - Rectangular fin
 - Triangular fin
 - Hyperbolic fin
 - 3.6.3 Convecting spines
 - Cylindrical spine
 - Conical spine
 - Concave parabolic spine
 - Convex parabolic spine
 - 3.6.4 Longitudinal radiating fins
 - 3.6.5 Longitudinal convecting–radiating fins
 - 3.6.6 Optimum dimensions of convecting fins and spines
 - Rectangular fin
 - Triangular fin
 - Concave parabolic fin
 - Cylindrical spine
 - Conical spine
 - Concave parabolic spine
 - Convex parabolic spine
- 3.7 Two-dimensional steady conduction
 - 3.7.1 Rectangular plate with specified boundary temperatures
 - 3.7.2 Solid cylinder with surface convection
 - 3.7.3 Solid hemisphere with specified base and surface temperatures
 - 3.7.4 Method of superposition
 - 3.7.5 Conduction of shape factor method
 - 3.7.6 Finite-difference method

- Cartesian coordinates
- Cylindrical coordinates

3.8 Transient conduction

3.8.1 Lumped thermal capacity model

- Internal energy generation
- Temperature-dependent specific heat
- Pure radiation cooling
- Simultaneous convective–radiative cooling
- Temperature-dependent heat transfer coefficient
- Heat capacity of the coolant pool

3.8.2 Semi-infinite solid model

- Specified surface temperature
- Specified surface heat flux
- Surface convection
- Constant surface heat flux and nonuniform initial temperature
- Constant surface heat flux and exponentially decaying energy generation

3.8.3 Finite-sized solid model

3.8.4 Multidimensional transient conduction

3.8.5 Finite-difference method

- Explicit method
- Implicit method
- Other methods

3.9 Periodic conduction

3.9.1 Cooling of a lumped system in an oscillating temperature environment

3.9.2 Semi-infinite solid with periodic surface temperature

3.9.3 Semi-infinite solid with periodic surface heat flux

3.9.4 Semi-infinite solid with periodic ambient temperature

3.9.5 Finite plane wall with periodic surface temperature

3.9.6 Infinitely long semi-infinite hollow cylinder with periodic surface temperature

3.10 Conduction-controlled freezing and melting

3.10.1 One-region Neumann problem

3.10.2 Two-region Neumann problem

3.10.3 Other exact solutions for planar freezing

3.10.4 Exact solutions in cylindrical freezing

3.10.5 Approximate analytical solutions

- One-region Neumann problem

- One-region Neumann problem with surface convection

- Outward cylindrical freezing

- Inward cylindrical freezing

- Outward spherical freezing

- Other approximate solutions

3.10.6 Multidimensional freezing (melting)

3.11 Contemporary topics

Nomenclature

References

3.1 INTRODUCTION

This chapter is concerned with the characterization of conduction heat transfer, which is a mode that pervades a wide range of systems and devices. Unlike convection, which pertains to energy transport due to fluid motion and radiation, which can propagate in a perfect vacuum, conduction requires the presence of an intervening medium. At microscopic levels, conduction in stationary fluids is a consequence of higher-temperature molecules interacting and exchanging energy with molecules at lower temperatures. In a nonconducting solid, the transport of energy is exclusively via lattice waves (phonons) induced by atomic motion. If the solid is a conductor, the transfer of energy is also associated with the translational motion of free electrons.

The microscopic approach is of considerable contemporary interest because of its applicability to miniaturized systems such as superconducting thin films, microsensors, and micromechanical devices (Duncan and Peterson, 1994; Tien and Chen, 1994; Tzou, 1997; Tien et al., 1998). However, for the vast majority of engineering applications, the macroscopic approach based on Fourier's law is adequate. This chapter is therefore devoted exclusively to macroscopic heat conduction theory, and the material contained herein is a unique synopsis of a wealth of information that is available in numerous works, such as those of Schneider (1955), Carslaw and Jaeger (1959), Gebhart (1993), Ozisik (1993), Poulikakos (1994), and Jiji (2000).

3.2 BASIC EQUATIONS

3.2.1 Fourier's Law

The basic equation for the analysis of heat conduction is *Fourier's law*, which is based on experimental observations and is

$$q_n'' = -k_n \frac{\partial T}{\partial n} \quad (3.1)$$

where the *heat flux* q_n'' (W/m²) is the heat transfer rate in the n direction per unit area perpendicular to the direction of heat flow, k_n (W/m · K) is the thermal conductivity in the direction n , and $\partial T/\partial n$ (K/m) is the *temperature gradient* in the direction n . The thermal conductivity is a thermophysical property of the material, which is, in general, a function of both temperature and location; that is, $k = k(T, n)$. For *isotropic materials*, k is the same in all directions, but for *anisotropic materials* such as wood and laminated materials, k is significantly higher along the grain or lamination than perpendicular to it. Thus for anisotropic materials, k can have a strong directional dependence. Although heat conduction in anisotropic materials is of current research interest, its further discussion falls outside the scope of this chapter and the interested reader can find a fairly detailed exposition of this topic in Ozisik (1993).

Because the thermal conductivity depends on the atomic and molecular structure of the material, its value can vary from one material to another by several orders of

magnitude. The highest values are associated with metals and the lowest values with gases and thermal insulators. Tabulations of thermal conductivity data are given in Chapter 2.

For three-dimensional conduction in a Cartesian coordinate system, the Fourier law of eq. (3.1) can be extended to

$$\mathbf{q}'' = \mathbf{i}q_x'' + \mathbf{j}q_y'' + \mathbf{k}q_z'' \quad (3.2)$$

where

$$q_x'' = -k \frac{\partial T}{\partial x} \quad q_y'' = -k \frac{\partial T}{\partial y} \quad q_z'' = -k \frac{\partial T}{\partial z} \quad (3.3)$$

and \mathbf{i} , \mathbf{j} , and \mathbf{k} are unit vectors in the x , y , and z coordinate directions, respectively.

3.2.2 General Heat Conduction Equations

The general equations of heat conduction in the rectangular, cylindrical, and spherical coordinate systems shown in Fig. 3.1 can be derived by performing an energy balance.

Cartesian coordinate system:

$$\frac{\partial}{\partial x} \left(k \frac{\partial T}{\partial x} \right) + \frac{\partial}{\partial y} \left(k \frac{\partial T}{\partial y} \right) + \frac{\partial}{\partial z} \left(k \frac{\partial T}{\partial z} \right) + \dot{q} = \rho c \frac{\partial T}{\partial t} \quad (3.4)$$

Cylindrical coordinate system:

$$\frac{1}{r} \frac{\partial}{\partial r} \left(kr \frac{\partial T}{\partial r} \right) + \frac{1}{r^2} \frac{\partial}{\partial \phi} \left(k \frac{\partial T}{\partial \phi} \right) + \frac{\partial}{\partial z} \left(k \frac{\partial T}{\partial z} \right) + \dot{q} = \rho c \frac{\partial T}{\partial t} \quad (3.5)$$

Spherical coordinate system:

$$\begin{aligned} \frac{1}{r^2} \frac{\partial}{\partial r} \left(kr^2 \frac{\partial T}{\partial r} \right) + \frac{1}{r^2 \sin^2 \theta} \frac{\partial}{\partial \phi} \left(k \frac{\partial T}{\partial \phi} \right) \\ + \frac{1}{r^2 \sin \theta} \frac{\partial}{\partial \theta} \left(k \sin \theta \frac{\partial T}{\partial \theta} \right) + \dot{q} = \rho c \frac{\partial T}{\partial t} \end{aligned} \quad (3.6)$$

In eqs. (3.4)–(3.6), \dot{q} is the volumetric energy addition (W/m^3), ρ the density of the material (kg/m^3), and c the specific heat ($\text{J/kg} \cdot \text{K}$) of the material. The general heat conduction equation can also be expressed in a general curvilinear coordinate system (Section 1.2.4). Ozisik (1993) gives the heat conduction equations in prolate spheroidal and oblate spheroidal coordinate systems.

3.2.3 Boundary and Initial Conditions

Each of the general heat conduction equations (3.4)–(3.6) is second order in the spatial coordinates and first order in time. Hence, the solutions require a total of six

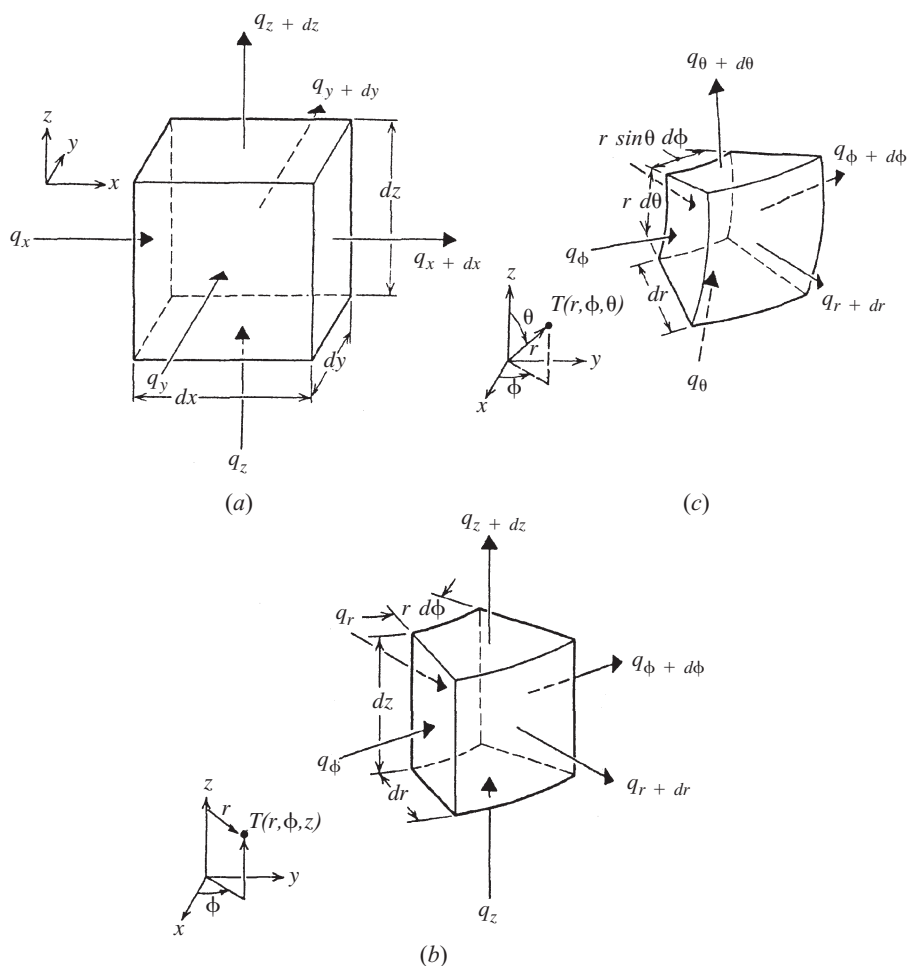


Figure 3.1 Differential control volumes in (a) Cartesian, (b) cylindrical, and (c) spherical coordinates.

boundary conditions (two for each spatial coordinate) and one initial condition. The initial condition prescribes the temperature in the body at time $t = 0$. The three types of boundary conditions commonly encountered are that of constant surface temperature (the boundary condition of the first kind), constant surface heat flux (the boundary condition of the second kind), and a prescribed relationship between the surface heat flux and the surface temperature (the convective or boundary condition of the third kind). The precise mathematical form of the boundary conditions depends on the specific problem.

For example, consider one-dimensional transient condition in a semi-infinite solid that is subject to heating at $x = 0$. Depending on the characterization of the heating, the boundary condition at $x = 0$ may take one of three forms. For constant surface temperature,

$$T(0, t) = T_s \quad (3.7)$$

For constant surface heat flux,

$$-k \frac{\partial T(0, t)}{\partial x} = q_s'' \quad (3.8)$$

and for convection at $x = 0$,

$$-k \frac{\partial T(0, t)}{\partial x} = h [T_\infty - T(0, t)] \quad (3.9)$$

where in eq. (3.9), $h(\text{W/m}^2 \cdot \text{K})$ is the convective heat transfer coefficient and T_∞ is the temperature of the hot fluid in contact with the surface at $x = 0$.

Besides the foregoing boundary conditions of eqs. (3.7)–(3.9), other types of boundary conditions may arise in heat conduction analysis. These include boundary conditions at the interface of two different materials in perfect thermal contact, boundary conditions at the interface between solid and liquid phases in a freezing or melting process, and boundary conditions at a surface losing (or gaining) heat simultaneously by convection and radiation. Additional details pertaining to these boundary conditions are provided elsewhere in the chapter.

3.3 SPECIAL FUNCTIONS

A number of special mathematical functions frequently arise in heat conduction analysis. These cannot be computed readily using a scientific calculator. In this section we provide a modest introduction to these functions and their properties. The functions include error functions, gamma functions, beta functions, exponential integral functions, Bessel functions, and Legendre polynomials.

3.3.1 Error Functions

The error function with argument (x) is defined as

$$\text{erf}(x) = \frac{2}{\sqrt{\pi}} \int_0^x e^{-t^2} dt \quad (3.10)$$

where t is a dummy variable. The error function is an odd function, so that

$$\text{erf}(-x) = -\text{erf}(x) \quad (3.11)$$

In addition,

$$\text{erf}(0) = 0 \quad \text{and} \quad \text{erf}(\infty) = 1 \quad (3.12)$$

The complementary error function with argument (x) is defined as

$$\text{erfc}(x) = 1 - \text{erf}(x) = \frac{2}{\sqrt{\pi}} \int_x^\infty e^{-t^2} dt \quad (3.13)$$

The derivatives of the error function can be obtained by repeated differentiations of eq. (3.10):

$$\frac{d}{dx} \operatorname{erf}(x) = \frac{2}{\sqrt{\pi}} e^{-x^2} \quad \text{and} \quad \frac{d^2}{dx^2} \operatorname{erf}(x) = -\frac{4}{\sqrt{\pi}} x e^{-x^2} \quad (3.14)$$

The repeated integrals of the complementary error function are defined by

$$i^n \operatorname{erfc}(x) = \int_x^\infty i^{n-1} \operatorname{erfc}(t) dt \quad (n = 1, 2, 3, \dots) \quad (3.15)$$

with

$$i^0 \operatorname{erfc}(x) = \operatorname{erfc}(x) \quad \text{and} \quad i^{-1} \operatorname{erfc}(x) = \frac{2}{\sqrt{\pi}} e^{-x^2} \quad (3.16)$$

The first two repeated integrals are

$$i \operatorname{erfc}(x) = \frac{1}{\sqrt{\pi}} e^{-x^2} - x \operatorname{erfc}(x) \quad (3.17)$$

$$i^2 \operatorname{erfc}(x) = \frac{1}{4} \left[(1 + 2x^2) \operatorname{erfc}(x) - \frac{2}{\sqrt{\pi}} x e^{-x^2} \right] \quad (3.18)$$

Table 3.1 lists the values of $\operatorname{erf}(x)$, $d \operatorname{erf}(x)/dx$, $d^2 \operatorname{erf}(x)/dx^2$, and $d^3 \operatorname{erf}(x)/dx^3$ for values of x from 0 to 3 in increments of 0.10. Table 3.2 lists the values of $\operatorname{erfc}(x)$, $i \operatorname{erfc}(x)$, $i^2 \operatorname{erfc}(x)$, and $i^3 \operatorname{erfc}(x)$ for the same values of x . Both tables were generated using Maple V (Release 6.0).

3.3.2 Gamma Function

The *gamma function*, denoted by $\Gamma(x)$, provides a generalization of the factorial $n!$ to the case where n is not an integer. It is defined by the *Euler integral* (Andrews, 1992):

$$\Gamma(x) = \int_0^\infty t^{x-1} e^{-t} dt \quad (x > 0) \quad (3.19)$$

and has the property

$$\Gamma(x + 1) = x \Gamma(x) \quad (3.20)$$

which for integral values of x (denoted by n) becomes

$$\Gamma(n + 1) = n! \quad (3.21)$$

Table 3.3 gives values of $\Gamma(x)$ for values of x from 1.0 through 2.0. These values were generated using Maple V, Release 6.0.

TABLE 3.1 Values of $\operatorname{erf}(x)$, $d \operatorname{erf}(x)/dx$, $d^2 \operatorname{erf}(x)/dx^2$, and $d^3 \operatorname{erf}(x)/dx^3$

x	$\operatorname{erf}(x)$	$d \operatorname{erf}(x)/dx$	$d^2 \operatorname{erf}(x)/dx^2$	$d^3 \operatorname{erf}(x)/dx^3$
0.00	0.00000	1.12838	0.00000	-2.25676
0.10	0.11246	1.11715	-0.22343	-2.18962
0.20	0.22270	1.08413	-0.43365	-1.99481
0.30	0.32863	1.03126	-0.61876	-1.69127
0.40	0.42839	0.96154	-0.76923	-1.30770
0.50	0.52050	0.87878	-0.87878	-0.87878
0.60	0.60386	0.78724	-0.94469	-0.44086
0.70	0.67780	0.69127	-0.96778	-0.02765
0.80	0.74210	0.59499	-0.95198	0.33319
0.90	0.79691	0.50197	-0.90354	0.62244
1.00	0.84270	0.41511	-0.83201	0.83021
1.10	0.88021	0.33648	-0.74026	0.95560
1.20	0.91031	0.26734	-0.64163	1.00521
1.30	0.93401	0.20821	-0.54134	0.99107
1.40	0.95229	0.15894	-0.44504	0.92822
1.50	0.96611	0.11893	-0.35679	0.83251
1.60	0.97635	0.08723	-0.27913	0.71877
1.70	0.98379	0.06271	-0.21322	0.59952
1.80	0.98909	0.04419	-0.15909	0.48434
1.90	0.99279	0.03052	-0.11599	0.37973
2.00	0.99532	0.02067	-0.08267	0.28934
2.10	0.99702	0.01372	-0.05761	0.21451
2.20	0.99814	0.00892	-0.03926	0.15489
2.30	0.99886	0.00569	-0.02617	0.10900
2.40	0.99931	0.00356	-0.01707	0.07481
2.50	0.99959	0.00218	-0.01089	0.05010
2.60	0.99976	0.00131	-0.00680	0.03275
2.70	0.99987	0.76992×10^{-3}	-0.00416	0.02091
2.80	0.99992	0.44421×10^{-3}	-0.00249	0.01305
2.90	0.99996	0.25121×10^{-3}	-0.00146	0.00795
3.00	0.99997	0.13925×10^{-3}	-0.83552×10^{-3}	0.00473

The *incomplete gamma function* is defined by the integral (Andrews, 1992)

$$\Gamma(a, x) = \int_x^\infty t^{a-1} e^{-t} dt \quad (3.22)$$

Values of $\Gamma(1.2, x)$ for $0 \leq x \leq 1$ generated using Maple V, Release 6.0 are given in Table 3.4.

3.3.3 Beta Functions

The *beta function*, denoted by $B(x, y)$, is defined by

$$B(x, y) = \int_0^1 (1-t)^{x-1} t^{y-1} dt \quad (3.23)$$

TABLE 3.2 Values of $\operatorname{erfc}(x)$, $i \operatorname{erfc}(x)$, $i^2 \operatorname{erfc}(x)$, and $i^3 \operatorname{erfc}(x)$

x	$\operatorname{erfc}(x)$	$i \operatorname{erfc}(x)$	$i^2 \operatorname{erfc}(x)$	$i^3 \operatorname{erfc}(x)$
0.00	1.00000	0.56419	0.25000	0.09403
0.10	0.88754	0.46982	0.19839	0.07169
0.20	0.77730	0.38661	0.15566	0.05406
0.30	0.67137	0.31422	0.12071	0.04030
0.40	0.57161	0.25213	0.09248	0.02969
0.50	0.47950	0.19964	0.06996	0.02161
0.60	0.39614	0.15594	0.05226	0.01554
0.70	0.32220	0.12010	0.03852	0.01103
0.80	0.25790	0.09117	0.02801	0.00773
0.90	0.20309	0.06820	0.02008	0.00534
1.00	0.15730	0.05025	0.01420	0.00364
1.10	0.11979	0.03647	0.00989	0.00245
1.20	0.08969	0.02605	0.00679	0.00162
1.30	0.06599	0.01831	0.00459	0.00106
1.40	0.04771	0.01267	0.00306	0.68381×10^{-3}
1.50	0.03389	0.00862	0.00201	0.43386×10^{-3}
1.60	0.02365	0.00577	0.00130	0.27114×10^{-3}
1.70	0.01621	0.00380	0.82298×10^{-3}	0.16686×10^{-3}
1.80	0.01091	0.00246	0.51449×10^{-3}	0.10110×10^{-3}
1.90	0.00721	0.00156	0.31642×10^{-3}	0.60301×10^{-4}
2.00	0.00468	0.97802×10^{-3}	0.19141×10^{-3}	0.35396×10^{-4}
2.10	0.00298	0.60095×10^{-3}	0.11387×10^{-3}	0.20445×10^{-4}
2.20	0.00186	0.36282×10^{-3}	0.66614×10^{-4}	0.11619×10^{-4}
2.30	0.00114	0.21520×10^{-3}	0.38311×10^{-4}	0.64951×10^{-5}
2.40	0.68851×10^{-3}	0.12539×10^{-3}	0.21659×10^{-4}	0.35711×10^{-5}
2.50	0.40695×10^{-3}	0.71762×10^{-4}	0.12035×10^{-4}	0.19308×10^{-5}
2.60	0.23603×10^{-3}	0.40336×10^{-4}	0.65724×10^{-5}	0.10265×10^{-5}
2.70	0.13433×10^{-3}	0.22264×10^{-4}	0.35268×10^{-5}	0.53654×10^{-6}
2.80	0.75013×10^{-4}	0.12067×10^{-4}	0.18595×10^{-5}	0.27567×10^{-6}
2.90	0.41098×10^{-4}	0.64216×10^{-5}	0.96315×10^{-6}	0.13922×10^{-6}
3.00	0.22090×10^{-4}	0.33503×10^{-5}	0.49007×10^{-6}	0.69101×10^{-7}

The beta function is related to the gamma function:

$$B(x, y) = \frac{\Gamma(x)\Gamma(y)}{\Gamma(x+y)} \quad (x > 0, y > 0) \quad (3.24)$$

has the symmetry property

$$B(x, y) = B(y, x) \quad (3.25)$$

and for nonnegative integers,

$$B(m, n) = \frac{(m-1)!(n-1)!}{(m+n-1)!} \quad m, n \text{ nonnegative integers} \quad (3.26)$$

TABLE 3.3 Gamma Function

x	$\Gamma(x)$	x	$\Gamma(x)$	x	$\Gamma(x)$	x	$\Gamma(x)$
1.00	1.00000	1.25	0.90640	1.50	0.88623	1.75	0.91906
1.01	0.99433	1.26	0.90440	1.51	0.88659	1.76	0.92137
1.02	0.98884	1.27	0.90250	1.52	0.88704	1.77	0.92376
1.03	0.98355	1.28	0.90072	1.53	0.88757	1.78	0.92623
1.04	0.97844	1.29	0.89904	1.54	0.88818	1.79	0.92877
1.05	0.97350	1.30	0.89747	1.55	0.88887	1.80	0.93138
1.06	0.96874	1.31	0.89600	1.56	0.88964	1.81	0.93408
1.07	0.96415	1.32	0.89464	1.57	0.89049	1.82	0.93685
1.08	0.95973	1.33	0.89338	1.58	0.89142	1.83	0.93969
1.09	0.95546	1.34	0.89222	1.59	0.89243	1.84	0.94261
1.10	0.95135	1.35	0.89115	1.60	0.89352	1.85	0.94561
1.11	0.94740	1.36	0.89018	1.61	0.89468	1.86	0.94869
1.12	0.94359	1.37	0.88931	1.62	0.89592	1.87	0.95184
1.13	0.93993	1.38	0.88854	1.63	0.89724	1.88	0.95507
1.14	0.93642	1.39	0.88785	1.64	0.89864	1.89	0.95838
1.15	0.93304	1.40	0.88726	1.65	0.90012	1.90	0.96177
1.16	0.92980	1.41	0.88676	1.66	0.90167	1.91	0.96523
1.17	0.92670	1.42	0.88636	1.67	0.90330	1.92	0.96877
1.18	0.92373	1.43	0.88604	1.68	0.90500	1.93	0.97240
1.19	0.92089	1.44	0.88581	1.69	0.90678	1.94	0.97610
1.20	0.91817	1.45	0.88566	1.70	0.90864	1.95	0.97988
1.21	0.91558	1.46	0.88560	1.71	0.91057	1.96	0.98374
1.22	0.91311	1.47	0.88563	1.72	0.91258	1.97	0.98768
1.23	0.91075	1.48	0.88575	1.73	0.91467	1.98	0.99171
1.24	0.90852	1.49	0.88595	1.74	0.91683	1.99	0.99581
						2.00	1.00000

TABLE 3.4 Incomplete Gamma Function, $\Gamma(a, x)$, $a = 1.2$

x	$\Gamma(a, x)$
0.00	0.91817
0.10	0.86836
0.20	0.80969
0.30	0.75074
0.40	0.69366
0.50	0.63932
0.60	0.58813
0.70	0.54024
0.80	0.49564
0.90	0.45426
1.00	0.41597

TABLE 3.5 Incomplete Beta Function, $B_t(0.3, 0.5)$

x	$B_t(0.3, 0.5)$
0.00	0.00000
0.10	0.64802
0.20	0.94107
0.30	1.18676
0.40	1.41584
0.50	1.64284
0.60	1.87920
0.70	2.13875
0.80	2.44563
0.90	2.86367
1.00	4.55444

The *incomplete beta function*, $B_t(x, y)$, is defined by

$$B_t(x, y) = \int_0^t (1 - t)^{x-1} t^{y-1} dt \tag{3.27}$$

Values of $B_t(0.3, 0.5)$ for the range $0 \leq t \leq 1$ generated using Maple V, Release 6.0 are given in Table 3.5.

3.3.4 Exponential Integral Function

The *exponential integral function* $E_1(x)$ or $-E_i(-x)$ for a real argument x is defined by

$$E_1(x) \quad \text{or} \quad -E_i(-x) = \int_x^\infty \frac{e^{-t}}{t} dt \tag{3.28}$$

and has the following properties:

$$E_1(0) = \infty \quad E_1(\infty) = 0 \quad \frac{dE_1(x)}{dx} = -\frac{e^{-x}}{x} \tag{3.29}$$

As indicated by the entries in Table 3.6, the function decreases monotonically from the value $E_1(0) = \infty$ to $E_1(\infty) = 0$ as x is varied from 0 to ∞ .

3.3.5 Bessel Functions

Bessel functions of the first kind of order n and argument x , denoted by $J_n(x)$, and *Bessel functions of the second kind* of order n and argument x , denoted by $Y_n(x)$, are defined, respectively, by the infinite series

TABLE 3.6 Exponential Integral Function

x	$E_1(x)$	x	$E_1(x)$
0.00	∞	0.80	0.31060
0.01	4.03793	0.90	0.26018
0.02	3.35471	1.00	0.21938
0.03	2.95912	1.10	0.18599
0.04	2.68126	1.20	0.15841
0.05	2.46790	1.30	0.13545
0.06	2.29531	1.40	0.11622
0.07	2.15084	1.50	0.10002
0.08	2.02694	1.60	0.08631
0.09	1.91874	1.70	0.07465
0.10	1.82292	1.80	0.06471
0.15	1.46446	1.90	0.05620
0.20	1.22265	2.00	0.04890
0.30	0.90568	2.20	0.03719
0.40	0.70238	2.40	0.02844
0.50	0.55977	2.60	0.02185
0.60	0.45438	2.80	0.01686
0.70	0.37377	3.00	0.01305

$$J_n(x) = \sum_{m=0}^{\infty} \frac{(-1)^m (x/2)^{2m+n}}{m! \Gamma(m+n+1)} \quad (3.30)$$

and

$$Y_n(x) = \frac{J_n(x) \cos n\pi - J_{-n}(x)}{\sin n\pi} \quad (n \neq 0, 1, 2, \dots) \quad (3.31a)$$

or

$$Y_n(x) = \lim_{m \rightarrow n} \frac{J_m(x) \cos m\pi - J_{-m}(x)}{\sin m\pi} \quad (n = 0, 1, 2, \dots) \quad (3.31b)$$

Numerous recurrence relationships involving the Bessel functions are available (Andrews, 1992). Some that are relevant in this chapter are

$$J_{-n}(x) = (-1)^n J_n(x) \quad (3.32)$$

$$\frac{dJ_n(x)}{dx} = J_{n-1}(x) - \frac{n}{x} J_n(x) = \frac{n}{x} J_n(x) - J_{n+1}(x) \quad (3.33)$$

$$\frac{d}{dx} [x^n J_n(x)] = x^n J_{n-1}(x) \quad (3.34)$$

$$\frac{d}{dx} [x^{-n} J_n(x)] = -x^{-n} J_{n+1}(x) \quad (3.35)$$

The relations given by eqs. (3.32)–(3.35) apply to the Bessel functions of the second kind when the J 's are replaced by Y 's.

Modified Bessel functions of the first kind of order n and argument x , denoted by $I_n(x)$, and *modified Bessel functions of the second kind* of order n and argument x , denoted by $K_n(x)$, are defined, respectively, by the infinite series

$$I_n(x) = \sum_{m=0}^{\infty} \frac{(x/2)^{2m+n}}{m! \Gamma(m+n+1)} \quad (3.36)$$

and

$$K_n(x) = \frac{\pi}{2 \sin n\pi} [I_{-n}(x) - I_n(x)] \quad (n \neq 0, 1, 2, \dots) \quad (3.37a)$$

or

$$K_n(x) = \lim_{m \rightarrow n} \frac{\pi}{2 \sin n\pi} [I_{-m}(x) - I_m(x)] \quad (n = 0, 1, 2, \dots) \quad (3.37b)$$

$I_n(x)$ and $K_n(x)$ are real and positive when $n > -1$ and $x > 0$.

A selected few of the numerous recurrence relationships involving the modified Bessel functions are

$$I_n(x) = (\iota)^{-n} J_n(\iota x) \quad (3.38)$$

$$I_{-n}(x) = (\iota)^n J_{-n}(\iota x) \quad (3.39)$$

$$\frac{dI_n(x)}{dx} = I_{n-1}(x) - \frac{n}{x} I_n(x) = \frac{n}{x} I_n(x) + I_{n+1}(x) \quad (3.40)$$

$$\frac{d}{dx} [x^n I_n(x)] = x^n I_{n-1}(x) \quad (3.41)$$

$$\frac{d}{dx} [x^{-n} I_n(x)] = x^{-n} I_{n+1}(x) \quad (3.42)$$

$$K_{-n}(x) = K_n(x) \quad (n = 0, 1, 2, 3, \dots) \quad (3.43)$$

$$\frac{dK_n(x)}{dx} = \frac{n}{x} K_n(x) - K_{n+1}(x) = -K_{n-1}(x) - \frac{n}{x} K_n(x) \quad (3.44)$$

$$\frac{d}{dx} [x^n K_n(x)] = -x^n K_{n-1}(x) \quad (3.45)$$

$$\frac{d}{dx} [x^{-n} K_n(x)] = -x^{-n} K_{n+1}(x) \quad (3.46)$$

Fairly extensive tables for the Bessel functions and modified Bessel functions of orders 1 and 2 and those of fractional order $I_{-1/3}(x)$, $I_{-2/3}(x)$, $I_{1/3}(x)$, and $I_{2/3}(x)$ in the range $0 \leq x \leq 5$ with a refined interval are given in Kern and Kraus (1972), and polynomial approximations are given by Kraus et al. (2001), culled from the work of Abramowitz and Stegun (1955). Maple V, Release 6.0 can also be used to

generate these tables. Figure 3.2 displays graphs of $J_0(x)$, $J_1(x)$, $Y_0(x)$, and $Y_1(x)$. These functions exhibit oscillatory behavior with amplitude decaying as x increases. Figure 3.3 provides plots of $I_0(x)$, $I_1(x)$, $K_0(x)$, and $K_1(x)$ as a function of x and these functions exhibit monotonic behavior.

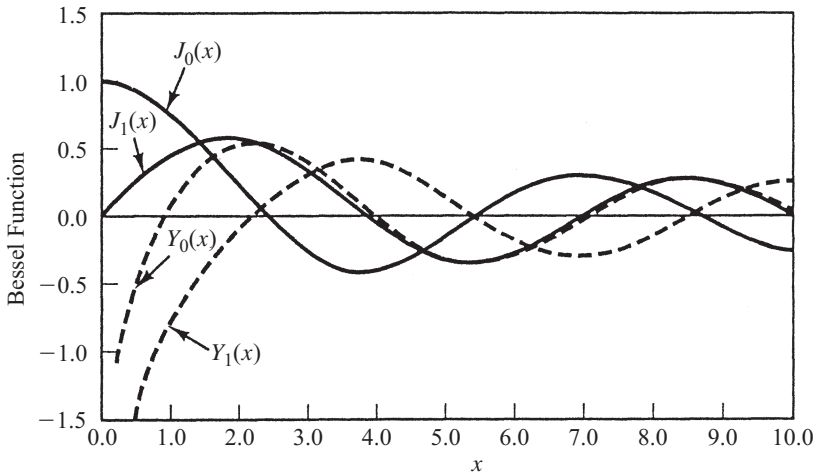


Figure 3.2 Graphs of $J_0(x)$, $J_1(x)$, $Y_0(x)$, and $Y_1(x)$.

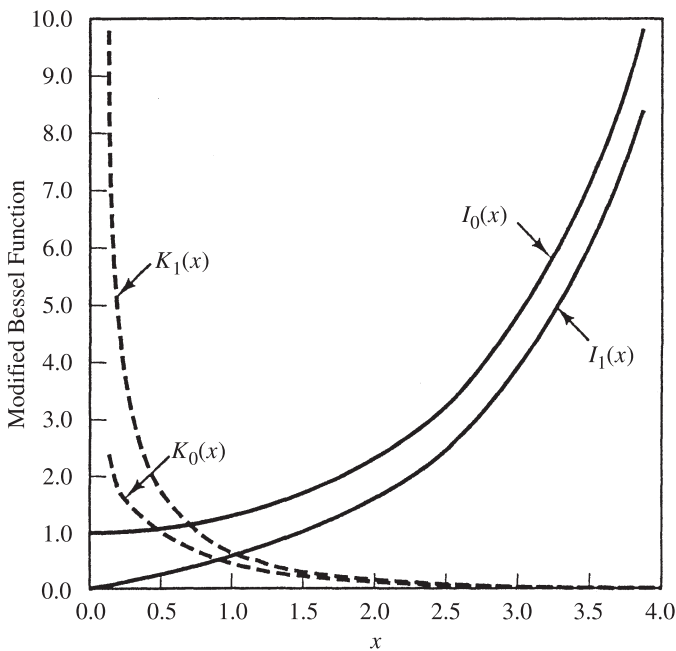


Figure 3.3 Graphs of $I_0(x)$, $I_1(x)$, $K_0(x)$, and $K_1(x)$.

Thomson functions $\text{ber}_i(x)$, $\text{bei}_i(x)$, $\text{ker}_i(x)$, and $\text{kei}_i(x)$ arise in obtaining the real and imaginary parts of the modified Bessel functions of imaginary argument. The subscripts i denote the order of the Thomson functions. Note that it is customary to omit the subscript when dealing with Thomson functions of zero order. Hence $\text{ber}_0(x)$, $\text{bei}_0(x)$, $\text{ker}_0(x)$, and $\text{kei}_0(x)$ are written as $\text{ber}(x)$, $\text{bei}(x)$, $\text{ker}(x)$, and $\text{kei}(x)$. The Thomson functions are defined by

$$I_0(x\sqrt{\imath}) = \text{ber}(x) + \imath \text{bei}(x) \tag{3.47}$$

$$K_0(x\sqrt{\imath}) = \text{ker}(x) + \imath \text{kei}(x) \tag{3.48}$$

with

$$\text{ber}(0) = 1 \qquad \text{bei}(0) = 0 \qquad \text{ker}(0) = \infty \qquad \text{kei}(0) = -\infty \tag{3.49}$$

Expressions for the derivatives of the Thomson functions are

$$\frac{d}{dx} [\text{ber}(x)] = \frac{1}{\sqrt{2}} [\text{ber}_1(x) + \text{bei}_1(x)] \tag{3.50}$$

$$\frac{d}{dx} [\text{bei}(x)] = \frac{1}{\sqrt{2}} [\text{bei}_1(x) - \text{ber}_1(x)] \tag{3.51}$$

$$\frac{d}{dx} [\text{ker}(x)] = \frac{1}{\sqrt{2}} [\text{ker}_1(x) + \text{kei}_1(x)] \tag{3.52}$$

$$\frac{d}{dx} [\text{kei}(x)] = \frac{1}{\sqrt{2}} [\text{kei}_1(x) - \text{ker}_1(x)] \tag{3.53}$$

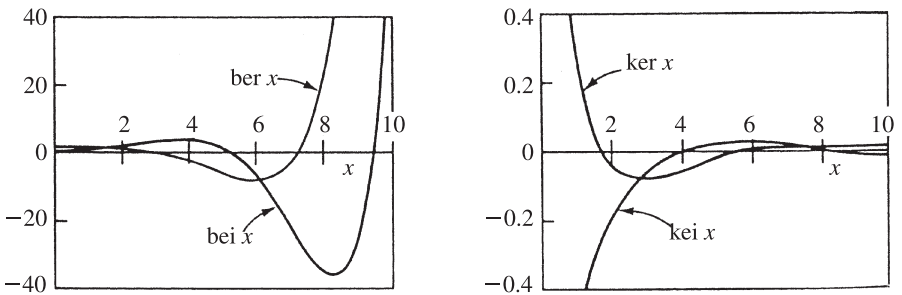
Table 3.7 gives the values of $\text{ber}(x)$, $\text{bei}(x)$, $\text{ker}(x)$, and $\text{kei}(x)$ for $1 \leq x \leq 5$, and the values of $d\text{ber}(x)/dx$, $d\text{bei}(x)/dx$, $d\text{ker}(x)/dx$, and $d\text{kei}(x)/dx$ are provided for the same range of x values in Table 3.8. Figure 3.4 displays graphs of $\text{ber}(x)$, $\text{bei}(x)$, $\text{ker}(x)$, and $\text{kei}(x)$.

TABLE 3.7 Functions $\text{ber}(x)$, $\text{bei}(x)$, $\text{ker}(x)$, and $\text{kei}(x)$

x	$\text{ber}(x)$	$\text{bei}(x)$	$\text{ker}(x)$	$\text{kei}(x)$
1.00	0.98438	0.24957	0.28671	−0.49499
1.50	0.92107	0.55756	0.05293	−0.33140
2.00	0.75173	0.97229	−0.04166	−0.20240
2.50	0.39997	1.45718	−0.06969	−0.11070
3.00	−0.22138	1.93759	−0.06703	−0.05112
3.50	−1.19360	2.28325	−0.05264	−0.01600
4.00	−2.56342	2.29269	−0.03618	0.00220
4.50	−4.29909	1.68602	−0.02200	0.00972
5.00	−6.23008	0.11603	−0.01151	0.01119

TABLE 3.8 Functions $d \operatorname{ber}(x)/dx$, $d \operatorname{bei}(x)/dx$, $d \operatorname{ker}(x)$, dx , and $d \operatorname{kei}(x)/dx$

x	$d \operatorname{ber}(x)/dx$	$d \operatorname{bei}(x)/dx$	$d \operatorname{ker}(x)/dx$	$d \operatorname{kei}(x)/dx$
1.00	-0.06245	0.49740	-0.69460	0.35237
1.50	-0.21001	0.73025	-0.29418	0.29561
2.00	-0.49307	0.91701	-0.10660	0.21981
2.50	-0.94358	0.99827	-0.01693	0.14890
3.00	-1.56985	0.88048	0.02148	0.09204
3.50	-2.33606	0.43530	0.03299	0.05098
4.00	-3.13465	-0.49114	0.03148	0.02391
4.50	-3.75368	-2.05263	0.02481	0.00772
5.00	-3.84534	-4.35414	0.01719	-0.00082

**Figure 3.4** Thomson functions.

3.3.6 Legendre Functions

The *Legendre function*, also known as the *Legendre polynomial* $P_n(x)$, and the associated Legendre function of the first kind $P_n^m(x)$, are defined by

$$P_n(x) = \frac{1}{2^n n!} \frac{d^n}{dx^n} (x^2 - 1)^n \quad (3.54)$$

$$P_n^m(x) = (1 - x^2)^{m/2} \frac{d^m}{dx^m} [P_n(x)] \quad (3.55)$$

The *Legendre function* $Q_n(x)$ and the associated Legendre function of the second kind, $Q_n^m(x)$, are defined by

$$Q_n(x) = \frac{(-1)^{n/2} \cdot 2^n [(n/2)!]^2}{n!} \times \left[x - \frac{(n-1)(n+2)}{3!} x^3 + \frac{(n-1)(n-3)(n+2)(n+4)}{5!} x^5 - \dots \right] \quad (n = \text{even}, |x| < 1) \quad (3.56)$$

$$Q_n(x) = \frac{(-1)^{(n+1)/2} \cdot 2^{n-1} \{[(n-1)/2]!\}^2}{1 \cdot 3 \cdot 5 \cdots n} \\ \times \left[1 - \frac{n(n+1)}{2!}x^2 - \frac{n(n-2)(n+1)(n+3)}{4!}x^4 - \cdots \right] \\ (n = \text{odd}, |x| < 1) \quad (3.57)$$

$$Q_n^m(x) = (1-x^2)^{m/2} \frac{d^m}{dx^m} [Q_n(x)] \quad (3.58)$$

Several relationships involving $P_n(x)$, $Q_n(x)$, $P_n^m(x)$, and $Q_n^m(x)$ are useful in heat conduction analysis. They are

$$P_n(-x) = (-1)^n P_n(x) \quad (3.59)$$

$$P_{n+1}(x) = \frac{2n+1}{n+1}x P_n(x) - \frac{n}{n+1}P_{n-1}(x) \quad (3.60)$$

$$\frac{d}{dx} [P_{n+1}(x)] - \frac{d}{dx} [P_{n-1}(x)] = 2(n+1)P_n(x) \quad (3.61)$$

$$Q_n(x = \pm 1) = \infty \quad (3.62)$$

$$P_n^m(x) = 0 \quad (m > n) \quad (3.63)$$

$$Q_n^m(x = \pm 1) = \infty \quad (3.64)$$

The numerical values of the Legendre functions and their graphs can be generated with Maple V, Release 6.0. Table 3.9 lists the values of $P_0(x)$ through $P_4(x)$ for the range $-1 \leq x \leq 1$, and a plot of these functions appears in Fig. 3.5.

3.4 STEADY ONE-DIMENSIONAL CONDUCTION

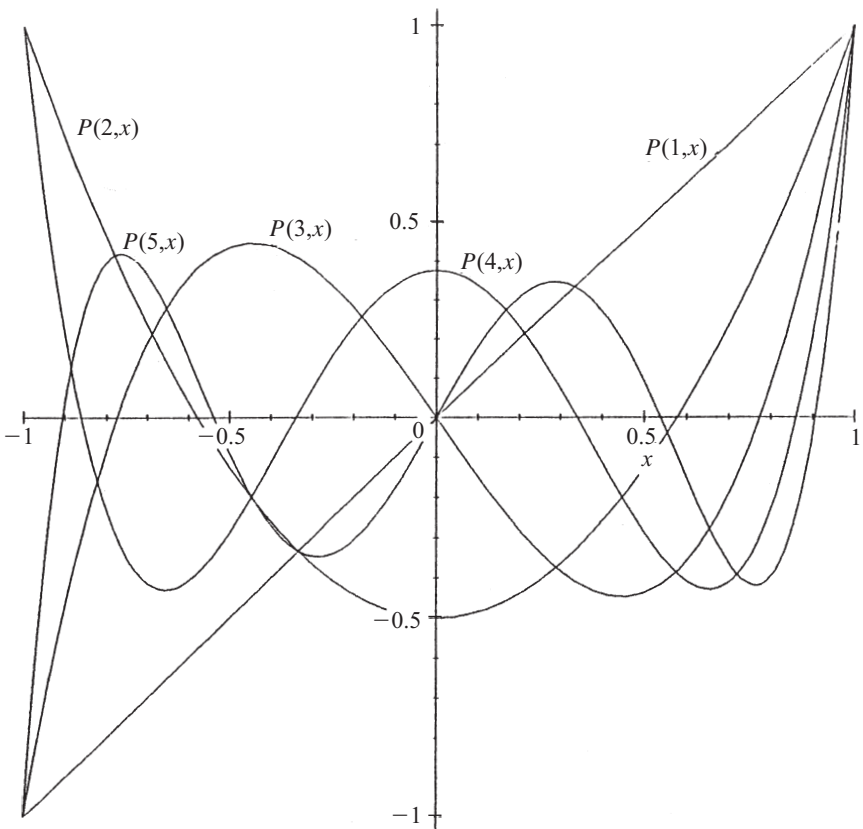
In this section we consider one-dimensional steady conduction in a plane wall, a hollow cylinder, and a hollow sphere. The objective is to develop expressions for the temperature distribution and the rate of heat transfer. The concept of thermal resistance is utilized to extend the analysis to composite systems with convection occurring at the boundaries. Topics such as contact conductance, critical thickness of insulation, and the effect of uniform internal heat generation are also discussed.

3.4.1 Plane Wall

Consider a plane wall of thickness L made of material with a thermal conductivity k , as illustrated in Fig. 3.6. The temperatures at the two faces of the wall are fixed at $T_{s,1}$ and $T_{s,2}$ with $T_{s,1} > T_{s,2}$. For steady conditions with no internal heat generation and constant thermal conductivity, the appropriate form of the general heat conduction equation, eq. (3.4), is

TABLE 3.9 Numerical Values of $P_n(x)$

x	$P_0(x)$	$P_1(x)$	$P_2(x)$	$P_3(x)$	$P_4(x)$
-1.00	1.00000	-1.00000	1.00000	-1.00000	1.00000
-0.80	1.00000	-0.80000	0.46000	-0.08000	-0.23300
-0.60	1.00000	-0.60000	0.04000	0.36000	-0.40800
-0.40	1.00000	-0.40000	-0.26000	0.44000	-0.11300
-0.20	1.00000	-0.20000	-0.44000	0.28000	0.23200
0.00	1.00000	0.00000	-0.50000	0.00000	0.37500
0.20	1.00000	0.20000	-0.44000	-0.28000	0.23200
0.40	1.00000	0.40000	-0.26000	-0.44000	-0.11300
0.60	1.00000	0.60000	0.04000	-0.36000	-0.40800
0.80	1.00000	0.80000	0.46000	0.08000	-0.23300
1.00	1.00000	1.00000	1.00000	1.00000	1.00000

**Figure 3.5** Legendre polynomials.

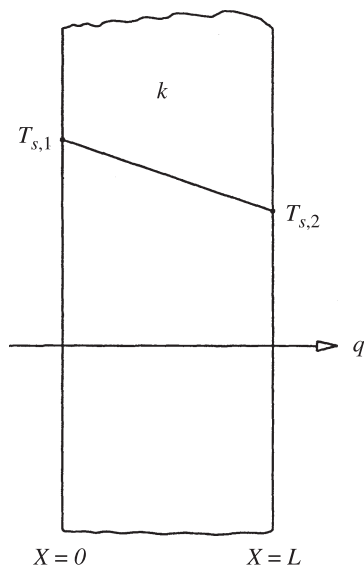


Figure 3.6 One-dimensional conduction through a plane wall.

$$\frac{d^2 T}{dx^2} = 0 \quad (3.65)$$

with the boundary conditions expressed as

$$T(x = 0) = T_{s,1} \quad \text{and} \quad T(x = L) = T_{s,2} \quad (3.66)$$

Integration of eq. (3.65) with subsequent application of the boundary conditions of eq. (3.66) gives the linear temperature distribution

$$T = T_{s,1} + (T_{s,2} - T_{s,1}) \frac{x}{L} \quad (3.67)$$

and application of Fourier's law gives

$$q = \frac{kA(T_{s,1} - T_{s,2})}{L} \quad (3.68)$$

where A is the wall area normal to the direction of heat transfer.

3.4.2 Hollow Cylinder

Figure 3.7 shows a hollow cylinder of inside radius r_1 , outside radius r_2 , length L , and thermal conductivity k . The inside and outside surfaces are maintained at constant temperatures $T_{s,1}$ and $T_{s,2}$, respectively with $T_{s,1} > T_{s,2}$. For steady-state conduction

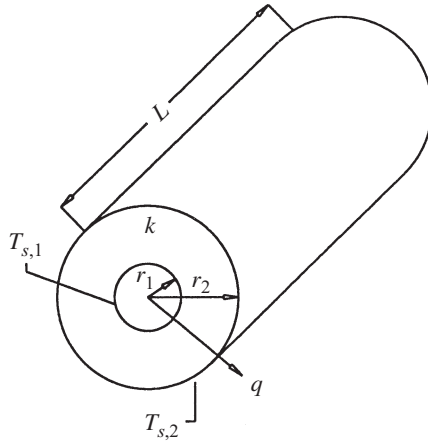


Figure 3.7 Radial conduction through a hollow cylinder.

in the radial direction with no internal heat generation and constant thermal conductivity, the appropriate form of the general heat conduction equation, eq. (3.5), is

$$\frac{d}{dr} \left(r \frac{dT}{dr} \right) = 0 \quad (3.69)$$

with the boundary conditions expressed as

$$T(r = r_1) = T_{s,1} \quad \text{and} \quad T(r = r_2) = T_{s,2} \quad (3.70)$$

Following the same procedure as that used for the plane wall will give the temperature distribution

$$T = T_{s,1} + \frac{T_{s,1} - T_{s,2}}{\ln(r_1/r_2)} \ln \frac{r}{r_1} \quad (3.71)$$

and the heat flow

$$q = \frac{2\pi k L (T_{s,1} - T_{s,2})}{\ln(r_2/r_1)} \quad (3.72)$$

3.4.3 Hollow Sphere

The description pertaining to the hollow cylinder also applies to the hollow sphere of Fig. 3.8 except that the length L is no longer relevant. The applicable form of eq. (3.6) is

$$\frac{d}{dr} \left(r^2 \frac{dT}{dr} \right) = 0 \quad (3.73)$$

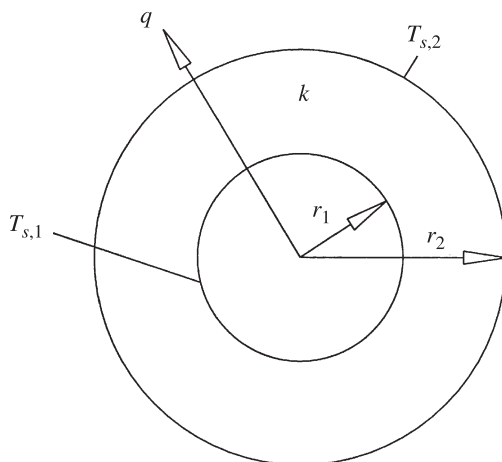


Figure 3.8 Radial conduction through a hollow sphere.

with the boundary conditions expressed as

$$T(r = r_1) = T_{s,1} \quad \text{and} \quad T(r = r_2) = T_{s,2} \quad (3.74)$$

The expressions for the temperature distribution and heat flow are

$$T = T_{s,1} + \frac{T_{s,1} - T_{s,2}}{1/r_2 - 1/r_1} \left(\frac{1}{r_1} - \frac{1}{r} \right) \quad (3.75)$$

$$q = \frac{4\pi k(T_{s,1} - T_{s,2})}{1/r_1 - 1/r_2} \quad (3.76)$$

3.4.4 Thermal Resistance

Thermal resistance is defined as the ratio of the temperature difference to the associated rate of heat transfer. This is completely analogous to electrical resistance, which, according to Ohm's law, is defined as the ratio of the voltage difference to the current flow. With this definition, the thermal resistance of the plane wall, the hollow cylinder, and the hollow sphere are, respectively,

$$R_{\text{cond}} = \frac{L}{kA} \quad (3.77)$$

$$R_{\text{cond}} = \frac{\ln(r_2/r_1)}{2\pi kL} \quad (3.78)$$

$$R_{\text{cond}} = \frac{1/r_1 - 1/r_2}{4\pi k} \quad (3.79)$$

When convection occurs at the boundaries of a solid, it is convenient to define the convection resistance from Newton's law of cooling:

$$q = hA(T_s - T_\infty) \quad (3.80)$$

where h is the convection heat transfer coefficient and T_∞ is the convecting fluid temperature. It follows from eq. (3.80) that

$$R_{\text{conv}} = \frac{T_s - T_\infty}{q} = \frac{1}{hA} \quad (3.81)$$

3.4.5 Composite Systems

The idea of thermal resistance is a useful tool for analyzing conduction through composite members.

Composite Plane Wall For the series composite plane wall and the associated thermal network shown in Fig. 3.9, the rate of heat transfer q is given by

$$q = \frac{T_{\infty,1} - T_{\infty,2}}{1/h_1A + L_1/k_1A + L_2/k_2A + 1/h_2A} \quad (3.82)$$

Once q has been determined, the surface and interface temperatures can be found:

$$T_{s,1} = T_{\infty,1} - q \frac{1}{h_1A} \quad (3.83)$$

$$T_2 = T_{\infty,1} - q \left(\frac{1}{h_1A} + \frac{L_1}{k_1A} \right) \quad (3.84)$$

$$T_{s,2} = T_{\infty,1} - q \left(\frac{1}{h_1A} + \frac{L_1}{k_1A} + \frac{L_2}{k_2A} \right) \quad (3.85)$$

Figure 3.10 illustrates a series-parallel composite wall. If materials 2 and 3 have comparable thermal conductivities, the heat flow may be assumed to be one-dimensional. The network shown in Fig. 3.10 assumes that surfaces normal to the direction of heat flow are isothermal. For a wall of unit depth, the heat transfer rate is

$$q = \frac{T_{s,1} - T_{s,2}}{L_1/k_1H_1 + L_2L_3/(k_2H_2L_3 + k_3H_3L_2) + L_4/k_4H_4} \quad (3.86)$$

where $H_1 = H_2 + H_3 = H_4$ and the rule for combining resistances in parallel has been employed. Once q has been determined, the interface temperatures may be computed:

$$T_1 = T_{s,1} - q \frac{L_1}{k_1H_1} \quad (3.87)$$

$$T_2 = T_{s,2} + q \frac{L_4}{k_4H_4} \quad (3.88)$$

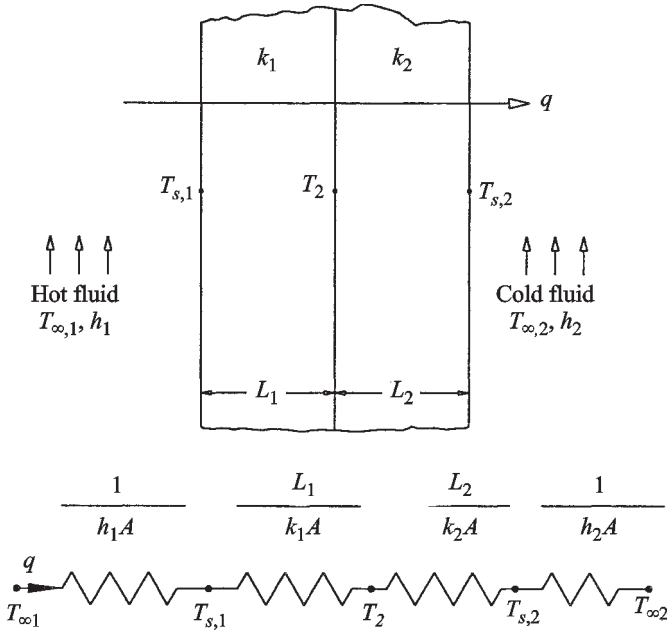


Figure 3.9 Series composite wall and its thermal network.

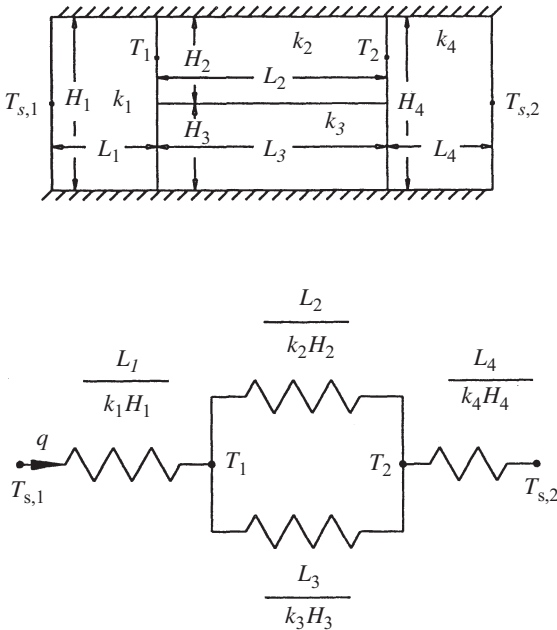


Figure 3.10 Series-parallel composite wall and its thermal network.

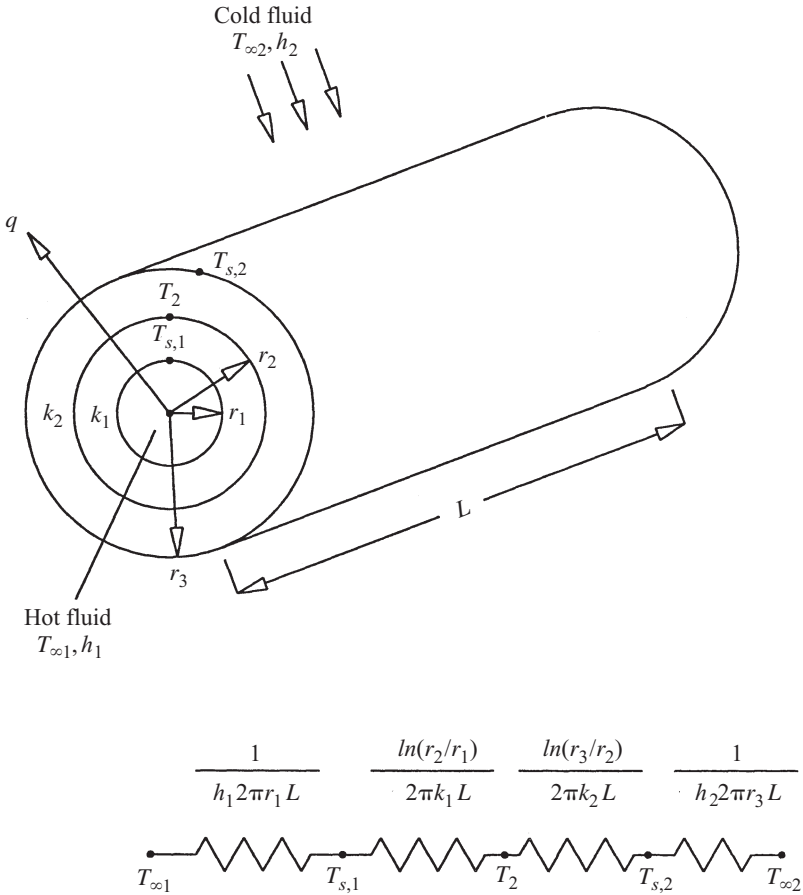


Figure 3.11 Series composite hollow cylinder and its thermal network.

Composite Hollow Cylinder A typical composite hollow cylinder with both inside and outside experiencing convection is shown in Fig. 3.11. The figure includes the thermal network that represents the system. The rate of heat transfer q is given by

$$q = \frac{T_{\infty,1} - T_{\infty,2}}{1/2\pi h_1 r_1 L + \ln(r_2/r_1)/2\pi k_1 L + \ln(r_3/r_2)/2\pi k_2 L + 1/2\pi h_2 r_3 L} \quad (3.89)$$

Once q has been determined, the inside surface $T_{s,1}$, the interface temperature T_2 , and the outside surface temperature $T_{s,2}$ can be found:

$$T_{s,1} = T_{\infty,1} - q \frac{1}{2\pi h_1 r_1 L} \quad (3.90)$$

$$T_2 = T_{\infty,1} - q \left[\frac{1}{2\pi h_1 r_1 L} + \frac{\ln(r_2/r_1)}{2\pi k_1 L} \right] \quad (3.91)$$

$$T_{s,2} = T_{\infty,2} + q \frac{1}{2\pi h_2 r_3 L} \quad (3.92)$$

Composite Hollow Sphere Figure 3.12 depicts a composite hollow sphere made of two layers and experiencing convective heating on the inside surface and convective cooling on the outside surface. From the thermal network, also shown in Fig. 3.12, the rate of heat transfer q can be determined as

$$q = \frac{T_{\infty,1} - T_{\infty,2}}{1/4\pi h_1 r_1^2 + (r_2 - r_1)/4\pi k_1 r_1 r_2 + (r_3 - r_2)/4\pi k_2 r_2 r_3 + 1/4\pi h_2 r_3^2} \quad (3.93)$$

Once q has been determined, temperatures $T_{s,1}$, T_2 , and $T_{s,2}$ can be found:

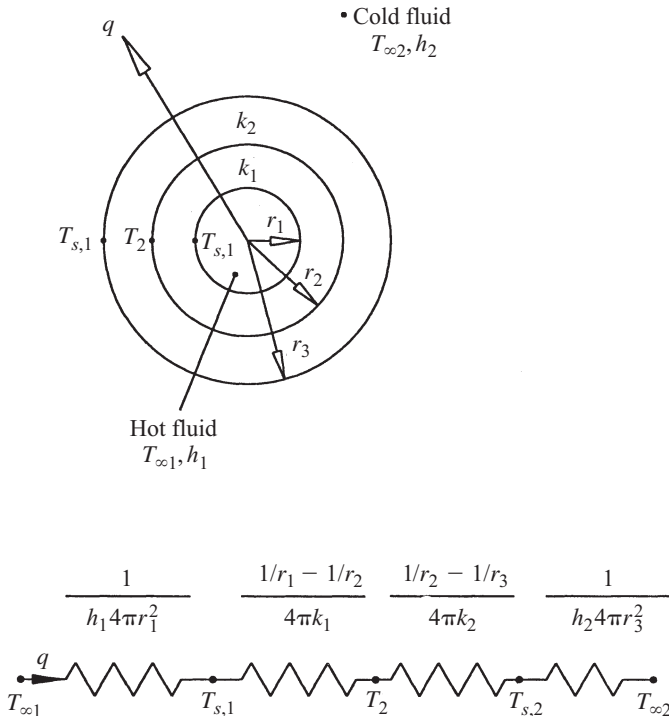


Figure 3.12 Series composite hollow sphere and its thermal network.

$$T_{s,1} = T_{\infty,1} - q \frac{1}{4\pi h_1 r_1^2} \quad (3.94)$$

$$T_2 = T_{\infty,1} - q \left[\frac{1}{4\pi h_1 r_1^2} + \frac{1}{4\pi k_1} \left(\frac{1}{r_1} - \frac{1}{r_2} \right) \right] \quad (3.95)$$

$$T_{s,2} = T_{\infty,2} + q \frac{1}{4\pi h_2 r_3^2} \quad (3.96)$$

3.4.6 Contact Conductance

The heat transfer analyses for the composite systems described in Section 3.4.5 assumed perfect contact at the interface between the two materials. In reality, however, the mating surfaces are rough and the actual contact occurs at discrete points (*asperities* or *peaks*), as indicated in Fig. 3.13. The gaps or voids are usually filled with air, and the heat transfer at the interface is the sum of solid conduction across the contact points and fluid conduction through the gaps. Because of the imperfect contact, there is a temperature drop across the gap or interface, ΔT_c . The contact conductance h_c ($\text{W}/\text{m}^2 \cdot \text{K}$) is defined as the ratio of the heat flux q/A through the interface to the interface temperature drop:

$$h_c = \frac{q/A}{\Delta T_c} = \frac{1}{R_c''} \quad (3.97)$$

where q/A is the heat flux through the interface and R_c'' ($\text{m}^2 \cdot \text{K}/\text{W}$), the inverse of h_c , is the contact resistance.

The topic of contact conductance is of considerable contemporary interest, as reflected by a review paper of Fletcher (1988), a book by Madhusudana (1996),

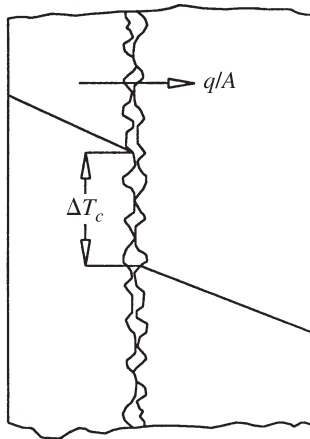


Figure 3.13 Contact interface for actual surfaces.

and numerous contributions from several research groups. Chapter 4 of this book is devoted exclusively to this subject.

3.4.7 Critical Thickness of Insulation

When a plane surface is covered with insulation, the rate of heat transfer always decreases. However, the addition of insulation to a cylindrical or spherical surface increases the conduction resistance but reduces the convection resistance because of the increased surface area. The *critical thickness of insulation* corresponds to the condition when the sum of conduction and convection resistances is a minimum. For a given temperature difference, this results in a maximum heat transfer rate, and the critical radius r_c is given by

$$r_c = \begin{cases} \frac{k}{h} & \text{(cylinder)} \\ \frac{2k}{h} & \text{(sphere)} \end{cases} \quad (3.98)$$

$$(3.99)$$

where k is the thermal conductivity of the insulation and h is the convective heat transfer coefficient for the outside surface.

The basic analysis for obtaining the critical radius expression has been modified to allow for:

- The variation of h with outside radius
- The variation of h with outside radius, including the effect of temperature-dependent fluid properties
- Circumferential variation of h
- Pure radiation cooling
- Combined natural convection and radiation cooling

The analysis for a circular pipe has also been extended to include insulation boundaries that form equilateral polygons, rectangles, and concentric circles. Such configurations require a two-dimensional conduction analysis and have led to the conclusion that the concept of critical perimeter of insulation, $P_c = 2\pi(k/h)$, is more general than that of critical radius. The comprehensive review article by Aziz (1997) should be consulted for further details.

3.4.8 Effect of Uniform Internal Energy Generation

In some engineering systems, it becomes necessary to analyze one-dimensional steady conduction with internal energy generation. Common sources of energy generation are the passage of an electric current through a wire or busbar or a rear window defroster in an automobile. In the fuel element of a nuclear reactor, the energy is generated due to neutron absorption. A vessel containing nuclear waste experiences energy generation as the waste undergoes a slow process of disintegration.

Plane Wall Consider first a plane wall of thickness $2L$, made of a material having a thermal conductivity k , as shown in Fig. 3.14. The volumetric rate of energy generation in the wall is \dot{q} (W/m³). Let $T_{s,1}$ and $T_{s,2}$ be the two surface temperatures, and assuming the thermal conductivity of the wall to be constant, the appropriate form of eq. (3.4) is

$$\frac{d^2T}{dx^2} + \frac{\dot{q}}{k} = 0 \quad (3.100)$$

and the boundary conditions are

$$T(x = -L) = T_{s,1} \quad \text{and} \quad T(x = L) = T_{s,2} \quad (3.101)$$

The solution for the temperature distribution is

$$T = \frac{\dot{q}}{2k} (L^2 - x^2) + \frac{T_{s,2} - T_{s,1}}{2L}x + \frac{T_{s,2} + T_{s,1}}{2} \quad (3.102)$$

The maximum temperature occurs at $x = k(T_{s,2} - T_{s,1})/2L\dot{q}$ and is given by

$$T_{\max} = \frac{\dot{q}L^2}{2k} + \frac{k(T_{s,2} - T_{s,1})^2}{8\dot{q}L^2} + \frac{T_{s,2} + T_{s,1}}{2} \quad (3.103)$$

If the face at $x = -L$ is cooled by convection with a heat transfer coefficient h_1 and coolant temperature $T_{\infty,1}$, and the face at $x = +L$ is cooled by convection with a heat transfer coefficient h_2 and coolant temperature $T_{\infty,2}$, the overall energy balance gives

$$2\dot{q}L = h_1(T_{s,1} - T_{\infty,1}) + h_2(T_{s,2} - T_{\infty,2}) \quad (3.104)$$

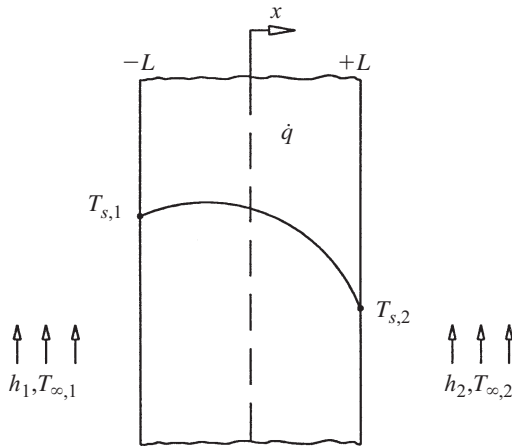


Figure 3.14 Conduction in a plane wall with uniform internal energy generation.

When $T_{s,1} = T_{s,2}$, the temperature distribution is symmetrical about $x = 0$ and is given by

$$T = \frac{\dot{q}}{2k} (L^2 - x^2) + T_s \quad (3.105)$$

and the maximum temperature occurs at the midplane ($x = 0$), which can be expressed as

$$T_{\max} = \frac{\dot{q}L^2}{2k} + T_s \quad (3.106)$$

When $T_{\infty,1} = T_{\infty,2} = T_{\infty}$ and $h_1 = h_2 = h$, eq. (3.104) reduces to

$$T_s - T_{\infty} = \frac{\dot{q}L}{h} \quad (3.107)$$

Hollow Cylinder For the hollow cylinder shown in Fig. 3.15, the appropriate form of eq. (3.5) for constant k is

$$\frac{1}{r} \frac{d}{dr} \left(r \frac{dT}{dr} \right) + \frac{\dot{q}}{k} = 0 \quad (3.108)$$

and the boundary conditions are

$$T(r = r_1) = T_{s,1} \quad \text{and} \quad T(r = r_2) = T_{s,2} \quad (3.109)$$

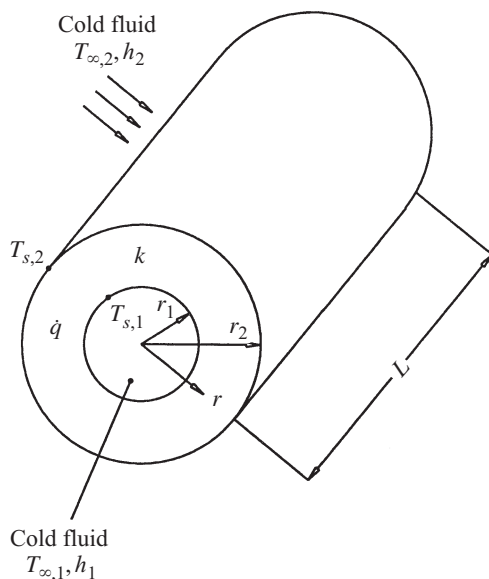


Figure 3.15 Conduction in a hollow cylinder with uniform internal energy generation.

The solution of eq. (3.108) that satisfies eqs. (3.109) is

$$T = T_{s,2} + \frac{\dot{q}r_2^2}{4k} \left[1 - \left(\frac{r}{r_2} \right)^2 \right] - \left\{ \frac{\dot{q}r_2^2}{4k} \left[1 - \left(\frac{r_1}{r_2} \right)^2 \right] + (T_{s,2} - T_{s,1}) \right\} \frac{\ln(r_2/r)}{\ln(r_2/r_1)} \quad (3.110)$$

If the inside and outside surfaces are cooled by convection, the inside with fluid at $T_{\infty,1}$ with heat transfer coefficient h_2 , the overall energy balance gives

$$\dot{q}(r_2^2 - r_1^2) = 2h_1r_1(T_{s,1} - T_{\infty,1}) + 2h_2r_2(T_{s,2} - T_{\infty,2}) \quad (3.111)$$

and for the case of $T_{s,1} = T_{s,2}$, eq. (3.110) is reduced to

$$T = T_s + \frac{\dot{q}r_2^2}{4k} \left[1 - \left(\frac{r}{r_2} \right)^2 \right] - \frac{\dot{q}r_2^2}{4k} \left[1 - \left(\frac{r_1}{r_2} \right)^2 \right] \frac{\ln(r_2/r)}{\ln(r_2/r_1)} \quad (3.112)$$

Similarly, when $T_{\infty,1} = T_{\infty,2} = T_{\infty}$ and $h_1 = h_2 = h$, eq. (3.111) is reduced to

$$T_s - T_{\infty} = \frac{\dot{q}(r_2 - r_1)}{2h} \quad (3.113)$$

Solid Cylinder Equation (3.108) also applies to the solid cylinder of Fig. 3.16, but the boundary conditions change to

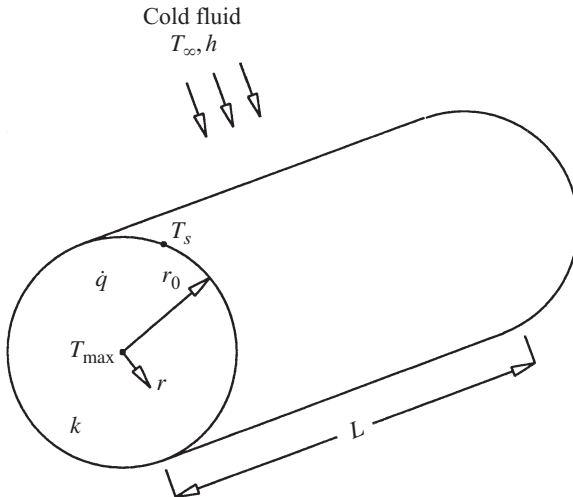


Figure 3.16 Conduction in a solid cylinder with uniform internal energy generation.

$$\left. \frac{dT}{dr} \right|_{r=0} = 0 \quad \text{and} \quad T(r = r_0) = T_s \quad (3.114)$$

The temperature distribution is given by

$$T = T_s + \frac{\dot{q}}{4k} (r_0^2 - r^2) \quad (3.115)$$

and the maximum temperature occurs along the centerline at $r = 0$:

$$T_{\max} = T_s + \frac{\dot{q}r_0^2}{4k} \quad (3.116)$$

If the outside surface of the cylinder is cooled by convection to a fluid at T_∞ through a heat transfer coefficient h , the overall energy balance gives

$$T_s - T_\infty = \frac{\dot{q}r_0}{2h} \quad (3.117)$$

Hollow Sphere For the hollow sphere shown in Fig. 3.17, the appropriate form of eq. (3.6) with constant thermal conductivity k is

$$\frac{1}{r^2} \frac{d}{dr} \left(r^2 \frac{dT}{dr} \right) + \frac{\dot{q}}{k} = 0 \quad (3.118)$$

and eq. (3.109) provides the boundary conditions

$$T(r = r_1) = T_{s,1} \quad \text{and} \quad T(r = r_2) = T_{s,2} \quad (3.109)$$

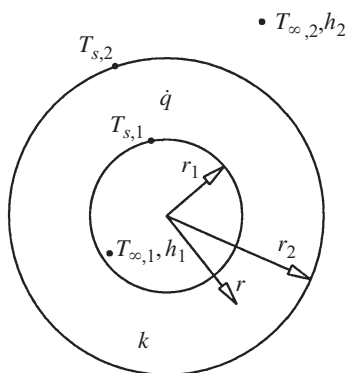


Figure 3.17 Conduction in a hollow sphere with uniform internal energy generation.

The temperature distribution is found to be

$$T = T_{s,2} + \frac{\dot{q}r_2^2}{6k} \left[1 - \left(\frac{r}{r_2} \right)^2 \right] - \left\{ \frac{\dot{q}r_2^2}{6k} \left[1 - \left(\frac{r_1}{r_2} \right)^2 \right] + (T_{s,2} - T_{s,1}) \right\} \frac{1/r - 1/r_2}{1/r_1 - 1/r_2} \quad (3.119)$$

If the inside and outside surfaces are cooled by convection, the inside with fluid at $T_{\infty,1}$ with heat transfer coefficient h_1 and the outside with fluid at $T_{\infty,2}$ with heat transfer coefficient h_2 , the overall energy balance gives

$$\frac{\dot{q} (r_2^3 - r_1^3)}{3} = h_1 r_1^2 (T_{s,1} - T_{\infty,1}) + h_2 r_2^2 (T_{s,2} - T_{\infty,2}) \quad (3.120)$$

and when $T_{s,1} = T_{s,2} = T_s$, eq. (3.119) reduces to

$$T = T_s + \frac{\dot{q}r_2^2}{6k} \left[1 - \left(\frac{r}{r_2} \right)^2 \right] - \frac{\dot{q}r_2^2}{6k} \left[1 - \left(\frac{r_1}{r_2} \right)^2 \right] \frac{1/r - 1/r_2}{1/r_1 - 1/r_2} \quad (3.121)$$

When $T_{\infty,1} = T_{\infty,2} = T_{\infty}$, and $h_1 = h_2 = h$, eq. (3.120) is reduced to

$$T_s - T_{\infty} = \frac{\dot{q} (r_2^3 - r_1^3)}{3h (r_1^2 + r_2^2)} \quad (3.122)$$

Solid Sphere For the solid sphere, eq. (3.118),

$$\frac{1}{r^2} \frac{d}{dr} \left(r^2 \frac{dT}{dr} \right) + \frac{\dot{q}}{k} = 0 \quad (3.118)$$

must be solved subject to the boundary conditions of eqs. (3.114):

$$\left. \frac{dT}{dr} \right|_{r=0} = 0 \quad \text{and} \quad T(r = r_0) = T_s \quad (3.114)$$

The solution is

$$T = T_s + \frac{\dot{q}}{6k} (r_0^2 - r^2) \quad (3.123)$$

The maximum temperature that occurs at the center of the sphere where $r = 0$ is

$$T_{\max} = T_s + \frac{\dot{q}r_0^2}{6k} \quad (3.124)$$

and if the cooling at the outside surface is to a fluid at T_∞ via a heat transfer coefficient of h , the overall energy balance gives

$$T_s - T_\infty = \frac{\dot{q}r_0}{3h} \quad (3.125)$$

For additional analytical results for one-dimensional steady conduction with uniform internal heat generation, the reader should consult Incropera and DeWitt (1996, App. C).

3.5 MORE ADVANCED STEADY ONE-DIMENSIONAL CONDUCTION

The results presented in Section 3.4 have been based on assumptions such as constant thermal conductivity, uniform heat generation, and pure convective cooling or heating at the boundary. In some applications, these assumptions may introduce significant errors in predicting the thermal behavior of the system.

The conducting medium may be nonhomogeneous, causing thermal conductivity to vary with location. Similarly, the temperature dependence of thermal conductivity cannot be ignored if the temperature difference driving the conduction process is large and the assumption of uniform heat generation may prove too restrictive. For example, when the shield of a nuclear reactor is irradiated with gamma rays, the resulting release of energy decays exponentially with distance from the irradiated surface, making the heat generation location dependent. A more realistic modeling of heat generation due to the passage of electric current or a chemical reaction requires that \dot{q} be treated as temperature dependent. Finally, if the heat transfer process at a boundary is driven by natural convection, radiation becomes equally important and must be taken into account. This section is devoted to a discussion of such situations.

3.5.1 Location-Dependent Thermal Conductivity

Plane Wall Consider the plane wall of Fig. 3.6 and let the thermal conductivity k increase linearly with x in accordance with

$$k = k_0(1 + ax) \quad (3.126)$$

where k_0 is the thermal conductivity at $x = 0$ and a is a measure of the variation of k with x . The equation governing the temperature distribution is

$$\frac{d}{dx} \left(k \frac{dT}{dx} \right) = 0 \quad (3.127)$$

Solving eq. (3.127) subject to the boundary conditions of eq. (3.66),

$$T(x = 0) = T_{s,1} \quad \text{and} \quad T(x = L) = T_{s,2} \quad (3.66)$$

gives

$$T = T_{s,1} + (T_{s,2} - T_{s,1}) \frac{\ln(1 + ax)}{\ln(1 + aL)} \quad (3.128)$$

and the rate of heat transfer will be

$$q = \frac{k_0 A a (T_{s,1} - T_{s,2})}{\ln(1 + aL)} \quad (3.129)$$

In the limit, as $a \rightarrow 0$, eqs. (3.128) and (3.129) reduce to eqs. (3.67) and (3.68), respectively.

Now consider the case where k is of the form

$$k = k_0(1 + ax^2) \quad (3.130)$$

The solutions for T and q are given by

$$T = T_{s,1} + (T_{s,2} - T_{s,1}) \frac{\arctan(\sqrt{ax})}{\arctan(\sqrt{aL})} \quad (3.131)$$

and the rate of heat transfer will be

$$q = \frac{k_0 A \sqrt{a} (T_{s,1} - T_{s,2})}{\arctan(\sqrt{aL})} \quad (3.132)$$

Hollow Cylinder When modified to allow for the location-dependent thermal conductivity of the form

$$k = a(1 + br) \quad (3.133)$$

analysis of Section 3.4.2 for a hollow cylinder (Fig. 3.7) gives the following results for the temperature distribution and the rate of heat transfer:

$$T = \frac{T_{s,1} \ln \left(\frac{r_2}{1 + br_2} \frac{1 + br}{r} \right) + T_{s,2} \ln \left(\frac{1 + br_1}{r_1} \frac{r}{1 + br} \right)}{\ln \left(\frac{1 + br_1}{1 + br_2} \frac{r_2}{r_1} \right)} \quad (3.134)$$

$$q = \frac{2\pi a L (T_{s,1} - T_{s,2})}{\ln \left(\frac{1 + br_1}{1 + br_2} \frac{r_2}{r_1} \right)} \quad (3.135)$$

When $b = 0$, $k = a$ and the thermal conductivity is constant. In this case, eqs. (3.134) and (3.135) are reduced to eqs. (3.71) and (3.72), respectively.

3.5.2 Temperature-Dependent Thermal Conductivity

Plane Wall Let the thermal conductivity k of the plane wall of Fig. 3.6 be a linear function of the temperature T , expressed as

$$k = k_0(1 + aT) \quad (3.136)$$

Equation (3.127) will then take the form

$$\frac{d}{dx} \left[k_0(1 + aT) \frac{dT}{dx} \right] = 0 \quad (3.137)$$

which must be integrated using the boundary conditions of eqs. (3.66):

$$T(x = 0) = T_{s,1} \quad \text{and} \quad T(x = L) = T_{s,2} \quad (3.66)$$

The solution is facilitated by the introduction of a new variable, T^* , defined by the Kirchhoff transformation:

$$T^* = \int_0^T (1 + aT) dT = T + \frac{1}{2}aT^2 \quad (3.138)$$

Differentiation of eq. (3.138) with respect to x gives

$$\frac{dT^*}{dx} = (1 + aT) \frac{dT}{dx} \quad (3.139)$$

which allows eq. (3.137) to be written as

$$\frac{d^2 T^*}{dx^2} = 0 \quad (3.140)$$

The boundary conditions of eq. (3.66) in terms of T^* become

$$T_{s,1}^*(x = 0) = T_{s,1} + \frac{1}{2}aT_{s,1}^2 \quad \text{and} \quad T_{s,2}^*(x = L) = T_{s,2} + \frac{1}{2}aT_{s,2}^2 \quad (3.141)$$

The solution for T^* is

$$T^* = T_{s,1}^* + (T_{s,2}^* - T_{s,1}^*) \frac{x}{L} \quad (3.142)$$

Once T^* has been found, T can be reclaimed by solving the quadratic of eq. (3.138), which gives

$$T = \frac{1}{a} \left(-1 + \sqrt{1 + 2aT^*} \right) \quad (3.143)$$

and the rate of heat transfer can be shown to be

$$q = \frac{k_m A (T_{s,1} - T_{s,2})}{L} \quad (3.144)$$

where $k_m = k_0(1 + aT_{s,m})$ is the thermal conductivity at the mean temperature,

$$T_{s,m} = \frac{T_{s,1} + T_{s,2}}{2}$$

For a variation of the thermal conductivity with temperature represented by

$$k = k_0(1 + aT^2) \quad (3.145)$$

the temperature distribution in the plane wall (Fig. 3.6) is given by the cubic equation

$$T + \frac{1}{3}aT^3 = T_{s,1} + \frac{1}{3}aT_{s,1}^3 + \left[\frac{1}{3}a(T_{s,2}^3 - T_{s,1}^3) + (T_{s,2} - T_{s,1}) \right] \frac{x}{L} \quad (3.146)$$

and the corresponding rate of heat transfer is

$$q = \frac{Ak_0(T_{s,1} - T_{s,2}) \left[1 + (a/3)(T_{s,1}^2 + T_{s,1}T_{s,2} + T_{s,2}^2) \right]}{L} \quad (3.147)$$

Hollow Cylinder For the thermal conductivity–temperature relation of eq. (3.136), the Kirchhoff transformation of eq. (3.138) can also be used for the hollow cylinder of Fig. 3.7. The final result for T^* is

$$T^* = T_{s,1}^* + \frac{T_{s,1}^* - T_{s,2}^*}{\ln(r_1/r_2)} \ln \frac{r}{r_1} \quad (3.148)$$

where $T_{s,1}^*$ and $T_{s,2}^*$ are as given in eq. (3.141). Once T^* for any radius r is found from eq. (3.148), eq. (3.143) can be used to find the corresponding value of T . The rate of heat transfer then follows as

$$q = \frac{2\pi k_m L (T_{s,1} - T_{s,2})}{\ln(r_2/r_1)} \quad (3.149)$$

where k_m is the thermal conductivity at the mean temperature,

$$T_{s,m} = \frac{T_{s,1} + T_{s,2}}{2}$$

Hollow Sphere The results for a hollow sphere (Fig. 3.8) whose thermal conductivity–temperature variation follows eq. (3.136) are

$$T^* = T_{s,1}^* + \frac{T_{s,1}^* - T_{s,2}^*}{1/r_2 - 1/r_1} \left(\frac{1}{r_1} - \frac{1}{r} \right) \quad (3.150)$$

$$T = \frac{1}{a} \left(-1 + \sqrt{1 + 2aT^*} \right) \quad (3.151)$$

$$q = \frac{4\pi k_m (T_{s,1} - T_{s,2})}{1/r_1 - 1/r_2} \quad (3.152)$$

Gebhart (1993) provides one-dimensional steady conduction analyses for single and composite solids when the thermal conductivity varies simultaneously with location and temperature. He also gives expressions for the conduction resistances of a plane wall, a hollow cylinder, and a hollow sphere for three cases of variable thermal conductivity: $k = k(T)$, $k = k(x)$ or $k(r)$, and $k = k(x, T) = k(T)f(x)$. Note that the last case assumes that $k(x, T)$ can be expressed as a product of two functions, $k(T)$ and $f(x)$, each a function of a single variable.

3.5.3 Location-Dependent Energy Generation

Plane Wall Figure 3.18 presents a plane wall that experiences location-dependent energy generation of the form

$$\dot{q} = \dot{q}_0 \left(1 - \frac{x}{L} \right) \quad (3.153)$$

The temperature distribution in the wall is given by

$$T = T_{s,1} + \frac{\dot{q}_0 L x}{2k} - \frac{\dot{q}_0}{2k} \left(x^2 - \frac{x^3}{3L} \right) \quad (3.154)$$

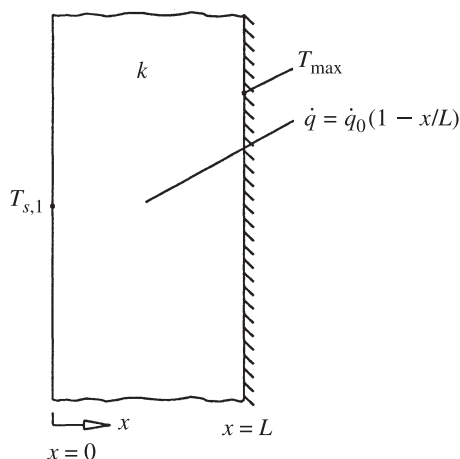


Figure 3.18 Plane wall with linearly decaying, location-dependent internal energy generation.

and the maximum temperature occurs at $x = L$ for an insulated face:

$$T = T_{s,1} + \frac{\dot{q}_0 L^2}{6k} \quad (3.155)$$

Next, assume that the plane wall of Fig. 3.6 represents the shield of a nuclear reactor. The absorption of gamma radiation at the left surface ($x = 0$) triggers energy release into the shield which decays exponentially with the penetration distance x and can be represented by the relation

$$\dot{q} = q_0'' a e^{-ax} \quad (3.156)$$

where q_0'' (W/m²) is the incident radiation heat flux and a (m⁻¹) is the absorption coefficient of the shield.

The temperature distribution in the shield is

$$T = T_{s,1} + \frac{q_0''}{ak} (1 - e^{-ax}) + \left[(T_{s,2} - T_{s,1}) + \frac{q_0''}{ak} (e^{-aL} - 1) \right] \frac{x}{L} \quad (3.157)$$

and the maximum temperature occurs at

$$x = \frac{1}{a} \ln \frac{q_0'' a L}{ak(T_{s,1} - T_{s,2}) + q_0''(1 - e^{-aL})} \quad (3.158)$$

Solid Cylinder Reconsidering the solid cylinder of Fig. 3.16, \dot{q} will now be assumed to vary linearly with the radial distance r , that is,

$$\dot{q} = ar \quad (3.159)$$

where a (W/m⁴) is a constant. The temperature distribution in this case is

$$T = T_\infty + \frac{ar_0^2}{3h} + \frac{a}{9k} (r_0^3 - r^3) \quad (3.160)$$

from which the centerline ($r = 0$) temperature T_c and the surface ($r = r_0$) temperature T_s follow as

$$T_c = T_\infty + \frac{ar_0^2}{3h} + \frac{ar_0^3}{9k} \quad (3.161)$$

$$T_s = T_\infty + \frac{ar_0^2}{3h} \quad (3.162)$$

3.5.4 Temperature-Dependent Energy Generation

In this section we present a collection of results for one-dimensional steady conduction in a plane wall, a solid cylinder, and a solid sphere when each experiences energy generation that increases linearly with local temperature in accordance with

$$\dot{q} = \dot{q}_s [1 + a(T - T_s)] \quad (3.163)$$

where \dot{q}_s is the energy generation at the surface temperature T_s and a is a constant.

Plane Wall For a plane wall of thickness $2L$ having identical surface temperatures T_s on both faces, the temperature distribution is

$$T = T_s + \frac{1}{a} \left(\frac{\cos nx}{\cos nL} - 1 \right) \quad (3.164)$$

where $n = \sqrt{a\dot{q}_s/k}$ and $nL < \pi/2$ to ensure that the temperatures remain finite.

If the convection cooling, characterized by the temperature T_∞ and heat transfer coefficient h , is identical on both faces of the wall, the relationship between T_s and T_∞ is given by

$$T_s = T_\infty + \frac{m}{h} \tan nL \quad (3.165)$$

where $m = \sqrt{\dot{q}_s k/a}$.

Solid Cylinder For a solid cylinder of radius r_0 , the temperature distribution is

$$T = T_s + \frac{1}{a} \left[\frac{J_0(nr)}{J_0(nr_0)} - 1 \right] \quad (3.166)$$

where $n = \sqrt{a\dot{q}_s/k}$ and J_0 is the Bessel function of the first kind of zero order (see Section 3.3.5). The parallel counterpart of eq. (3.165) is

$$T_s = T_\infty + \frac{m}{h} \frac{J_1(nr_0)}{J_0(nr_0)} \quad (3.167)$$

where $m = \sqrt{\dot{q}_s k/a}$, $n = \sqrt{a\dot{q}_s/k}$, and J_1 is the Bessel function of the first kind of order 1. In eqs. (3.166) and (3.167), $nr_0 < 2.4048$ to assure finite temperatures in the cylinder.

Solid Sphere For a solid sphere of radius r_0 , the temperature distribution is

$$T = T_s + \frac{1}{a} \left(\frac{r_0}{r} \frac{\sin nr}{\sin nr_0} - 1 \right) \quad (3.168)$$

where $nr_0 < \pi$ to assure finite temperatures in the sphere and the relationship between T_s and the coolant temperature T_∞ is

$$T = T_s + \frac{k}{hr_0 a} [1 - (nr_0) \cot nr_0] \quad (3.169)$$

where, here too, $nr_0 < \pi$ to assure finite temperatures in the sphere.

3.5.5 Radiative–Convective Cooling of Solids with Uniform Energy Generation

The solutions obtained in Section 3.4.8 for a plane wall (the thermal symmetry case), a solid cylinder, and a solid sphere are now extended to accommodate surface cooling by simultaneous convection and radiation. The surface energy balance for each geometry gives

$$h(T_s - T_\infty) + \epsilon\sigma(T_s^4 - T_\infty^4) + k \left. \frac{dT}{dx} \right|_{x=L} = 0 \quad (\text{plane wall}) \quad (3.170)$$

$$h(T_s - T_\infty) + \epsilon\sigma(T_s^4 - T_\infty^4) + k \left. \frac{dT}{dr} \right|_{r=r_0} = 0 \quad (\text{solid cylinder and sphere}) \quad (3.171)$$

where ϵ is the surface emissivity, σ the Stefan–Boltzmann constant, and T_∞ represents the surrounding or ambient temperature for both convection and radiation. In eqs. (3.170) and (3.171), the last terms can be evaluated using eqs. (3.105), (3.115), and (3.123), respectively.

Because eqs. (3.170) and (3.171) require a numerical approach for their solutions, it is convenient to recast them in dimensionless form as

$$N_1(\theta_s - 1) + N_2(\theta_s^4 - 1) + \left. \frac{d\theta}{dX} \right|_{X=1} = 0 \quad (\text{plane wall}) \quad (3.173)$$

$$N_1(\theta_s - 1) + N_2(\theta_s^4 - 1) + \left. \frac{d\theta}{dR} \right|_{R=1} = 0 \quad (\text{cylinder and sphere}) \quad (3.173)$$

where $\theta = T_s/T_\infty$, $N_1 = hL/k$ for the plane wall, $N_1 = hr_0/k$ for the cylinder and sphere, $N_2 = \epsilon\sigma T_\infty^3 L/k$ for the plane wall, and $N_2 = \epsilon\sigma T_\infty^3 r_0/k$ for the cylinder and sphere, $X = x/L$, $R = r/r_0$, and $\theta = T/T_\infty$. The numerical values for θ_s are given in Table 3.10 for a range of values of N_1 and N_2 and $\dot{q}L^2/kT_\infty = 1$ for the plane wall and $\dot{q}r_0^2/kT_\infty = 1$ for the cylinder and sphere.

3.6 EXTENDED SURFACES

The term *extended surface* is used to describe a system in which the area of a surface is increased by the attachment of *fins*. A fin accommodates energy transfer by conduction within its boundaries, while its exposed surfaces transfer energy to the surroundings by convection or radiation or both. Fins are commonly used to augment heat transfer from electronic components, automobile radiators, engine and compressor cylinders, control devices, and a host of other applications. A comprehensive treatment of extended surface technology is provided by Kraus et al. (2001).

In this section we provide the performance characteristics (temperature distribution, rate of heat transfer, and fin efficiency) for convecting, radiating, and convecting–radiating fins. Configurations considered include longitudinal fins, radial fins, and spines. The section concludes with a discussion of optimum fin designs.

TABLE 3.10 Dimensionless Surface Temperature in Solids with Uniform Energy Generation and Radiative–Convective Surface Cooling

N_1	N_2	θ_s		
		Plane Wall	Solid Cylinder	Solid Sphere
0.25	0.25	1.4597	1.2838	1.2075
0.50	0.25	1.4270	1.2559	1.1840
0.75	0.25	1.3970	1.2320	1.1646
1.00	0.25	1.3698	1.2115	1.1484
0.25	0.50	1.2993	1.1759	1.1254
0.50	0.50	1.2838	1.1640	1.1159
0.75	0.50	1.2693	1.1534	1.1076
1.00	0.50	1.2559	1.1439	1.1004
0.25	0.75	1.2258	1.1288	1.0905
0.50	0.75	1.2164	1.1221	1.0853
0.75	0.75	1.2075	1.1159	1.0807
1.00	0.75	1.1991	1.1103	1.0764
0.25	1.00	1.1824	1.1020	1.0710
0.50	1.00	1.1759	1.0976	1.0677
0.75	1.00	1.1698	1.0935	1.0647
1.00	1.00	1.1640	1.0897	1.0619

3.6.1 Longitudinal Convecting Fins

The five common profiles of longitudinal fins shown in Fig. 3.19 are rectangular, trapezoidal, triangular, concave parabolic, and convex parabolic. The analytical expressions obtained are based on several assumptions.

1. The heat conduction in the fin is steady and one-dimensional.
2. The fin material is homogeneous and isotropic.
3. There is no energy generation in the fin.
4. The convective environment is characterized by a uniform and constant heat transfer coefficient and temperature.
5. The fin has a constant thermal conductivity.
6. The contact between the base of the fin and the primary surface is perfect.
7. The fin has a constant base temperature.

Rectangular Fin For the rectangular fin (Fig. 3.19a), the temperature distribution, rate of heat transfer, and fin efficiency are given for five cases of thermal boundary conditions.

1. *Constant base temperature and convecting tip:*

$$\frac{\theta}{\theta_b} = \frac{\cosh m(b-x) + H \sinh m(b-x)}{\cosh mb + H \sinh mb} \tag{3.174}$$

$$q_f = kmA\theta_b \frac{\sinh mb + H \cosh mb}{\cosh mb + H \sinh mb} \quad (3.175)$$

$$q_{id} = (hPb + h_t A)_{\theta_b} \quad (3.176)$$

$$\eta = \frac{q_f}{q_{id}} \quad (3.177)$$

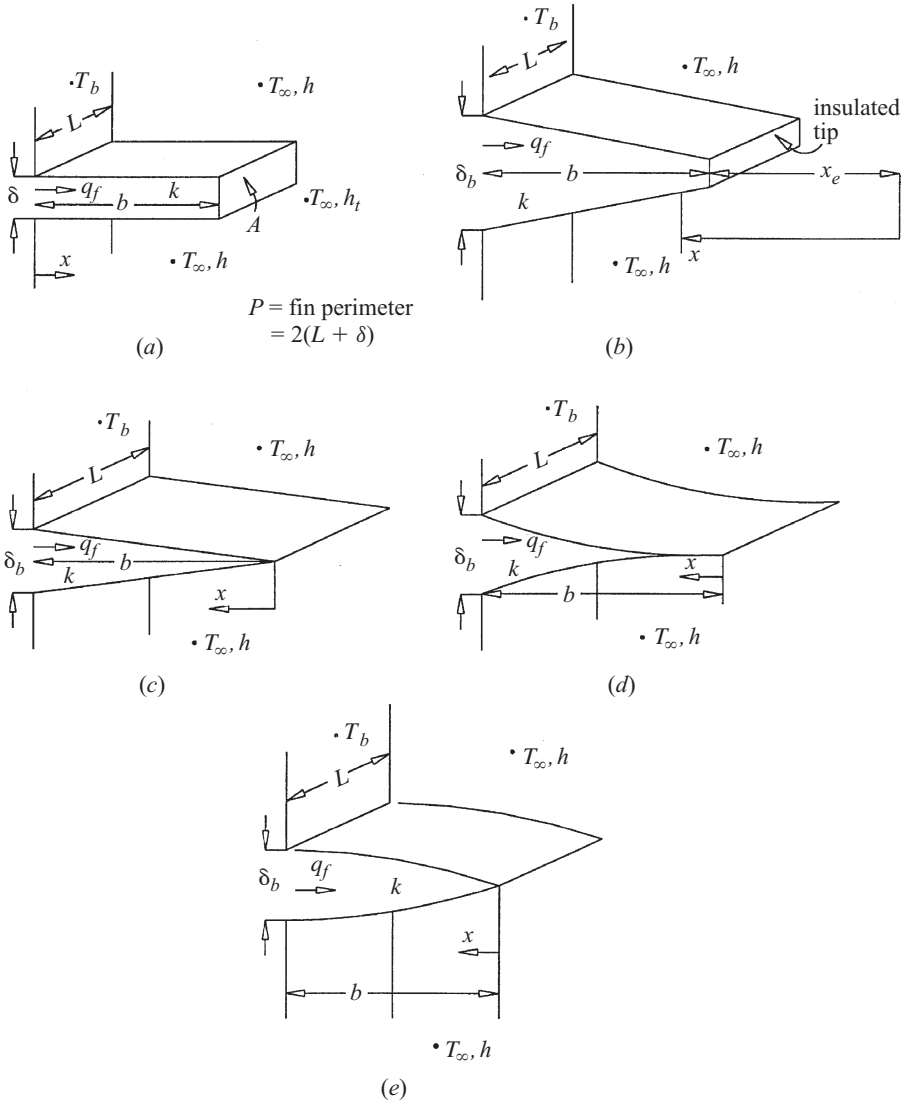


Figure 3.19 Longitudinal fins of (a) rectangular, (b) trapezoidal, (c) triangular, (d) concave parabolic, and (e) convex parabolic profiles.

where $\theta = T - T_\infty$, $\theta_b = T_b - T_\infty$, $m^2 = hP/kA = 2h/k\delta$, $H = h_t/km$, and T_b is the fin base temperature, T the fin temperature at location x , T_∞ the convective environmental temperature, b the fin height, A the fin cross-sectional area, P the fin perimeter, k the fin thermal conductivity, h the convective heat transfer coefficient for surfaces other than the fin tip, h_t the tip convective heat transfer coefficient, q_f the fin heat dissipation, and q_{id} the ideal fin heat dissipation.

2. *Constant base temperature and insulated tip ($H = 0$):*

$$\frac{\theta}{\theta_b} = \frac{\cosh m(b-x)}{\cosh mb} \quad (3.178)$$

$$q_f = kmA\theta_b \tanh mb \quad (3.179)$$

$$\eta = \frac{\tanh mb}{mb} \quad (3.180)$$

3. *Constant base and tip temperatures:*

$$\frac{\theta}{\theta_b} = \frac{(\theta_t/\theta_b) \sinh mx + \sinh m(b-x)}{\sinh mb} \quad (3.181)$$

$$q_f = kmA\theta_b \frac{\cosh mb - (\theta_t/\theta_b)}{\sinh mb} \quad (3.182)$$

with q_{id} and η given by eqs. (3.176) and (3.177), respectively, T_t taken as the prescribed tip temperature, and $\theta_t = T_t - T_\infty$.

4. *Convective heating at the base and insulated tip:*

$$\frac{\theta}{\theta_f} = \frac{\text{Bi} \cosh(mb-x)}{\text{Bi} \cosh mb + mb \sinh mb} \quad (3.183)$$

$$q_f = kmA\theta_f \frac{\text{Bi} \sinh mb}{\text{Bi} \cosh mb + mb \sinh mb} \quad (3.184)$$

where $\text{Bi} = h_f b/k$, $\theta_f = T_f - T_\infty$, and h_f and T_f characterize the convection process at the fin base. Equations (3.176) and (3.177) can be used to find q_{id} and η , but θ_b must be found first from eq. (3.183).

5. *Infinitely high fin with constant base temperature:*

$$\frac{\theta}{\theta_b} = e^{-mx} \quad (3.185)$$

$$q_f = kmA\theta_b \quad (3.186)$$

Because the fin is infinitely high, q_{id} and η cannot be calculated. Instead, one may calculate the *fin effectiveness* ϵ as the ratio of q_f to the rate of heat transfer from the *base surface* without the fin, $hA\theta_b$. Thus

$$\epsilon = \frac{q_f}{hA\theta_b} = \left(\frac{kP}{hA} \right)^{1/2} \quad (3.187)$$

Several important conclusions can be drawn from eq. (3.187). First, the fin effectiveness is enhanced by choosing a material with high thermal conductivity. Copper has a high value ($k = 401 \text{ W/m} \cdot \text{K}$ at 300K), but it is heavy and expensive. Aluminum alloys have lower k ($k = 168$ to $237 \text{ W/m} \cdot \text{K}$ at 300 K) but are lighter, offer lower cost, and in most instances are preferable to copper. Second, the fins are more effective when the convecting fluid is a gas (low h) rather than a liquid (higher h). Moreover, there is a greater incentive to use the fin under natural convection (lower h) than under forced convection (higher h). Third, the greater the perimeter/area (P/A) ratio, the higher the effectiveness. This, in turn, suggests the use of thin, closely spaced fins. However, the gap between adjacent fins must be sufficient to prevent interference of the boundary layers on adjacent surfaces.

Trapezoidal Fin For a constant base temperature and insulated tip, the temperature distribution, rate of heat transfer, ideal rate of heat transfer, and fin efficiency for a trapezoidal fin (Fig. 3.19b) are

$$\frac{\theta}{\theta_b} = \frac{I_0(2m\sqrt{bx})K_1(2m\sqrt{bx_e}) + K_0(2m\sqrt{bx})I_1(2m\sqrt{bx_e})}{I_0(2mb)K_1(2m\sqrt{bx_e}) + K_0(2mb)I_1(2m\sqrt{bx_e})} \quad (3.188)$$

$$q_f = km\delta_b L\theta_b \frac{I_1(2mb)K_1(2m\sqrt{bx_e}) - K_1(2mb)I_1(2m\sqrt{bx_e})}{I_0(2mb)K_1(2m\sqrt{bx_e}) + K_0(2mb)I_1(2m\sqrt{bx_e})} \quad (3.189)$$

$$q_{id} = 2Lbh\theta_b \quad (3.190)$$

and eq. (3.177) gives the fin efficiency. In eqs. (3.188) and (3.189), $m = \sqrt{2h/k\delta_b}$ and x_e is the distance to the fin tip. The modified Bessel functions appearing here and in subsequent sections are discussed in Section 3.3.5.

Triangular Fin The rectangular fin (Fig. 3.19c) is a special case of the trapezoidal fin with $x_e = 0$ and

$$\frac{\theta}{\theta_b} = \frac{I_0(2m\sqrt{bx})}{I_0(2mb)} \quad (3.191)$$

$$q_f = km\delta_b L\theta_b \frac{I_1(2mb)}{I_0(2mb)} \quad (3.192)$$

$$\eta = \frac{I_1(2mb)}{mbI_0(2mb)} \quad (3.193)$$

Concave Parabolic Fin For the concave parabolic fin shown in Fig. 2.19d, the temperature distribution, rate of heat transfer, and fin efficiency are

$$\frac{\theta}{\theta_b} = \left(\frac{x}{b}\right)^{-1/2+1/2(1+4m^2b^2)^{1/2}} \quad (3.194)$$

$$q_f = \frac{k\delta_b L\theta_b}{2b} \left[-1 + (1 + 4m^2b^2)^{1/2} \right] \quad (3.195)$$

$$\eta = \frac{2}{1 + (1 + 4m^2b^2)^{1/2}} \quad (3.196)$$

Convex Parabolic Fin For the convex parabolic fin shown in Fig. 3.19e, the temperature distribution, rate of heat transfer, and fin efficiency are

$$\frac{\theta}{\theta_b} = \left(\frac{x}{b}\right)^{1/4} \left[\frac{I_{-1/3} \left(\frac{4}{3}mb^{1/4}x^{3/4} \right)}{I_{-1/3} \left(\frac{4}{3}mb \right)} \right] \quad (3.197)$$

$$q_f = km\delta_b L\theta_b \frac{I_{2/3} \left(\frac{4}{3}mb \right)}{I_{-1/3} \left(\frac{4}{3}mb \right)} \quad (3.198)$$

$$\eta = \frac{1}{mb} \frac{I_{2/3} \left(\frac{4}{3}mb \right)}{I_{-1/3} \left(\frac{4}{3}mb \right)} \quad (3.199)$$

The efficiency of longitudinal fins of rectangular, triangular, concave parabolic, and convex parabolic fins are plotted as a function of mb in Fig. 3.20.

3.6.2 Radial Convecting Fins

The radial fin is also referred to as an *annular fin* or *circumferential fin*, and the performance of three radial fin profiles is considered. These are the rectangular, triangular, and hyperbolic profiles. Analytical results are presented for the rectangular profile, and graphical results are provided for all three profiles.

Rectangular Fin For the radial fin of rectangular profile shown in the inset of Fig. 3.21, the expressions for the temperature distribution, rate of heat transfer, and fin efficiency are

$$\frac{\theta}{\theta_b} = \frac{K_1(mr_a)I_0(mr) + I_1(mr_a)K_0(mr)}{I_0(mr_b)K_1(mr_a) + I_1(mr_a)K_0(mr_b)} \quad (3.200)$$

$$q_f = 2\pi r_b km\delta_b \frac{I_1(mr_a)K_1(mr_b) - K_1(mr_a)I_1(mr_b)}{I_0(mr_b)K_1(mr_a) + I_1(mr_a)K_0(mr_b)} \quad (3.201)$$

$$\eta = \frac{2r_b}{m(r_a^2 - r_b^2)} \frac{I_1(mr_a)K_1(mr_b) - K_1(mr_a)I_1(mr_b)}{I_0(mr_b)K_1(mr_a) + I_1(mr_a)K_0(mr_b)} \quad (3.202)$$

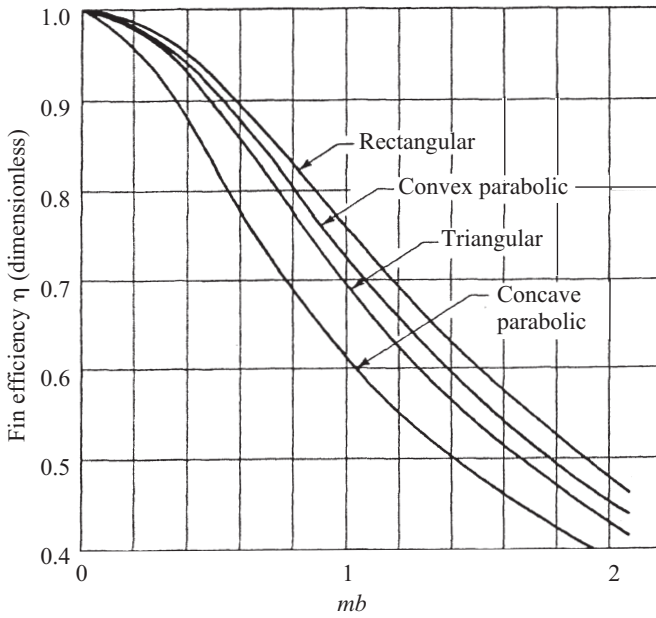


Figure 3.20 Efficiencies of longitudinal convecting fins.

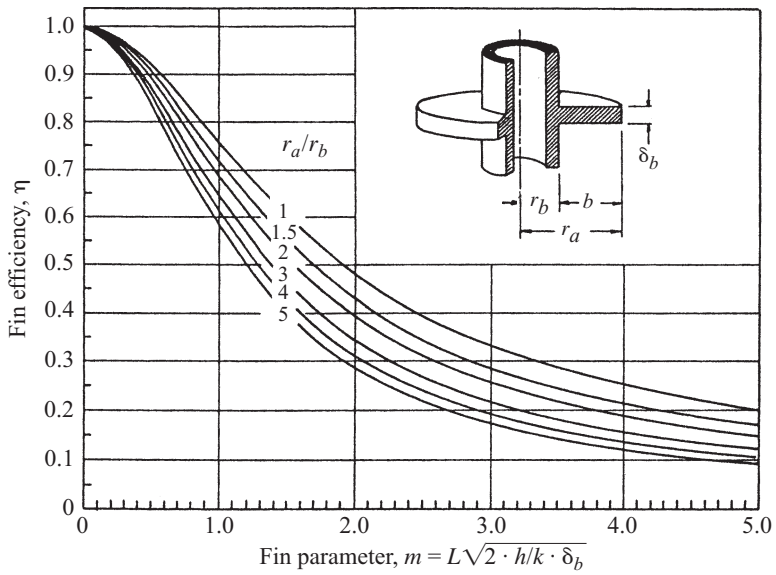


Figure 3.21 Efficiency of radial (annular) fins of rectangular profile. (Adapted from Ullman and Kalman, 1989.)

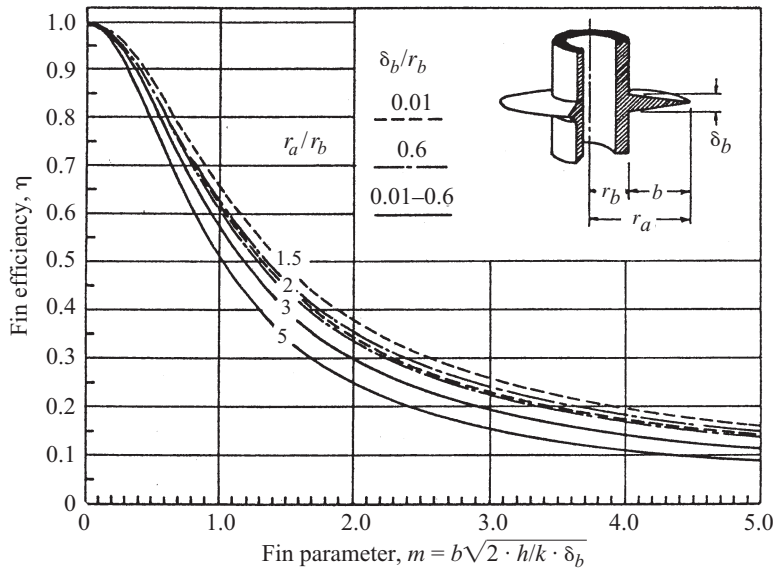


Figure 3.22 Efficiency of radial (annular) fins of triangular profile. (Adapted from Ullman and Kalman, 1989.)

The efficiency of a radial fin of rectangular profile given by eq. (3.202) is plotted as a function of mb in the main body of Fig. 3.21 for $r_a/r_b = 1$ (longitudinal fin), 1.5, 2.0, 3.0, 4.0, and 5.0.

Triangular Fin The inset in Fig. 3.22 shows a radial fin of triangular profile. The analysis for this profile is given in Kraus et al. (2001) and involves an infinite series that is omitted in favor of numerical results for the fin efficiency, which are graphed in Fig. 3.22. Note that η is a function of m , r_a/r_b , and δ_b/r_b . Once η is known, $q_f = 2\pi(r_a^2 - r_b^2)h\theta_b\eta$.

Hyperbolic Fin A radial fin of hyperbolic profile appears as an inset in Fig. 3.23. The lengthy analytical results are presented in Kraus et al. (2001) and a graph of the fin efficiency is presented in Fig. 3.23. Note that η is a function of m , r_a/r_b , and δ_b/r_b , and once η is known, $q_f = 2\pi(r_a^2 - r_b^2)h\theta_b\eta$.

3.6.3 Convecting Spines

Four commonly used shapes of spines, shown in Fig. 3.24, are the cylindrical, conical, concave parabolic, and convex parabolic. Analytical results for the temperature distribution, rate of heat transfer, and fin efficiency are furnished.

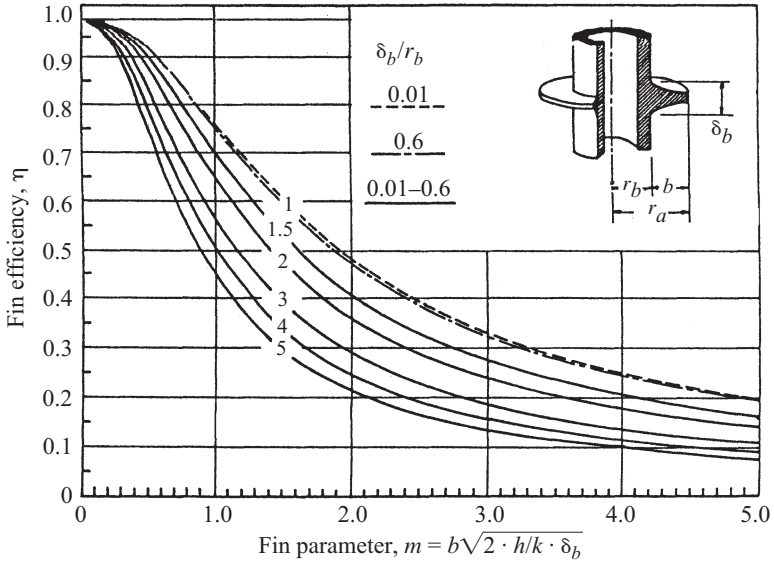


Figure 3.23 Efficiency of radial (annular) fins of hyperbolic profile. (Adapted from Ullman and Kalman, 1989.)

Cylindrical Spine For the cylindrical spine, the results for the rectangular fins are applicable if $m = (4h/kd)^{1/2}$ is used instead of $m = (2h/k\delta)^{1/2}$. If the spine tip is insulated, eqs. (3.178)–(3.180) can be used.

Conical Spine

$$\frac{\theta}{\theta_b} = \left(\frac{b}{x}\right)^{1/2} \frac{I_1(2M\sqrt{x})}{I_1(2M\sqrt{b})} \quad (3.203)$$

$$q_f = \frac{\pi k d_b^2 M \theta_b}{4\sqrt{b}} \frac{I_2(2M\sqrt{b})}{I_1(2M\sqrt{b})} \quad (3.204)$$

$$\eta = \frac{2}{M\sqrt{b}} \frac{I_2(2M\sqrt{b})}{I_1(2M\sqrt{b})} \quad (3.205)$$

where $M = (4hb/kd_b)^{1/2}$.

Concave Parabolic Spine

$$\frac{\theta}{\theta_b} = \left(\frac{x}{b}\right)^{-3/2+1/2(9+4M^2)^{1/2}} \quad (3.206)$$

$$q_f = \frac{\pi k d_b^2 \theta_b [-3 + (9 + 4M^2)^{1/2}]}{8b} \quad (3.207)$$

$$\eta = \frac{2}{1 + (1 + \frac{8}{9}m^2b^2)^{1/2}} \quad (3.208)$$

where $M = (4hb/kd_b)^{1/2}$ and $m = (2h/kd_b)^{1/2}$.

Convex Parabolic Spine

$$\frac{\theta}{\theta_b} = \frac{I_0(\frac{4}{3}Mx^{3/4})}{I_0(\frac{4}{3}Mb^{3/4})} \quad (3.209)$$

$$q_f = \frac{\pi k d_b^2 M \theta_b}{2b^{1/4}} \frac{I_1(\frac{4}{3}Mb^{3/4})}{I_0(\frac{4}{3}Mb^{3/4})} \quad (3.210)$$

$$\eta = \frac{3}{2\sqrt{2}} \frac{I_1(\frac{4}{3}\sqrt{2}mb)}{mb I_0(\frac{4}{3}\sqrt{2}mb)} \quad (3.211)$$

where $M = (4hb^{1/2}/kd_b)^{1/2}$ and $m = (2h/kd_b)^{1/2}$.

Figure 3.25 is a plot of η as a function of mb for the four spines discussed.

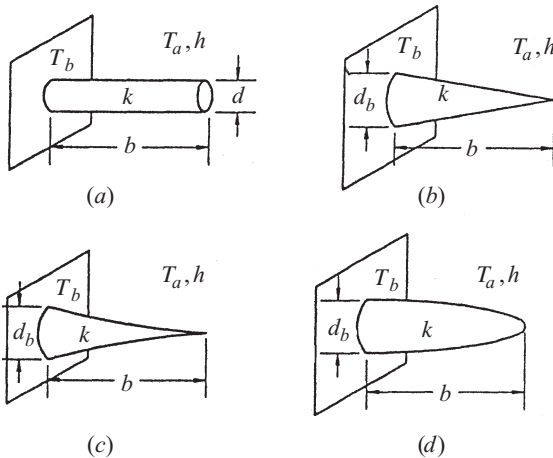


Figure 3.24 Spines: (a) cylindrical; (b) conical; (c) concave parabolic; (d) convex parabolic.

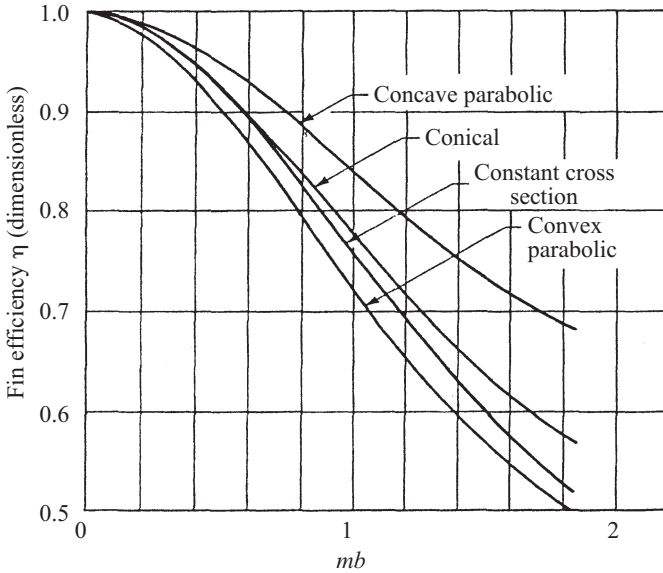


Figure 3.25 Efficiencies of convecting spines.

3.6.4 Longitudinal Radiating Fins

Unlike convecting fins, for which exact analytical solutions abound, few such solutions are available for radiating fins. Consider the longitudinal fin of rectangular profile shown in Fig. 3.19a and let the fin radiate to free space at 0 K. The differential equation governing the temperature in the fin is

$$\frac{d^2 T}{dx^2} = \frac{2\sigma\epsilon}{k\delta} T^4 \quad (3.212)$$

with the boundary conditions

$$T(x=0) = T_b \quad \text{and} \quad \left. \frac{dT}{dx} \right|_{x=b} = 0 \quad (3.213)$$

where ϵ is the emissivity of the fin surface and σ is the Stefan–Boltzmann constant ($\sigma = 5.667 \times 10^{-8} \text{ W/m}^2 \cdot \text{K}^4$).

The solution for the temperature distribution, rate of heat transfer, and fin efficiency are

$$B(0.3, 0.5) - B_u(0.3, 0.5) = b \left(\frac{20\sigma\epsilon T_b^3}{k\delta} \right)^{1/2} \quad (3.214)$$

$$q_f = 2k\delta L \left(\frac{\sigma\epsilon}{5k\delta} \right)^{1/2} (T_b^5 - T_i^5)^{1/2} \quad (3.215)$$

$$\eta = \frac{2k\delta L(\sigma\epsilon/5k\delta)^{1/2} \left(T_b^5 - T_i^5\right)^{1/2}}{2\sigma\epsilon bLT_b^4} \tag{3.216}$$

where B and B_u are complete and incomplete beta functions discussed in Section 3.3.3, $u = (T_i/T)^5$ and T_i is the unknown tip temperature. Because T_i is not known, the solution involves a trial-and-error procedure.

Sen and Trinh (1986) reported the solution of eqs. (3.212) and (3.213) when the surface heat dissipation is proportional to T^m rather than T^4 . Their solution appears in terms of hypergeometric functions which bear a relationship to the incomplete beta function. Kraus et al. (2001) provide an extensive collection of graphs to evaluate the performance of radiating fins of different profiles.

3.6.5 Longitudinal Convecting–Radiating Fins

A finite-difference approach was taken by Nguyen and Aziz (1992) to evaluate the performance of longitudinal fins (Fig. 3.19) of rectangular, trapezoidal, triangular, and concave parabolic profiles when the fin surface loses heat by simultaneous convection and radiation. For each profile, the performance depends on five parameters, $2b/\delta_b$, $h\delta_b/2k$, T_∞/T_b , T_s/T_b , and $2b^2\sigma\epsilon T_b^3/k\delta_b$, where T_s is the effective sink temperature for radiation. A sample result for the fin efficiency is provided in Table 3.11. These results reveal a more general trend—that a convecting–radiating fin has a lower efficiency than that of a purely convecting fin ($2b^2\sigma\epsilon T_b^3/k\delta_b = 0$).

3.6.6 Optimum Dimensions of Convecting Fins and Spines

The classical fin or spine optimization involves finding the profile so that for a prescribed volume, the fin or spine rate of heat transfer is maximized. Such optimizations result in profiles with curved boundaries that are difficult and expensive to fabricate. From a practical point of view, a better approach is to select the profile first and then find the optimum dimensions so that for a given profile area or volume, the fin or spine rate of heat transfer is maximized. The results of the latter approach are provided here. For each shape, two sets of expressions for optimum dimensions are given, one set for

TABLE 3.11 Efficiency of Longitudinal Convecting–Radiating Fins, $T_\infty/T_b = T_s/T_b = 0.8$, $2hb^2/k\delta_b = 1$

$2b^2\sigma\epsilon T_b^3/k\delta$	Rectangular	Trapezoidal $\delta t/\delta_b = 0.25$	Triangular	Concave Parabolic
0.00	0.6968	0.6931	0.6845	0.6240
0.20	0.4679	0.4677	0.4631	0.4244
0.40	0.3631	0.3644	0.3616	0.3324
0.60	0.3030	0.3051	0.3033	0.2811
0.80	0.2638	0.2666	0.2655	0.2471
1.00	0.2365	0.2396	0.2390	0.2233

when the profile area or volume is specified and another set for when the fin or spine rate of heat transfer is specified. Note that q_f for fins in the expressions to follow is the fin rate of heat transfer per unit length L of fin.

Rectangular Fin When the weight or profile area A_p is specified,

$$\delta_{\text{opt}} = 0.9977 \left(\frac{A_p^2 h}{k} \right)^{1/3} \quad (3.217)$$

$$b_{\text{opt}} = 1.0023 \left(\frac{A_p k}{h} \right)^{1/3} \quad (3.218)$$

and when the fin rate of heat transfer (per unit length) q_f is specified,

$$\delta_{\text{opt}} = \frac{0.6321 [q_f / (T_b - T_\infty)]^2}{hk} \quad (3.219)$$

$$b_{\text{opt}} = \frac{0.7978 q_f}{h(T_b - T_\infty)} \quad (3.220)$$

Triangular Fin When the weight or profile area A_p is specified,

$$\delta_{b,\text{opt}} = 1.6710 \left(\frac{A_p^2 h}{k} \right)^{1/3} \quad (3.221)$$

$$b_{\text{opt}} = 1.1969 \left(\frac{A_p k}{h} \right)^{1/3} \quad (3.222)$$

and when the fin rate of heat transfer (per unit length) q_f is specified,

$$\delta_{b,\text{opt}} = \frac{0.8273 [q_f / (T_b - T_\infty)]^2}{hk} \quad (3.223)$$

$$b_{\text{opt}} = \frac{0.8422 q_f}{h(T_b - T_\infty)} \quad (3.224)$$

Concave Parabolic Fin When the weight or profile area A_p is specified,

$$\delta_{\text{opt}} = 2.0801 \left(\frac{A_p^2 h}{k} \right)^{1/3} \quad (3.225)$$

$$b_{\text{opt}} = 1.4422 \left(\frac{A_p k}{h} \right)^{1/3} \quad (3.226)$$

and when the fin rate of heat transfer (per unit length) q_f is specified,

$$\delta_{b,\text{opt}} = \left(\frac{1}{hk} \right) \left[\frac{q_f}{(T_b - T_\infty)} \right]^2 \quad (3.227)$$

$$b_{\text{opt}} = \frac{q_f}{h(T_b - T_\infty)} \quad (3.228)$$

Cylindrical Spine When the weight or volume V is specified,

$$d_{\text{opt}} = 1.5031 \left(\frac{hV^2}{k} \right)^{1/5} \quad (3.229)$$

$$b_{\text{opt}} = 0.5636 \left(\frac{Vk^2}{h^2} \right)^{1/5} \quad (3.230)$$

and when the spine rate of heat transfer q_f is specified,

$$d_{\text{opt}} = 0.9165 \left[\frac{q_f^2}{hk(T_b - T_\infty)^2} \right]^{1/3} \quad (3.231)$$

$$b_{\text{opt}} = 0.4400 \left[\frac{q_f k}{h^2(T_b - T_\infty)} \right]^{1/3} \quad (3.232)$$

Conical Spine When the weight or volume V is specified,

$$d_{b,\text{opt}} = 1.9536 \left(\frac{hV^2}{k} \right)^{1/5} \quad (3.233)$$

$$b_{\text{opt}} = 1.0008 \left(\frac{Vk^2}{h^2} \right)^{1/5} \quad (3.234)$$

and when the spine rate of heat transfer q_f is specified,

$$d_{b,\text{opt}} = 1.0988 \left[\frac{q_f^2}{hk(T_b - T_\infty)^2} \right]^{1/3} \quad (3.235)$$

$$b_{\text{opt}} = 0.7505 \left[\frac{q_f k}{h^2(T_b - T_\infty)^2} \right]^{1/3} \quad (3.236)$$

Concave Parabolic Spine When the weight or volume V is specified,

$$d_{b,\text{opt}} = 2.0968 \left(\frac{hV^2}{k} \right)^{1/5} \quad (3.237)$$

$$b_{\text{opt}} = 1.4481 \left(\frac{Vk^2}{h^2} \right)^{1/5} \quad (3.238)$$

and when the spine rate of heat transfer q_f is specified,

$$d_{b,\text{opt}} = 1.1746 \left[\frac{q_f^2}{hk(T_b - T_\infty)^2} \right]^{1/3} \quad (3.239)$$

$$b_{\text{opt}} = 1.0838 \left[\frac{q_f k}{h^2(T_b - T_\infty)^2} \right]^{1/3} \quad (3.240)$$

Convex Parabolic Spine When the weight or volume V is specified,

$$d_{b,\text{opt}} = 1.7980 \left(\frac{hV^2}{k} \right)^{1/5} \quad (3.241)$$

$$b_{\text{opt}} = 0.7877 \left(\frac{Vk^2}{h^2} \right)^{1/5} \quad (3.242)$$

and when the spine rate of heat transfer q_f is specified,

$$d_{b,\text{opt}} = 1.0262 \left[\frac{q_f^2}{hk(T_b - T_\infty)^2} \right]^{1/3} \quad (3.243)$$

$$b_{\text{opt}} = 0.5951 \left[\frac{q_f k}{h^2(T_b - T_\infty)^2} \right]^{1/3} \quad (3.244)$$

The material presented here is but a small fraction of the large body of literature on the subject of optimum shapes of extended surfaces. The reader should consult Aziz (1992) for a comprehensive compilation of results for the optimum dimensions of convecting extended surfaces. Another article by Aziz and Kraus (1996) provides similar coverage for radiating and convecting–radiating extended surfaces. Both articles contain a number of examples illustrating the design calculations, and both are summarized in Kraus et al. (2001).

3.7 TWO-DIMENSIONAL STEADY CONDUCTION

The temperature field in a two-dimensional steady-state configuration is controlled by a second-order partial differential equation whose solution must satisfy four boundary conditions. The analysis is quite complex, and consequently, exact analytical solutions are limited to simple geometries such as a rectangular plate, a cylinder, and a sphere under highly restrictive boundary conditions. Problems that involve complex geometries and more realistic boundary conditions can only be solved by using an

approximate technique or a numerical method. Approximate techniques that are employed include the integral method, the method of scale analysis, and the method of conduction shape factors. The two most popular numerical techniques are the finite-difference and finite-element methods. There are numerous sources for information on approximate and numerical techniques, some of which are Bejan (1993), Ozisik (1993, 1994), Comini et al. (1994), and Jaluria and Torrance (1986). In the following section we provide an example of an exact solution, a table of conduction shape factors, and a brief discussion of the finite-difference method and its application to two-dimensional conduction in a square plate and a solid cylinder.

3.7.1 Rectangular Plate with Specified Boundary Temperatures

Figure 3.26 shows a rectangular plate with three sides maintained at a constant temperature T_1 , while the fourth side is maintained at another constant temperature, T_2 ($T_2 \neq T_1$). Defining

$$\theta = \frac{T - T_1}{T_2 - T_1} \quad (3.245)$$

the governing two-dimensional temperature distribution becomes

$$\frac{\partial^2 \theta}{\partial x^2} + \frac{\partial^2 \theta}{\partial y^2} = 0 \quad (3.246)$$

with the boundary conditions

$$\theta(0, y) = 1 \quad (3.247a)$$

$$\theta(x, 0) = 0 \quad (3.247b)$$

$$\theta(L, y) = 0 \quad (3.247c)$$

$$\theta(x, H) = 0 \quad (3.247d)$$

Use of the separation of variables method gives the solution for θ as

$$\theta = \frac{4}{\pi} \sum_{n=0}^{\infty} \frac{\sinh [(2n+1)\pi(L-x)/H]}{\sinh [(2n+1)\pi L/H]} \frac{\sin [(2n+1)\pi y/H]}{2n+1} \quad (3.248)$$

Using eq. (3.248), Bejan (1993) developed a network of isotherms and heat flux lines, which is shown in Fig. 3.27 for $H/L = 2$ (a rectangular plate) and for $H/L = 1$ (a square plate).

The heat flow into the plate from a hot left face is given by

$$\frac{q}{W} = \frac{8}{\pi} k(T_2 - T_1) \sum_{n=0}^{\infty} \frac{1}{(2n+1) \tanh [(2n+1)\pi L/H]} \quad (3.249)$$

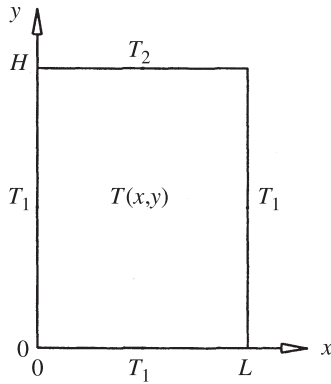


Figure 3.26 Two-dimensional steady conduction in a rectangular plate.

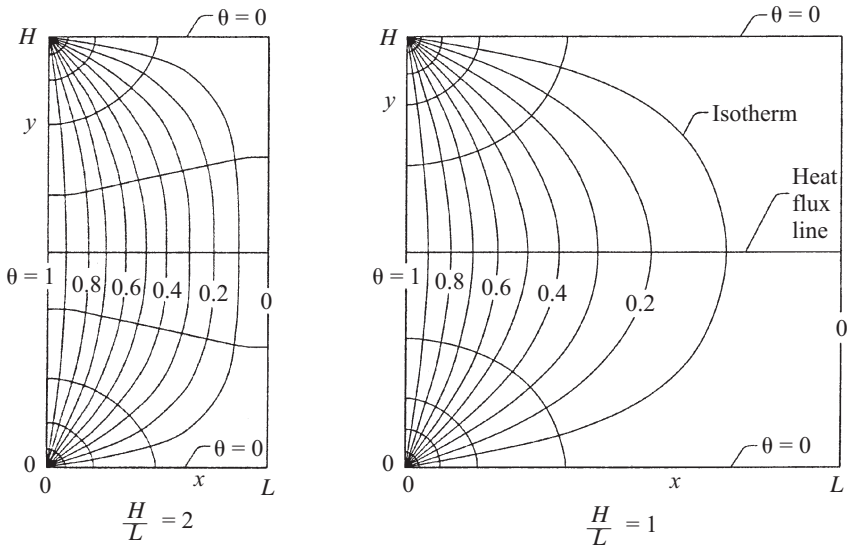


Figure 3.27 Isotherms and heat flux lines in a rectangular plate and a square plate. (From Bejan, 1993.)

where W is the plate dimension in the z direction. Solutions for the heat flux and convective boundary conditions are given in Ozisik (1993) and Poulidakos (1994).

3.7.2 Solid Cylinder with Surface Convection

Figure 3.28 illustrates a solid cylinder of radius r_0 and length L in which conduction occurs in both radial and axial directions. The face at $z = 0$ is maintained at a constant

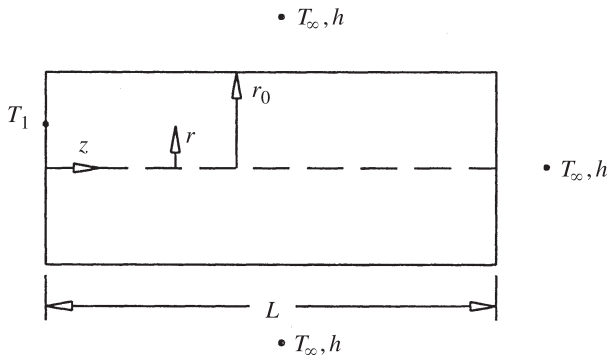


Figure 3.28 Radial and axial conduction in a hollow cylinder.

temperature T_1 , while both the lateral surface and the face at $z = L$ lose heat by convection to the environment at T_∞ via the heat transfer coefficient h . The system described represents a two-dimensional (r, z) convecting spine discussed by Aziz and Lunardini (1995). The equation governing the two-dimensional heat conduction in the cylinder is

$$\frac{\partial^2 \theta}{\partial R^2} + \frac{1}{R} \frac{\partial \theta}{\partial R} + \frac{\partial^2 \theta}{\partial Z^2} = 0 \quad (3.250)$$

where

$$\theta = \frac{T - T_\infty}{T_1 - T_\infty} \quad R = \frac{r}{r_0} \quad Z = \frac{z}{L} \quad \gamma = \frac{L}{r_0}$$

and Bi is the *Biot number*, $\text{Bi} = hr_0/k$. The boundary conditions are

$$\theta(R, 0) = 1 \quad (3.251a)$$

$$\frac{\partial \theta}{\partial R}(0, Z) = 0 \quad (3.251b)$$

$$\frac{\partial \theta}{\partial R}(1, Z) = -\text{Bi} \cdot \theta(1, Z) \quad (3.251c)$$

$$\frac{\partial \theta}{\partial R}(R, 1) = -\text{Bi} \cdot \gamma \theta(R, 1) \quad (3.251d)$$

The solution obtained via the separation of the variables is

$$\theta = \sum_{n=1}^{\infty} \frac{2\lambda_n J_1(\lambda_n) J_0(\lambda_n R)}{(\lambda_n^2 + \text{Bi}^2) [J_0(\lambda_n)]^2} (\cosh \lambda_n \gamma Z - \gamma \sinh \lambda_n \gamma Z) \quad (3.252)$$

where

$$\Upsilon = \frac{\lambda_n \sinh \lambda_n \gamma + \text{Bi} \cosh \lambda_n \gamma}{\lambda_n \cosh \lambda_n \gamma + \text{Bi} \sinh \lambda_n \gamma}$$

and where J_0 and J_1 are the Bessel functions of the first kind (Section 3.3.5) and the eigenvalues λ_n are given by

$$\lambda_n J_1(\lambda_n) = \text{Bi} \cdot J_0(\lambda_n) \quad (3.253)$$

The heat flow into the cylinder from the hot left face is

$$q = 4\pi k r_0 (T_1 - T_\infty) \sum_{n=1}^{\infty} \frac{\lambda_n [J_1(\lambda_n)]^2}{(\lambda_n^2 + \text{Bi}^2) [J_0(\lambda_n)]^2} \Upsilon \quad (3.254)$$

A three-dimensional plot of θ as a function of r and z is shown in Fig. 3.29 for $r_0 = 1$, $L = 1$, and $h/k = 1$. This plot was generated using Maple V, Release 5.0. As expected, the temperature decreases along both the radial and axial directions. Ozisik (1993) has devoted a complete chapter to the method of separation of variables in cylindrical coordinates and provides solutions for several other configurations.

3.7.3 Solid Hemisphere with Specified Base and Surface Temperatures

Poulikakos (1994) considers a hemispherical droplet condensing on a cold horizontal surface as shown in Fig. 3.30. The heat conduction equation for the two-dimensional (r, θ) steady-state temperature distribution in the droplet is given by

$$\frac{\partial}{\partial r} \left(r^2 \frac{\partial \phi}{\partial r} \right) + \frac{1}{\sin \theta} \frac{\partial}{\partial \theta} \left(\sin \theta \frac{\partial \phi}{\partial \theta} \right) = 0 \quad (3.255)$$

where $\phi = T - T_c$. Two of the boundary conditions are

$$\theta(r_0, \theta) = T_s - T_c = \phi_s \quad (3.256a)$$

$$\phi \left(r, \frac{\pi}{2} \right) = 0 \quad (3.256b)$$

Because the boundary condition at $r = 0$ falls on the $\theta = \pi/2$ plane, which is the base of the hemispherical droplet, it must meet the boundary condition of eq. (3.256b), that is,

$$\phi \left(r, \frac{\pi}{2} \right) = 0 \quad (3.256c)$$

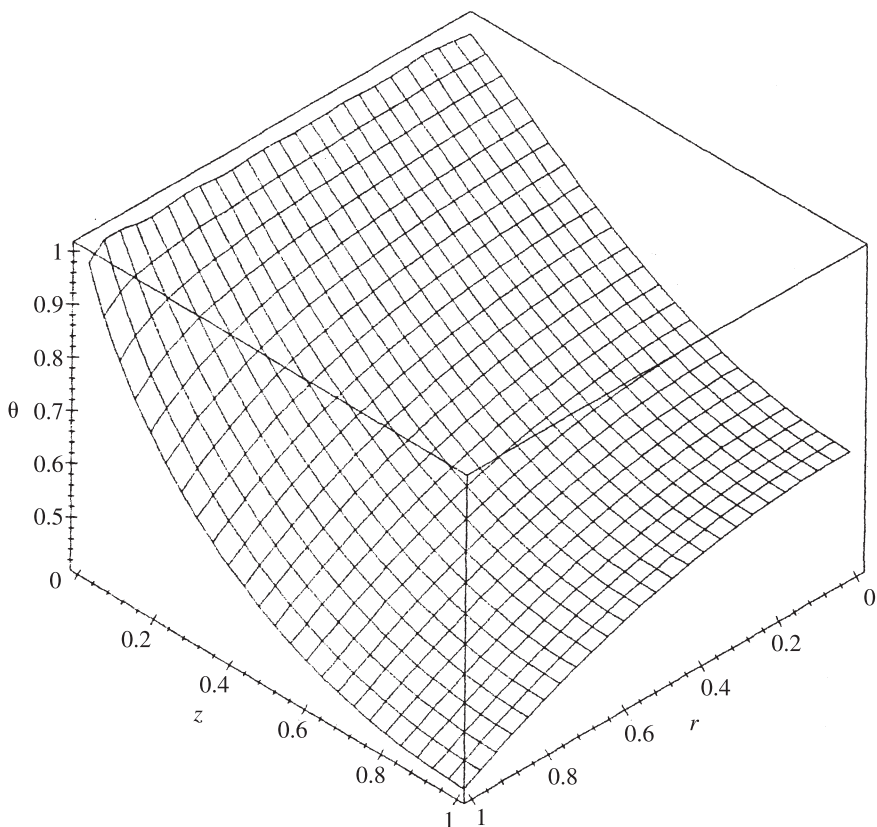


Figure 3.29 Three-dimensional plot of the temperature distribution in a solid cylinder. (From Aziz, 2001.)

The fourth boundary condition at $\theta = 0$ is obtained by invoking the condition of thermal symmetry about $\theta = 0$, giving

$$\frac{\partial \phi}{\partial \theta}(r, 0) = 0 \quad (3.256d)$$

Use of the method of separation of the variables provides the solution for ϕ as

$$\phi = \phi_s \sum_{n=1}^{\infty} \left[P_{n+1}(1) - P_{n-1}(1) - P_{n+1}(0) + P_{n-1}(0) \right] \left(\frac{r}{r_0} \right)^n P_n(\cos \theta) \quad (3.257)$$

where the P 's are the Legendre functions of the first kind, discussed in Section 3.3.6.

Ozisik (1993) may be consulted for a comprehensive discussion of the method of separation of the variables in spherical coordinates.

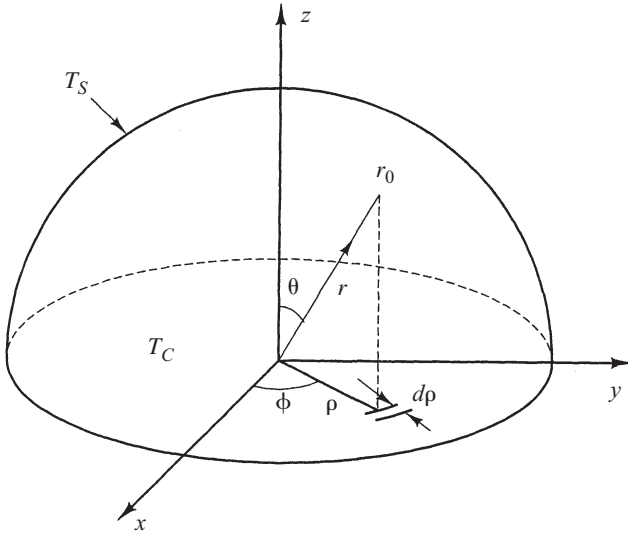


Figure 3.30 Hemispherical droplet condensing on an isothermal surface. (Adapted from Poulikakos, 1994.)

3.7.4 Method of Superposition

The configuration considered in the preceding section involved one nonhomogeneous boundary condition [either eq. (3.247a), (3.251a), or (3.256a)]. When two or more nonhomogeneous boundary conditions occur, the analysis can be split into two subanalyses each containing one nonhomogeneous boundary condition. Each subanalysis can then be solved using the method of separation of the variables, and the sum of the solutions to the two subanalyses will provide the solution to the overall problem. This approach is illustrated in Fig. 3.31 for a rectangular plate with two homogeneous boundary conditions.

The mathematical description of the problem is

$$\frac{\partial^2 \theta}{\partial x^2} + \frac{\partial^2 \theta}{\partial y^2} = 0 \quad (3.258)$$

where $\theta = T - T_3$. The boundary conditions are

$$\theta(0, y) = \theta_1 = T_1 - T_3 \quad (3.259a)$$

$$\theta(x, 0) = \theta_2 = T_2 - T_3 \quad (3.259b)$$

$$\theta(L, y) = 0 \quad (3.259c)$$

$$\theta(x, H) = 0 \quad (3.259d)$$

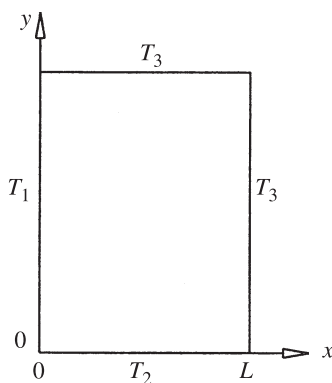


Figure 3.31 Rectangular plate with two nonhomogeneous boundary conditions.

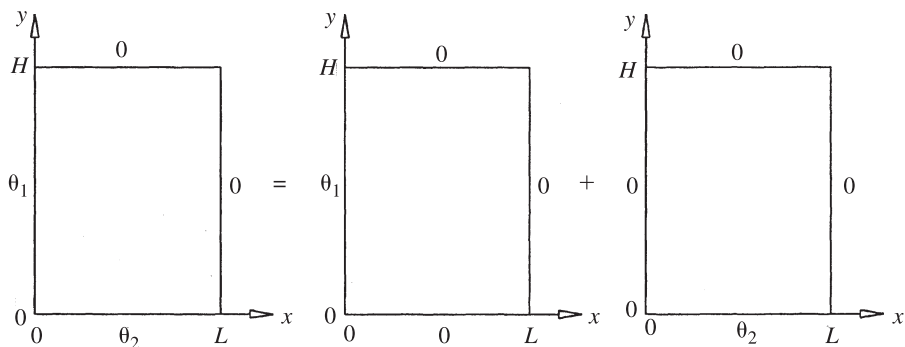


Figure 3.32 Splitting the problem of Fig. 3.31 into two subproblems with known solutions.

The problem is split into two subproblems, as indicated in Fig. 3.32, and the two solutions can be obtained from eq. (3.248) with appropriate adjustment to account for the definition of θ and the coordinates, x and y . The sum of the two solutions is

$$\begin{aligned} \theta = & \frac{4\theta_1}{\pi} \sum_{n=0}^{\infty} \frac{\sinh [(2n+1)\pi(L-x)/H]}{\sinh [(2n+1)\pi L/H]} \frac{\sin [(2n+1)(\pi y/H)]}{2n+1} \\ & + \frac{4\theta_2}{\pi} \sum_{n=0}^{\infty} \frac{\sinh [(2n+1)\pi(H-y)/L]}{\sinh [(2n+1)(\pi H/L)]} \frac{\sin [(2n+1)(\pi x/L)]}{2n+1} \end{aligned} \quad (3.260)$$

3.7.5 Conduction Shape Factor Method

Although the conduction shape factor method does not give the temperature distribution, it provides a simple equation for the rate of heat transfer:

$$q = kS \Delta T \quad (3.261)$$

where k is the thermal conductivity of the conducting medium, ΔT the temperature difference driving the heat flow, and S the conduction shape factor. Table 3.12 provides expressions for the conduction shape factor for various two-dimensional configurations.

The conduction resistance for a two-dimensional system follows from eq. (3.261) as

$$R_{\text{cond}} = \frac{1}{Sk} \quad (3.262)$$

3.7.6 Finite-Difference Method

Cartesian Coordinates In the finite-difference approach, the conducting region is covered with a grid consisting of intersecting lines. The points of intersection are called *nodes*. For a rectangular region, the grid lines are drawn parallel to the boundaries. For simplicity, the spacings Δx and Δy are chosen so that $\Delta x = \Delta y$. Nodes are identified by double-subscript notation, ij , where i and j count the grid lines along the x - and y -coordinate directions, respectively. The node i, j , which represents a particular subvolume, is presumed to be isothermal at the temperature, $T_{i,j}$. In Fig. 3.33, five different types of nodes are identified together with their control volumes, which are shown as dashed enclosures. The finite-difference approximation for each type of node is given here with the control volume assumed to have no energy generation.

1. *Internal node:*

$$-T_{i,j} + \frac{1}{4}(T_{i+1,j} + T_{i,j+1} + T_{i-1,j} + T_{i,j-1}) = 0 \quad (3.263)$$

2. *Node on plane convecting surface:*

$$2T_{i-1,j} + T_{i,j-1} + T_{i,j+1} + \frac{2h \Delta x}{k} T_{\infty} - 2 \left(\frac{h \Delta x}{k} + 2 \right) T_{i,j} = 0 \quad (3.264)$$

3. *External corner node with convection:*

$$T_{i,j-1} + T_{i-1,j} + \frac{2h \Delta x}{k} T_{\infty} - 2 \left(1 + \frac{h \Delta x}{k} \right) T_{i,j} = 0 \quad (3.265)$$

4. *Internal corner node with convection:*

$$\begin{aligned} 2(T_{i,j-1} + T_{i,j+1}) + T_{i+1,j} + T_{i,j-1} + \frac{2h \Delta x}{k} T_{\infty} \\ - 2 \left(3 + \frac{h \Delta x}{k} \right) T_{i,j} = 0 \end{aligned} \quad (3.266)$$

TABLE 3.12 Conduction Shape Factors for Selected Two-Dimensional Systems
[$q = Sk(T_1 - T_2)$]

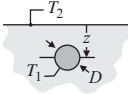
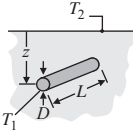
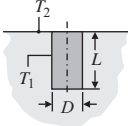
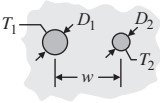
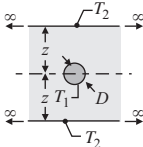
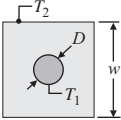
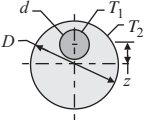
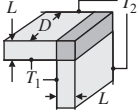
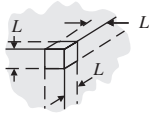
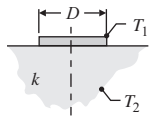
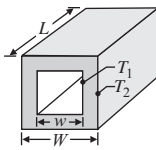
System	Schematic	Restrictions	Shape Factor
Case 1: Isothermal sphere buried in a semi-infinite medium		$z > D/2$	$\frac{2\pi D}{1 - D/4z}$
Case 2: Horizontal isothermal cylinder of length L buried in a semi-infinite medium		$L \gg D$ $L \gg D$ $z > 3D/2$	$\frac{2\pi L}{\cosh^{-1}(2z/D)}$ $\frac{2\pi L}{\ln(4z/D)}$
Case 3: Vertical cylinder in a semi-infinite medium		$L \gg D$	$\frac{2\pi L}{\ln(4L/D)}$
Case 4: Conduction between two cylinders of length L in infinite medium		$L \gg D_1, D_2$ $L \gg w$	$\frac{2\pi L}{\cosh^{-1}\left(\frac{4w^2 - D_1^2 - D_2^2}{2D_1 D_1}\right)}$
Case 5: Horizontal circular cylinder of length L midway between parallel planes of equal length and infinite width		$z \gg D/2$ $L \gg z$	$\frac{2\pi L}{\ln(8z/\pi D)}$
Case 6: Circular cylinder of length L centered in a square solid of equal length		$w > D$ $L \gg w$	$\frac{2\pi L}{\ln(1.08w/D)}$
Case 7: Eccentric circular cylinder of length L in a cylinder of equal length		$D > d$ $L \gg D$	$\frac{2\pi L}{\cosh^{-1}\left(\frac{D^2 + d^2 - 4z^2}{2Dd}\right)}$
Case 8: Conduction through the edge of adjoining walls		$D > L/5$	$0.54D$

TABLE 3.12 Conduction Shape Factors for Selected Two-Dimensional Systems
[$q = Sk(T_1 - T_2)$] (Continued)

System	Schematic	Restrictions	Shape Factor
Case 9: Conduction through corner of three walls with a temperature difference ΔT_{1-2} across the wall		$L \ll \text{length and width of wall}$	$0.15L$
Case 10: Disk of diameter D and T_1 on a semi-infinite medium of thermal conductivity k and T_2		None	$2D$
Case 11: Square channel of length L		$\frac{W}{w} < 1.4$ $\frac{W}{w} > 1.4$	$\frac{2\pi L}{0.785 \ln(W/w)}$ $\frac{2\pi L}{0.930(W/w) - 0.050}$

5. Node on a plane surface with a uniform heat flux:

$$(2T_{i+1,j} + T_{i,j+1} + T_{i,j-1}) + \frac{2q'' \Delta x}{k} - 4T_{i,j} = 0 \quad (3.267)$$

In eqs. (3.264)–(3.266), $h = 0$ applies to a node on an adiabatic boundary and $h = \infty$ applies to a node on an isothermal boundary.

By writing an appropriate finite-difference approximation for each node in the grid, a set of n -linear algebraic equations (one for each of the n nodes) in the unknown node temperatures can be produced. A standard numerical procedure or a computer code can be used to solve the system of equations giving the temperatures at all the nodes.

Consider the square plate shown in Fig. 3.34. For $\Delta x = \Delta y = 0.1/16 = 0.00625$ m, the finite-difference solution generated by Aziz (2001) gives the temperatures on the convecting surface. For $j = 1, 3, 5, 7, \dots, 17$,

$T_{17,j} = 67.85, 68.24, 70.19, 73.24, 77.13, 81.67, 86.81, 92.66$, and 100.00 all in $^{\circ}\text{C}$.

Cylindrical Coordinates Consider the solid cylinder of radius r_0 and length L (Fig. 3.35) in which steady conduction occurs along the r and z directions. The conduction equation is

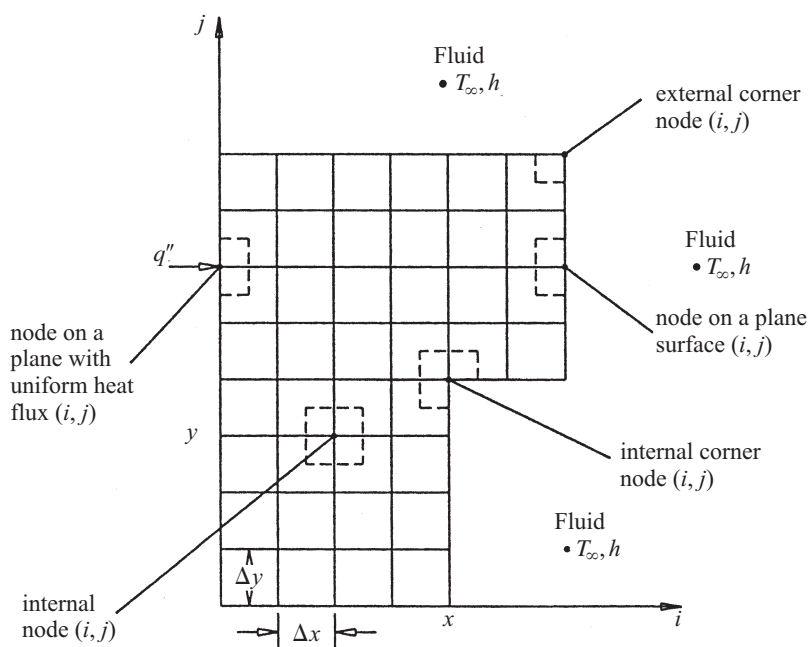


Figure 3.33 Types of nodes and the corresponding control volumes.

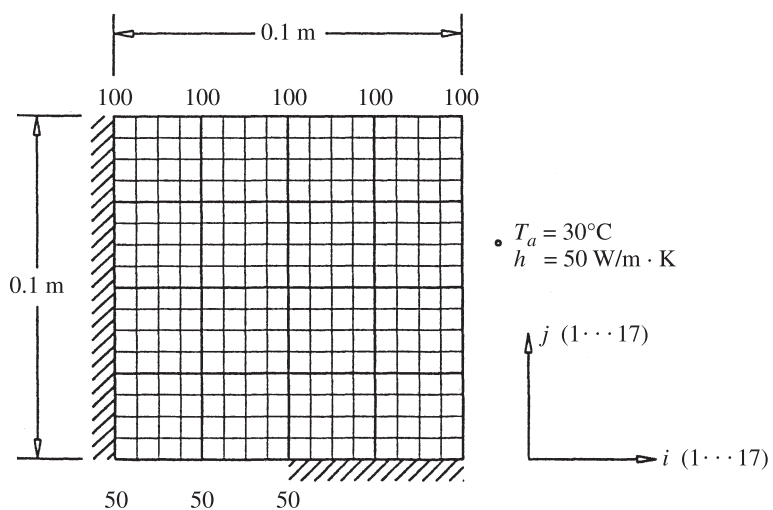


Figure 3.34 Grid for two-dimensional conduction in a square plate.

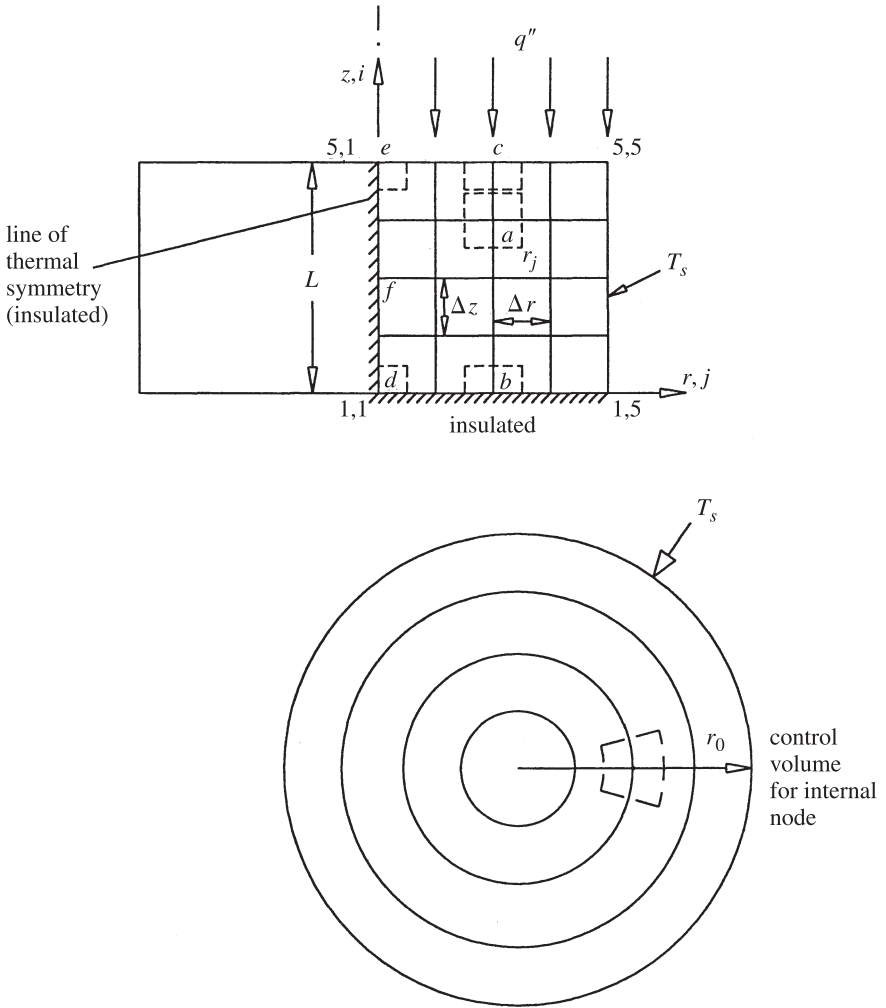


Figure 3.35 Finite-difference grid for radial and axial conduction in a solid cylinder with six different types of nodes.

$$\frac{\partial^2 T}{\partial r^2} + \frac{1}{r} \frac{\partial T}{\partial r} + \frac{\partial^2 T}{\partial z^2} = 0 \quad (3.268)$$

Let the outer surface temperature of the cylinder be T_s . The face at $z = 0$ is insulated while the face at $z = L$ experiences a constant heat flux q'' . This description gives the boundary conditions

$$\frac{\partial T(0,z)}{\partial r} = 0 \quad (\text{thermal symmetry}) \quad (3.269a)$$

$$T(r_0, z) = T_s \quad (3.269b)$$

$$\frac{\partial T(r, 0)}{\partial z} = 0 \quad (3.269c)$$

$$\frac{\partial T(r, L)}{\partial z} = q'' \quad (3.269d)$$

Six different nodes (*a*, *b*, *c*, *d*, *e*, and *f*) have been identified in Fig. 3.35. The finite-difference approximations for these nodes are as follows:

1. *Node a (internal node):*

$$-T_{i,j} + \frac{1}{4} \left[\left(1 - \frac{\Delta r}{2r_j}\right) T_{i,j-1} + \left(1 + \frac{\Delta r}{2r_j}\right) T_{i,j+1} + T_{i+1,j} + T_{i-1,j} \right] = 0 \quad (3.270)$$

2. *Node b (node on an insulated surface, $z = 0$):*

$$-T_{i,j} + \frac{1}{4} \left[2T_{i+1,j} + \left(1 - \frac{\Delta r}{2r_j}\right) T_{i,j-1} + \left(1 + \frac{\Delta r}{2r_j}\right) T_{i,j+1} \right] = 0 \quad (3.271)$$

3. *Node c (node on a constant heat flux surface, $z = L$):*

$$\begin{aligned} -T_{i,j} + \frac{1}{4} \left[\left(1 - \frac{\Delta r}{2r_j}\right) T_{i,j-1} + \left(1 + \frac{\Delta r}{2r_j}\right) T_{i,j+1} + 2T_{i-1,j} \right] \\ + \frac{q'' \Delta r}{2k} = 0 \end{aligned} \quad (3.272)$$

4. *Node d (node at the corner of two insulated surfaces):*

$$-T_{i,j} + \frac{1}{3} (T_{i+1,j} + 2T_{i,j+1}) = 0 \quad (i = 1, j = 1) \quad (3.273)$$

5. *Node e (node at the corner of an insulated surface and a constant heat flux surface):*

$$-T_{i,j} + \frac{1}{3} \left(T_{i-1,j} + 2T_{i,j+1} + \frac{q'' \Delta r}{k} \right) = 0 \quad (3.274)$$

6. *Node f (node on the longitudinal axis):*

$$-T_{i,j} + \frac{1}{6} (T_{i-1,j} + T_{i+1,j} + 4T_{i,j+1}) = 0 \quad (3.275)$$

Taking $r_0 = 1\text{m}$, $L = 1\text{m}$, $T_s = 25^\circ\text{C}$, $k = 20\text{W/m} \cdot \text{K}$, and $q'' = 1000\text{W/m}^2$, Aziz (2001) produced the following temperatures at the 20 nodes shown in Fig. 3.35:

$T_{1,1} = 31.03^{\circ}\text{C}$	$T_{3,3} = 32.33^{\circ}\text{C}$
$T_{1,2} = 30.54^{\circ}\text{C}$	$T_{3,4} = 28.95^{\circ}\text{C}$
$T_{1,3} = 29.14^{\circ}\text{C}$	$T_{4,1} = 41.42^{\circ}\text{C}$
$T_{1,4} = 27.13^{\circ}\text{C}$	$T_{4,2} = 40.43^{\circ}\text{C}$
$T_{2,1} = 32.02^{\circ}\text{C}$	$T_{4,3} = 37.38^{\circ}\text{C}$
$T_{2,2} = 31.46^{\circ}\text{C}$	$T_{4,4} = 32.15^{\circ}\text{C}$
$T_{2,3} = 29.87^{\circ}\text{C}$	$T_{5,1} = 51.59^{\circ}\text{C}$
$T_{2,4} = 27.53^{\circ}\text{C}$	$T_{5,2} = 50.42^{\circ}\text{C}$
$T_{3,1} = 35.24^{\circ}\text{C}$	$T_{5,3} = 46.69^{\circ}\text{C}$
$T_{3,2} = 34.50^{\circ}\text{C}$	$T_{5,4} = 39.35^{\circ}\text{C}$

A thorough discussion of the finite-difference method appears in Ozisik (1994). The book also features a large number of examples.

3.8 TRANSIENT CONDUCTION

The term *transient conduction* is used when the temperature in a heat conduction process depends on both time and the spatial coordinates. Three models that are commonly used to study transient conduction are the lumped thermal capacity model, the semi-infinite solid model and the finite-sized model. The finite-difference method provides one of many numerical methods that are used to analyze complicated configurations.

3.8.1 Lumped Thermal Capacity Model

The lumped thermal capacity model assumes that spatial temperature variations within the body are negligible and the temperature variation is solely a function of time. Consider a body of arbitrary shape of volume V , surface area A_s , density ρ , and specific heat c , initially at a temperature T_i , as indicated in Fig. 3.36. At time $t \geq 0$, the body is immersed in a convective environment (T_{∞}, h) , where $T_{\infty} < T_i$, and allowed to cool. The differential equation describing the cooling process is

$$\rho V c \frac{dT}{dt} = -h A_s (T - T_{\infty}) \quad (3.276)$$

with the initial condition

$$T(t = 0) = T_i \quad (3.277)$$

The solution is

$$\frac{T - T_{\infty}}{T_i - T_{\infty}} = e^{-h A_s t / \rho V c} \quad (3.278)$$

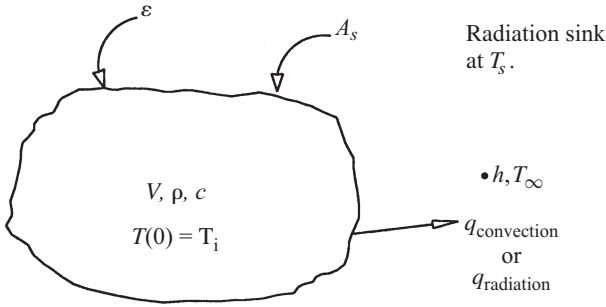


Figure 3.36 Cooling of a lumped thermal capacity body.

and the cumulative energy transfer to the coolant Q over a period of time t is

$$Q = \rho V c (T_i - T_\infty) (1 - e^{-h A_s t / \rho V c}) \quad (3.279)$$

The lumped thermal capacity model is valid for $Bi = hV/kA_s < 0.10$, a condition that is met in many engineering applications, such as the annealing of metals.

Attention now turns to some refinements of the basic lumped thermal capacity model.

Internal Energy Generation If the body experiences uniform thermal energy generation \dot{E}_g (W) at time $t = 0$, the temperature variation in the body is given by

$$\frac{\dot{E}_g - h A_s (T - T_\infty)}{\dot{E}_g - h A_s (T_i - T_\infty)} = e^{-h A_s t / \rho V c} \quad (3.280)$$

This situation occurs when an electronic component is suddenly energized.

Temperature-Dependent Specific Heat If the specific heat varies linearly with temperature, that is,

$$c = c_\infty [1 \pm \beta (T - T_\infty)] \quad (3.281)$$

the temperature variation given by Aziz and Hamad (1977) is

$$\ln \frac{T - T_\infty}{T_i - T_\infty} \pm \beta (T_i - T_\infty) \frac{T - T_i}{T_i - T_a} = -\frac{h A_s t}{\rho V c_\infty} \quad (3.282)$$

Pure Radiation Cooling If the body is cooled solely by radiation, the term $h A_s (T - T_\infty)$ is replaced in eq. (3.276) by $\epsilon \sigma A_s (T^4 - T_s^4)$, where ϵ is the surface emissivity and T_s is the effective sink temperature for radiation. The solution for T in this case is given by Aziz and Hamad (1977):

$$\ln \left(\frac{T_s + T}{T_s - T} \frac{T_s - T_i}{T_s + T_i} \right) + 2 \left(\arctan \frac{T}{T_s} - \arctan \frac{T_i}{T_s} \right) = \frac{4\epsilon\sigma A_s T_s^3 t}{\rho V c} \quad (3.283)$$

Equation (3.283) is useful, for example, in designing liquid droplet radiation systems for heat rejection on a permanent space station.

Simultaneous Convective–Radiative Cooling In this case, the radiative term, $-\sigma A_s(T^4 - T_s^4)$ appears on the right-hand side of eq. (3.276) in addition to $-hA_s(T - T_\infty)$. An exact solution for this case does not exist except when $T_\infty = T_s = 0$. For this special case the exact solution is

$$\frac{1}{3} \ln \left[\frac{1 + (\epsilon\sigma T_i^3) / h(T/T_i)^3}{(1 + \epsilon\sigma T_i^3 / h)(T/T_i)^3} \right] = \frac{hA_s t}{\rho V c} \quad (3.284)$$

Temperature-Dependent Heat Transfer Coefficient For natural convection cooling, the heat transfer coefficient is a function of the temperature difference, and the functional relationship is

$$h = C(T - T_\infty)^n \quad (3.285)$$

where C and n are constants. Using eq. (3.285) in (3.276) and solving the resulting differential equation gives

$$\frac{T - T_\infty}{T_i - T_\infty} = \left(1 + \frac{nh_i A_s t}{\rho V c} \right)^{-1/n} \quad (3.286)$$

where $n \neq 0$ and $h_i = C(T_i - T_\infty)^n$.

Heat Capacity of the Coolant Pool If the coolant pool has a finite heat capacity, the heat transfer to the coolant causes T_∞ to increase. Denoting the properties of the hot body by subscript 1 and the properties of the coolant pool by subscript 2, the temperature–time histories as given by Bejan (1993) are

$$T_1(t) = T_1(0) - \frac{T_1(0) - T_2(0)}{1 + \rho_1 V_1 c_1 / \rho_2 V_2 c_2} (1 - e^{-nt}) \quad (3.287)$$

$$T_2(t) = T_2(0) + \frac{T_1(0) + T_2(0)}{1 + (\rho_2 V_2 c_2 / \rho_1 V_1 c_1)} (1 - e^{-nt}) \quad (3.288)$$

where $T_1(0)$ and $T_2(0)$ are the initial temperatures and

$$n = hA_s \frac{\rho_1 V_1 c_1 + \rho_2 V_2 c_2}{(\rho_1 V_1 c_1)(\rho_2 V_2 c_2)} \quad (3.289)$$

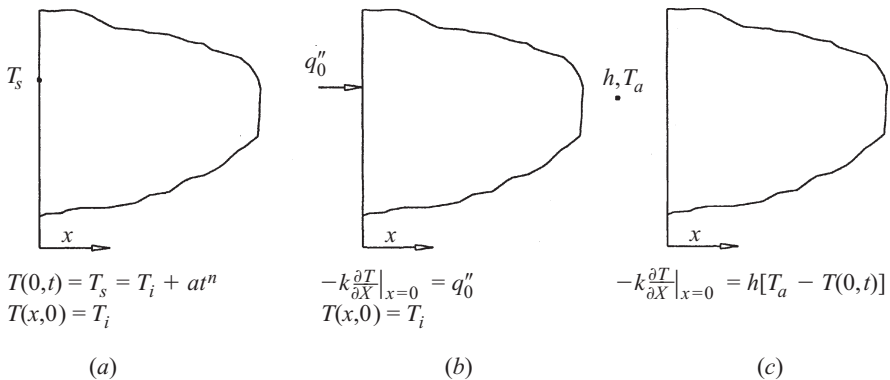


Figure 3.37 Semi-infinite solid with (a) specified surface temperature, (b) specified surface heat flux, and (c) surface convection.

3.8.2 Semi-infinite Solid Model

As indicated in Fig. 3.37, the semi-infinite solid model envisions a solid with one identifiable surface and extending to infinity in all other directions. The parabolic partial differential equation describing the one-dimensional transient conduction is

$$\frac{\partial^2 T}{\partial x^2} = \frac{1}{\alpha} \frac{\partial T}{\partial t} \quad (3.290)$$

Specified Surface Temperature If the solid is initially at a temperature T_i , and if for time $t > 0$ the surface at $x = 0$ is suddenly subjected to a specified temperature–time variation $f(t)$, the initial and boundary conditions can be written as

$$T(x, 0) = T_i \quad (x \geq 0) \quad (3.291a)$$

$$T(0, t) = f(t) = T_i + at^{n/2} \quad (3.291b)$$

$$T(\infty, t) = T_i \quad (t \geq 0) \quad (3.291c)$$

where a is a constant and n is a positive integer.

Using the Laplace transformation, the solution for T is obtained as

$$T = T_i + a\Gamma\left(1 + \frac{n}{2}\right)(4t)^{n/2}i^n \operatorname{erfc}\left(\frac{x}{2\sqrt{\alpha t}}\right) \quad (3.292)$$

where Γ is the gamma function (Section 3.3.2) and $i^n \operatorname{erfc}$ is the n th repeated integral of the complementary error function (Section 3.3.1). The surface heat flux q_0'' is

$$q_0'' = \frac{2^{n-1}}{\sqrt{\alpha}} t^{(n-1)/2} ka\Gamma\left(1 + \frac{n}{2}\right)\left[i^{n-1} \operatorname{erfc}\left(\frac{x}{2\sqrt{\alpha t}}\right)\right]_{x=0} \quad (3.293)$$

Several special cases can be deduced from eqs. (3.292) and (3.293).

Case 1: $f(t) = T_0$ This is the case of constant surface temperature which occurs when $n = 0$ and $a = T_0 - T_i$:

$$\frac{T(x, t) - T_i}{T_0 - T_i} = \operatorname{erfc}\left(\frac{x}{2\sqrt{\alpha t}}\right) \quad (3.294)$$

$$q_0'' = \frac{k(T_0 - T_i)}{(\pi\alpha t)^{1/2}} \quad (3.295)$$

Case 2: $f(t) = T_i + at$ This is the case of a linear variation of surface temperature with time which occurs when $n = 2$:

$$T(x, t) = T_i + 4ati^2 \operatorname{erfc}\left(\frac{x}{2\sqrt{\alpha t}}\right) \quad (3.296)$$

$$q_0'' = \frac{2kat}{(\pi\alpha t)^{1/2}} \quad (3.297)$$

Case 3: $f(t) = T_i + at^{1/2}$ This is the case of a parabolic surface temperature variation with time with $n = 1$.

$$T(x, t) = T_i + a\sqrt{\pi t} i \operatorname{erfc}\left(\frac{x}{2\sqrt{\alpha t}}\right) \quad (3.298)$$

$$q_0'' = \frac{ka}{2} \sqrt{\frac{\pi}{\alpha}} \quad (3.299)$$

Specified Surface Heat Flux For a constant surface heat flux q_0'' , the boundary conditions of eq. (3.291b) is replaced by

$$-k \frac{\partial T(0, t)}{\partial x} = q_0'' \quad (3.300)$$

and the solution is

$$T(x, t) = T_i + \frac{2q_0''\sqrt{\alpha t}}{k} i \operatorname{erfc}\left(\frac{x}{2\sqrt{\alpha t}}\right) \quad (3.301)$$

Surface Convection The surface convection boundary condition

$$-k \frac{\partial T(0, t)}{\partial x} = h [T_\infty - T(0, t)] \quad (3.302)$$

replaces eq. (3.291b) and the solution is

$$\frac{T(x, t) - T_i}{T_\infty - T_i} = \operatorname{erfc}\left(\frac{x}{2\sqrt{\alpha t}}\right) - e^{(hx/k) + (h^2\alpha t/k^2)} \operatorname{erfc}\left(\frac{h}{k}\sqrt{\alpha t} + \frac{x}{2\sqrt{\alpha t}}\right) \quad (3.303)$$

Constant Surface Heat Flux and Nonuniform Initial Temperature Zhuang et al. (1995) considered a nonuniform initial temperature of the form

$$T(x, 0) = a + bx \quad (3.304)$$

where a and b are constants to find a modified version of eq. (3.301) as

$$T(x, t) = a + bx + 2\sqrt{\alpha t} \left(\frac{q_0''}{k} + b \right) i \operatorname{erfc} \left(\frac{x}{2\sqrt{\alpha t}} \right) \quad (3.305)$$

The surface temperature is obtained by putting $x = 0$ in eq. (3.305), which gives

$$T(0, t) = a + 2\sqrt{\frac{\alpha t}{\pi}} \left(\frac{q_0''}{k} + b \right) \quad (3.306)$$

Zhuang et al. (1995) found that the predictions from eqs. (3.305) and (3.306) matched the experimental data obtained when a layer of asphalt is heated by a radiant burner, producing a heat flux of 41.785 kW/m^2 . They also provided a solution when the initial temperature distribution decays exponentially with x .

Constant Surface Heat Flux and Exponentially Decaying Energy Generation When the surface of a solid receives energy from a laser source, the effect of this penetration of energy into the solid can be modeled by adding an exponentially decaying heat generation term, $\dot{q}_0 e^{-ax}/k$ (where a is the surface absorption coefficient), to the left side of eq. (3.290). The solution for this case has been reported by Sahin (1992) and Blackwell (1990):

$$\begin{aligned} T = T_i + (T_0 + T_i) \operatorname{erfc} \left(\frac{x}{2\sqrt{\alpha t}} \right) \\ + \frac{\dot{q}_0}{ka^2} \left[\operatorname{erfc} \left(\frac{x}{2\sqrt{\alpha t}} \right) - \frac{1}{2} e^{a^2 \alpha t + ax} \operatorname{erfc} \left(\frac{x}{2\sqrt{\alpha t}} + a\sqrt{\alpha t} \right) \right. \\ \left. - \frac{1}{2} e^{a^2 \alpha t - ax} \operatorname{erfc} \left(\frac{x}{2a\sqrt{\alpha t}} - a\sqrt{\alpha t} \right) + e^{-ax} e^{(a^2 \alpha t - 1)} \right] \quad (3.307) \end{aligned}$$

Both Sahin (1992) and Blackwell (1990) have also solved this case for a convective boundary condition (h, T_∞) at $x = 0$. Blackwell's results show that for a given absorption coefficient a , thermal properties of α and k , initial temperature T_i , and surface heat generation \dot{q}_0 , the location of the maximum temperature moves deeper into the solid as time progresses. If h is allowed to vary, for a given time the greater value of h provides the greater depth at where the maximum temperature occurs. The fact that the maximum temperature occurs inside the solid provides a possible explanation for the "explosive removal of material" that has been observed to occur when the surface of a solid is given an intense dose of laser energy.

3.8.3 Finite-Sized Solid Model

Consider one-dimensional transient conduction in a plane wall of thickness $2L$, a long solid cylinder of radius r_0 , and a solid sphere of radius r_0 , each initially at a uniform temperature T_i . At time $t = 0$, the exposed surface in each geometry is exposed to a hot convective environment (h, T_∞). The single parabolic partial differential equation describing the one-dimensional transient heating of all three configurations can be written as

$$\frac{1}{s^n} \frac{\partial}{\partial s} \left(s^n \frac{\partial T}{\partial s} \right) = \frac{1}{\alpha} \frac{\partial T}{\partial t} \quad (3.308)$$

where $s = x, n = 0$ for a plane wall, $s = r, n = 1$ for a cylinder, and $s = r, n = 2$ for a sphere. In the case of a plane wall, x is measured from the center plane. The initial and boundary conditions for eq. (3.308) are

$$T(s, 0) = T_i \quad (3.309a)$$

$$\frac{\partial T(0, t)}{\partial s} = 0 \quad (\text{thermal symmetry}) \quad (3.309b)$$

$$k \frac{\partial T(L \text{ or } r_0, t)}{\partial s} = h [T_\infty - T(L \text{ or } r_0, t)] \quad (3.309c)$$

According to Adebisi (1995), the separation of variables method gives the solution for θ as

$$\theta = \sum_{n=1}^{\infty} \frac{2 \text{Bi}}{\lambda_n^2 + \text{Bi}^2 + 2\nu \cdot \text{Bi}} \frac{R^\nu J_{-\nu}(\lambda_n R)}{J_{-\nu}(\lambda_n)} e^{-\lambda_n^2 \tau} \quad (3.310)$$

where $\theta = (T_\infty - T)/(T_\infty - T_i)$, $R = x/L$ for a plane wall, $R = r/r_0$ for both cylinder and sphere, $\text{Bi} = hL/k$ or hr_0/k , $\tau = \alpha t/L^2$ or $\tau = \alpha t/r_0^2$, $\nu = (1 - n)/2$, and the λ_n are the eigenvalues given by

$$\lambda_n J_{-(\nu-1)}(\lambda_n) = \text{Bi} \cdot J_{-\nu}(\lambda_n) \quad (3.311)$$

The cumulative energy received over the time t is

$$Q = \rho c V (T_\infty - T_i) \sum_{n=1}^{\infty} \frac{2(1+n) \text{Bi}^2 (1 - e^{-\lambda_n^2 \tau})}{\lambda_n^2 (\lambda_n^2 + \text{Bi}^2 + 2\nu \cdot \text{Bi})} \quad (3.312)$$

Solutions for a plane wall, a long cylinder, and a sphere can be obtained from eqs. (3.310) and (3.312) by putting $n = 0$, ($\nu = \frac{1}{2}$), $n = 1$ ($\nu = 0$), and $n = 2$ ($\nu = -\frac{1}{2}$), respectively. It may be noted that

$$J_{-1/2}(z) = \left(\frac{2}{\pi z} \right)^{1/2} \cos z$$

$$J_{1/2}(z) = \left(\frac{2}{\pi z}\right)^{1/2} \sin z$$
$$J_{3/2}(z) = \left(\frac{2}{\pi z}\right)^{1/2} \left(\frac{\sin z}{z} - \cos z\right)$$

With these representations, eqs. (3.310) and (3.312) reduce to the standard forms appearing in textbooks. Graphical representations of eqs. (3.310) and (3.312) are called *Heisler charts*.

3.8.4 Multidimensional Transient Conduction

For some configurations it is possible to construct multidimensional transient conduction solutions as the product of one-dimensional results given in Sections 3.8.2 and 3.8.3. Figure 3.38 is an example of a two-dimensional transient conduction situation in which the two-dimensional transient temperature distribution in a semi-infinite plane wall is the product of the one-dimensional transient temperature distribution in an infinitely long plane wall and the one-dimensional transient temperature distribution in a semi-infinite solid. Several other examples of product solutions are given by Bejan (1993).

3.8.5 Finite-Difference Method

Explicit Method For two-dimensional transient conduction in Cartesian coordinates, the governing partial differential equation is

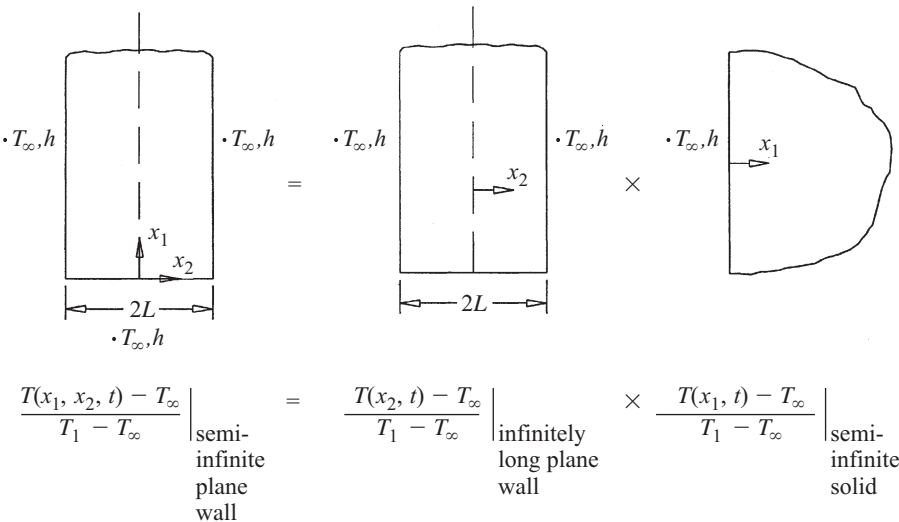


Figure 3.38 Product solution for a two-dimensional transient conduction problem.

$$\frac{\partial^2 T}{\partial x^2} + \frac{\partial^2 T}{\partial y^2} = \frac{1}{\alpha} \frac{\partial T}{\partial t} \quad (3.313)$$

which assumes no internal heat generation and constant thermal properties. Approximating the second-order derivatives in x and y and the first-order derivative in t by *forward differences*, the explicit finite-difference approximations (using $\Delta x = \Delta y$) for various nodes (see Fig. 3.33) can be expressed using the Fourier modulus, $Fo = \alpha \Delta t / (\Delta x)^2$, $Bi = h \Delta x / k$, and $t = p \Delta t$.

- *Internal node:* With $Fo \leq \frac{1}{4}$,

$$T_{i,j}^{p+1} = Fo \left(T_{i+1,j}^p + T_{i-1,j}^p + T_{i,j+1}^p + T_{i,j-1}^p \right) + (1 - 4Fo) T_{i,j}^p \quad (3.314)$$

- *Node at interior corner with convection:* With $Fo(3 + Bi) \leq \frac{3}{4}$,

$$T_{i,j}^{p+1} = \frac{2}{3} Fo \left(T_{i+1,j}^p + 2T_{i-1,j}^p + 2T_{i,j+1}^p + T_{i,j-1}^p + 2Bi T_{\infty} \right) + \left(1 - 4Fo - \frac{4}{3} Bi \cdot Fo \right) T_{i,j}^p \quad (3.315)$$

- *Node on a plane surface with convection:* With $Fo(2 + Bi) \leq \frac{1}{2}$,

$$T_{i,j}^{p+1} = Fo \left(2T_{i-1,j}^p + T_{i,j+1}^p + T_{i,j-1}^p + 2Bi \cdot T_{\infty} \right) + (1 - 4Fo - 2Bi \cdot Fo) T_{i,j}^p \quad (3.316)$$

- *Node at exterior corner with convection:* With $Fo(1 + Bi) \leq \frac{1}{4}$,

$$T_{i,j}^{p+1} = 2Fo \left(T_{i-1,j}^p + T_{i,j-1}^p + 2Bi \cdot T_{\infty} \right) + (1 - 4Fo - 4Bi \cdot Fo) T_{i,j}^p = 0 \quad (3.317)$$

- *Node on a plane surface with uniform heat flux:* With $Fo \leq \frac{1}{4}$,

$$T_{i,j}^{p+1} = (1 - 4Fo) T_{i,j}^p + Fo \left(2T_{i-1,j}^p + T_{i,j+1}^p + T_{i,j-1}^p \right) + 2Fo \cdot q'' \frac{\Delta x}{k} \quad (3.318)$$

The choice of Δx and Δt must satisfy the stability constraints, introducing each of the approximations given by eqs. (3.314)–(3.318) to ensure a solution free of numerically induced oscillations. Once the approximations have been written for each node on the grid, the numerical computation is begun with $t = 0$ ($p = 0$), for which the node temperatures are known from the initial conditions prescribed. Because eqs. (3.313)–(3.318) are explicit, node temperatures at $t = \Delta t$ ($p = 1$) can be determined from a knowledge of the node temperatures the preceding time, $t = 0$ ($p = 0$). This

“marching out” in time type of computation permits the transient response of the solid to be determined in a straightforward manner. However, the computational time necessary to cover the entire transient response is excessive because extremely small values of Δt are needed to meet the stability constraints.

Implicit Method In the implicit method, the second derivatives in x and y are approximated by *central differences* but with the use of temperatures at a subsequent time, $p + 1$, rather than the current time, p , while the derivative in t is replaced by a *backward difference* instead of a forward difference. Such approximations lead to the following equations:

- *Internal node:*

$$(1 + 4\text{Fo})T_{i,j}^{p+1} - \text{Fo} \left(T_{i+1,j}^{p+1} + T_{i-1,j}^{p+1} + T_{i,j+1}^{p+1} + T_{i,j-1}^{p+1} \right) = T_{i,j}^p \quad (3.319)$$

- *Node at interior corner with convection:*

$$\begin{aligned} \left[(1 + 4\text{Fo}) \left(1 + \frac{1}{3}\text{Bi} \right) \right] T_{i,j}^{p+1} - \frac{2}{3}\text{Fo} \left(T_{i+1,j}^{p+1} + 2T_{i-1,j}^{p+1} \right. \\ \left. + 2T_{i,j+1}^{p+1} + T_{i,j-1}^{p+1} \right) = T_{i,j}^p + \frac{4}{3}\text{Fo} \cdot \text{Bi} \cdot T_{\infty} \end{aligned} \quad (3.320)$$

- *Node on a plane surface with convection:*

$$\begin{aligned} [1 + 2\text{Fo}(2 + \text{Bi})] T_{i,j}^{p+1} - \text{Fo} \left(2T_{i-1,j}^{p+1} + T_{i,j+1}^{p+1} + T_{i,j-1}^{p+1} \right) \\ = T_{i,j}^p + 2\text{Bi} \cdot \text{Fo} \cdot T_{\infty} \end{aligned} \quad (3.321)$$

- *Node at exterior corner with convection:*

$$1 + 4\text{Fo}(1 + \text{Bi})T_{i,j}^{p+1} - 2\text{Fo} \left(T_{i-1,j}^{p+1} + T_{i,j-1}^{p+1} \right) = T_{i,j}^p + 4\text{Bi} \cdot \text{Fo} \cdot T_{\infty} \quad (3.322)$$

- *Node on a plane surface with uniform heat flux:*

$$(1 + 4\text{Fo})T_{i,j}^{p+1} + \text{Fo} \left(2T_{i-1,j}^{p+1} + T_{i,j+1}^{p+1} + T_{i,j-1}^{p+1} \right) = T_{i,j}^p + \frac{2\text{Fo} \cdot q'' \Delta x}{k} \quad (3.323)$$

The implicit method is unconditionally stable and therefore permits the use of higher values of Δt , thereby reducing the computational time. However, at each time t , the implicit method requires that the node equations be solved *simultaneously* rather than *sequentially*.

Other Methods Several improvements of the explicit and implicit methods have been advocated in the numerical heat transfer literature. These include the three-time-level scheme of Dufort and Fankel, the Crank–Nicholson method, and alternating

direction explicit methods. For a discussion of these methods as well as stability analysis, the reader should consult Pletcher et al. (1988).

3.9 PERIODIC CONDUCTION

Examples of periodic conduction are the penetration of atmospheric temperature cycles into the ground, heat transfer through the walls of internal combustion engines, and electronic components under cyclic operation. The periodicity may appear in the differential equation or in a boundary condition or both. The complete solution to a periodic heat conduction problem consists of a transient component that decays to zero with time and a steady oscillatory component that persists. It is the steady oscillatory component that is of prime interest in most engineering applications. In this section we present several important solutions.

3.9.1 Cooling of a Lumped System in an Oscillating Temperature Environment

Revisit the lumped thermal capacity model described in Section 3.8.1 and consider a scenario in which the convective environmental temperature T_∞ oscillates sinusoidally, that is,

$$T_\infty = T_{\infty,m} + a \sin \omega t \quad (3.324)$$

where a is the amplitude of oscillation, $\omega = 2\pi f$ the angular frequency, f the frequency in hertz, and $T_{\infty,m}$ the mean temperature of the environment.

The method of complex combination described by Arpaci (1966), Myers (1998), Poulikakos (1994), and Aziz and Lunardini (1994) gives the steady periodic solution as

$$\theta = \frac{1}{\sqrt{1+B^2}} \sin(B\tau - \beta) \quad (3.325)$$

where

$$\theta = \frac{T - T_{\infty,m}}{a} \quad B = \frac{\rho V c}{h A} \omega \quad \tau = \frac{h A t}{\rho V c} \quad \beta = \arctan B \quad (3.326)$$

A comparison of eq. (3.325) with the dimensionless environmental temperature variation ($\sin B\tau$) shows that the temperature of the body oscillates with the same frequency as that of the environment but with a phase lag of β . As the frequency of oscillation increases, the phase angle $\beta = \arctan B$ increases, but the amplitude of oscillation $1/(1+B^2)^{1/2}$ decreases.

3.9.2 Semi-infinite Solid with Periodic Surface Temperature

Consider the semi-infinite solid described in Section 3.8.2 and let the surface temperature be of the form

$$T(0, t) = T_s = T_i + a \cos \omega t \quad (3.327)$$

In this case, eqs. (3.291) are still applicable, although the initial condition of eq. (3.291a) becomes irrelevant for the steady periodic solution, which is

$$T(x, t) = T_i + ae^{-[(\omega/2\alpha)^{1/2}x]} \cos \left[\omega t - \left(\frac{\omega}{2\alpha} \right)^{1/2} x \right] \quad (3.328)$$

Three conclusions can be drawn from this result. First, the temperatures at all locations oscillate with the same frequency as the thermal disturbance at the surface. Second, the amplitude of oscillation decays exponentially with x . This makes the solution applicable to the finite thickness plane wall. Third, the amplitude of oscillation decays exponentially with the square root of the frequency ω . Thus, higher-frequency disturbances damp out more rapidly than those at lower frequencies. This explains why daily oscillations of ambient temperature do not penetrate as deeply into the ground as annual and millennial oscillations. The surface heat flux variation follows directly from eq. (3.328):

$$q''(0, t) = -k \frac{\partial T(0, t)}{\partial x} = ka \left(\frac{\omega}{\alpha} \right)^{1/2} \cos \left(\omega t - \frac{\pi}{4} \right) \quad (3.329)$$

and this shows that $q''(0, t)$ leads $T(0, t)$ by $\pi/4$ radians.

3.9.3 Semi-infinite Solid with Periodic Surface Heat Flux

In this case, the boundary condition of eq. (3.327) is replaced with

$$q''(0, t) = -k \frac{\partial T}{\partial x}(0, t) = q_0'' \cos \omega t \quad (3.330)$$

and the solution takes the form

$$T(x, t) = T_i + \frac{q_0''}{k} \left(\frac{\alpha}{\omega} \right)^{1/2} e^{-[(\omega/2\alpha)^{1/2}x]} \cos \left[\omega t - \left(\frac{\omega}{2\alpha} \right)^{1/2} x - \frac{\pi}{4} \right] \quad (3.331)$$

It is interesting to note that the phase angle increases as the depth x increases with the minimum phase angle of $\pi/4$ occurring at the surface ($x = 0$). A practical situation in which eq. (3.331) becomes useful is in predicting the steady temperature variations induced by frictional heating between two reciprocating parts in contact in a machine. This application has been described by Poulikakos (1994).

3.9.4 Semi-infinite Solid with Periodic Ambient Temperature

The surface boundary condition in this case is

$$T_\infty = T_{\infty, m} + a \cos \omega t \quad (3.332)$$

and the steady periodic temperature distribution is given by

$$\theta = \frac{\text{Bi}}{(\text{Bi}^2 + 2\text{Bi} + 2)^{1/2}} e^{-\sqrt{\pi} X} \cos(2\pi\tau - \sqrt{\pi} X - \beta) \quad (3.333)$$

where

$$\theta = \frac{T - T_{\infty, m}}{a} \quad (3.334a)$$

$$X = \left(\frac{\omega}{2\pi\alpha} \right)^{1/2} x \quad (3.334b)$$

$$\tau = \frac{\omega t}{2\pi} \quad (3.334c)$$

$$\text{Bi} = \frac{h}{k} \left(\frac{2}{\alpha} \right)^{1/2} \omega \quad (3.334d)$$

$$\beta = \arctan \frac{1}{1 + \text{Bi}} \quad (3.334e)$$

Note that as $h \rightarrow \infty$, $\text{Bi} \rightarrow \infty$, and $\beta \rightarrow 0$, eqs. (3.333) reduce to eq. (3.328) with $T_{\infty, m} = T_i$. The presence of the factor $\text{Bi}/(\text{Bi} + 2\text{Bi} + 2)^{1/2}$ in eq. (3.333) shows that convection enhances the damping effect and that it also increases the phase angle by an amount $\beta = \arctan 1/(1 + \text{Bi})$.

3.9.5 Finite Plane Wall with Periodic Surface Temperature

Consider a plane wall of thickness L with the face at $x = 0$ insulated and the face at $x = L$ subjected to a periodic temperature change of the form

$$T(L, t) = T_i + a \cos \omega t \quad (3.335)$$

where T_i is the initial temperature of the wall and the insulated boundary condition at $x = 0$ gives

$$\frac{\partial T(0, t)}{\partial x} = 0 \quad (3.336)$$

The steady periodic solution is

$$T(x, t) = T_i + a\phi_1 \left[\frac{x}{L}, \left(\frac{\omega}{2\alpha} \right)^{1/2} L \right] \cos \left\{ \omega t + \phi_2 \left[\frac{x}{L}, \left(\frac{\omega}{2\alpha} \right)^{1/2} L \right] \right\} \quad (3.337)$$

where the numerical values of ϕ_1 as a function of x/L and $(w/2\alpha)^{1/2}L$ are supplied in Table 3.13, and ϕ_2 , which is also a function of x/L and $(w/2\alpha)^{1/2}L$, is given by

$$\phi_2 = \arctan \frac{\phi_a \phi_d - \phi_b \phi_c}{\phi_a \phi_b - \phi_c \phi_d} \quad (3.338)$$

TABLE 3.13 Values of the Amplitude Decay Function, ϕ as a Function of x/L and $\sigma = (\omega/2\alpha)^{1/2}L$

σ	$x/L = 0$	0.125	0.250	0.375	0.500	0.625	0.750	0.875	1.000
0.0	1.00	1.00	1.00	1.00	1.00	1.00	1.00	1.00	1.00
0.5	0.98	0.98	0.98	0.98	0.98	0.98	0.98	0.99	1.00
1.0	0.77	0.77	0.77	0.78	0.79	0.81	0.85	0.91	1.00
1.5	0.47	0.47	0.47	0.48	0.52	0.58	0.68	0.83	1.00
2.0	0.27	0.27	0.28	0.30	0.36	0.45	0.58	0.77	1.00
4.0	0.04	0.04	0.05	0.08	0.13	0.22	0.37	0.64	1.00
8.0	0.00	0.00	0.01	0.01	0.02	0.05	0.14	0.36	1.00
∞	0.00	0.00	0.00	0.00	0.00	0.00	0.00	0.00	

where

$$\phi_a = \cos \left[\left(\frac{\omega}{2\alpha} \right)^{1/2} L \right] \cosh \left[\left(\frac{\omega}{2\alpha} \right)^{1/2} L \right] \quad (3.339a)$$

$$\phi_b = \cos \left[\left(\frac{\omega}{2\alpha} \right)^{1/2} x \right] \cosh \left[\left(\frac{\omega}{2\alpha} \right)^{1/2} x \right] \quad (3.339b)$$

$$\phi_c = \sin \left[\left(\frac{\omega}{2\alpha} \right)^{1/2} L \right] \sinh \left[\left(\frac{\omega}{2\alpha} \right)^{1/2} L \right] \quad (3.339c)$$

$$\phi_d = \sin \left[\left(\frac{\omega}{2\alpha} \right)^{1/2} x \right] \sinh \left[\left(\frac{\omega}{2\alpha} \right)^{1/2} x \right] \quad (3.339d)$$

3.9.6 Infinitely Long Semi-infinite Hollow Cylinder with Periodic Surface Temperature

Consider an infinitely long cylinder of inside radius, r_i , extending to infinity in the radial direction. The inner surface is subjected to a periodic temperature variation of the form

$$T(r_i, t) = T_i + a \cos \omega t \quad (3.340)$$

where T_i is the initial temperature of the cylinder. The equation governing the temperature distribution is

$$\frac{\partial^2 T}{\partial r^2} + \frac{1}{r} \frac{\partial T}{\partial r} = \frac{1}{\alpha} \frac{\partial T}{\partial t} \quad (3.341)$$

The other boundary condition is

$$T(\infty, t) = T_i, \quad \frac{\partial T(\infty, t)}{\partial r} = 0 \quad (3.342)$$

and the initial condition is

$$T(r, 0) = T_i \quad (3.343)$$

An application of the method of complex combination gives the steady-state periodic solution as

$$\theta = \frac{T - T_i}{a} = \Lambda_1 \cos \omega t - \Lambda_2 \sin \omega t \quad (3.344)$$

where

$$\Lambda_1 = \frac{\ker(\sqrt{\omega/\alpha} r_i) \ker(\sqrt{\omega/\alpha} r) + \operatorname{kei}(\sqrt{\omega/\alpha} r_i) \operatorname{kei}(\sqrt{\omega/\alpha} r)}{\ker^2(\sqrt{\omega/\alpha} r_i) + \operatorname{kei}^2(\sqrt{\omega/\alpha} r_i)} \quad (3.345a)$$

$$\Lambda_2 = \frac{\ker(\sqrt{\omega/\alpha} r_i) \operatorname{kei}(\sqrt{\omega/\alpha} r) - \operatorname{kei}(\sqrt{\omega/\alpha} r_i) \ker(\sqrt{\omega/\alpha} r)}{\ker^2(\sqrt{\omega/\alpha} r_i) + \operatorname{kei}^2(\sqrt{\omega/\alpha} r_i)} \quad (3.345b)$$

and \ker and kei are the Thomson functions discussed in Section 3.3.5.

As indicated in Section 3.9.1, the method of complex combination is described by Arpaci (1966), Myers (1998), Poulidakos (1994), and Aziz and Lunardini (1994). The method may be extended to numerous other periodic heat problems of engineering interest.

3.10 CONDUCTION-CONTROLLED FREEZING AND MELTING

Heat conduction with freezing (melting) occurs in a number of applications, such as ice formation, permafrost melting, metal casting, food preservation, storage of latent energy, and organ preservation and cryosurgery. Books and review articles on the subject include those of Lunardini (1991), Cheng and Seki (1991), Rubinsky and Eto (1990), Aziz and Lunardini (1993), Viskanta (1983, 1988), and Alexiades and Solomon (1993). Because of the vastness of the literature, only selected results that are judged to be of fundamental importance are discussed in this section.

3.10.1 One-Region Neumann Problem

The one-region Neumann problem deals with a semi-infinite region of liquid initially at its freezing temperature, T_f . At time $t > 0$, the face at $x = 0$ is suddenly reduced and kept at T_0 such that $T_0 < T_f$, as shown in Fig. 3.39. This initiates the extraction of heat by conduction from the saturated liquid to the surface and the liquid begins to freeze. As the cooling continues, the interface (assumed sharp) between the solid and liquid phases penetrates deeper into the liquid region. The prediction of the location of the interface calls for determination of the one-dimensional transient temperature distribution in the solid assuming that the liquid continues to remain at T_f at all times. The governing partial differential equation is

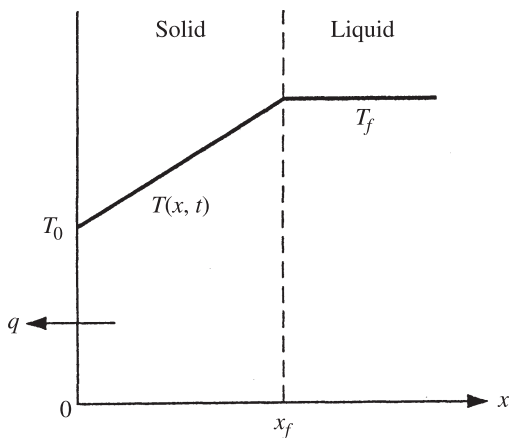


Figure 3.39 One-region Neumann problem (freezing).

$$\frac{\partial^2 T}{\partial x^2} = \frac{1}{\alpha} \frac{\partial T}{\partial t} \quad (3.346)$$

with the boundary conditions

$$T(0, t) = T_0 \quad (3.347a)$$

$$T(x_f, t) = T_f \quad (3.347b)$$

where x_f denotes the location of the interface, which is not known a priori and must be determined as part of the solution. An energy balance at the interface gives

$$k \left. \frac{\partial T}{\partial x} \right|_{x=x_f} = \rho L \frac{\partial x_f}{\partial t} \quad (3.348)$$

where k and ρ are the thermal conductivity and density of the solid phase, respectively, and L is the latent heat.

The temperature distribution in the solid is given as

$$\frac{T_f - T}{T_f - T_0} = 1 - \frac{\operatorname{erf}(x/2\sqrt{\alpha t})}{\operatorname{erf}(x_f/2\sqrt{\alpha t})} \quad (3.349)$$

where $x_f/2\sqrt{\alpha t}$, denoted by λ , is a root of the transcendental equation

$$\sqrt{\pi} \lambda \operatorname{erf}(\lambda e^{\lambda^2}) = \operatorname{St} \quad (3.350)$$

TABLE 3.14 Interface Location Parameter λ

λ	St
0.0	0.0000
0.2	0.0822
0.4	0.3564
0.6	0.9205
0.8	1.9956
1.0	4.0601
1.2	8.1720

and

$$\text{St} = \frac{c(T_f - T_0)}{L} \quad (3.351)$$

is the *Stefan number*, the ratio of the sensible heat to the latent heat. For water, St is about 0.10, for paraffin wax about 0.90, for copper about 2.64, and for silicon dioxide about 436. Table 3.14 gives selected values of λ and St that satisfy eq. (3.350). Viskanta (1983) reports that the Neumann model accurately predicts the solidification of *n*-octadecane on a horizontal plate.

The solution presented here applies to the one-region melting problem if T_f is replaced by the melting temperature T_m . With $T_0 > T_m$, eq. (3.349) gives the temperature in the liquid region.

3.10.2 Two-Region Neumann Problem

The two-region Neumann problem allows for heat conduction in both the solid and liquid phases. For the configuration in Fig. 3.40, the mathematical description of the problem is

$$\frac{\partial^2 T_s}{\partial x^2} = \frac{1}{\alpha_s} \frac{\partial T_s}{\partial t} \quad (0 < x < x_f \text{ and } t > 0) \quad (3.352)$$

$$\frac{\partial^2 T_l}{\partial x^2} = \frac{1}{\alpha_l} \frac{\partial T_l}{\partial t} \quad (x_f < x < \infty \text{ and } t > 0) \quad (3.353)$$

with initial and boundary conditions

$$T_l(x, 0) = T_i \quad (3.354a)$$

$$T_s(0, t) = T_0 \quad (3.354b)$$

$$T_s(x_f, t) = T_l(x_f, t) = T_f \quad (3.354c)$$

$$\left(k_s \frac{\partial T_s}{\partial x} - k_l \frac{\partial T_l}{\partial x} \right)_{x=x_f} = \rho L \frac{dx_f}{dt} \quad (3.354d)$$

where the subscripts s and l refer to the solid and liquid phases, respectively.

The solutions for T_s and T_l are

$$\frac{T_s - T_0}{T_f - T_0} = \frac{\operatorname{erf}(x/2\sqrt{\alpha_s t})}{\operatorname{erf}(x_f/2\sqrt{\alpha_s t})} \quad (3.355)$$

$$\frac{T_i - T_l}{T_i - T_f} = \frac{\operatorname{erfc}(x/2\sqrt{\alpha_l t})}{\operatorname{erfc}(x_f/2\sqrt{\alpha_l t})} \quad (3.356)$$

With $x_f/2\sqrt{\alpha_s t}$ denoted by λ , the interface energy balance given by eq. (3.354d) leads to the transcendental equation for λ :

$$\frac{e^{-\lambda^2}}{\lambda \operatorname{erf}(\lambda)} - \frac{T_i - T_f}{T_f - T_0} \left[\frac{(k\rho c)_l}{(k\rho c)_s} \right]^{1/2} \frac{e^{-\lambda^2(\alpha_s/\alpha_l)}}{\lambda \operatorname{erfc}[\lambda(\alpha_s/\alpha_l)^{1/2}]} = \frac{\sqrt{\pi} L}{c(T_f - T_0)} \quad (3.357)$$

Churchill and Evans (1971) noted that λ is a function of three parameters:

$$\theta^* = \frac{T_i - T_f}{T_f - T_0} \left[\frac{(k\rho c)_l}{(k\rho c)_s} \right]^{1/2} \quad \alpha^* = \frac{\alpha_s}{\alpha_l} \quad \text{St} = \frac{c(T_f - T_0)}{L}$$

and solved eq. (3.357) for a range of values of these parameters. Table 3.15 summarizes these results for λ .

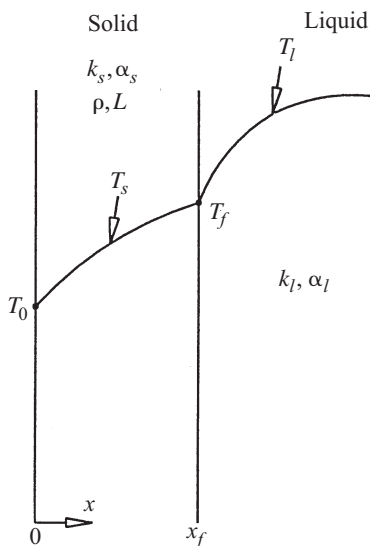


Figure 3.40 Two-region Neumann problem (freezing).

TABLE 3.15 Values of λ

St	α^*	θ^*						
		0.50	1.0	1.5	2.0	3.0	5.0	10.0
0.1	2.0	0.202	0.187	0.173	0.161	0.141	0.111	0.071
0.1	1.5	0.203	0.188	0.175	0.163	0.142	0.113	0.072
0.1	1.0	0.204	0.189	0.176	0.164	0.144	0.114	0.073
0.2	2.0	0.270	0.241	0.216	0.195	0.165	0.123	0.074
0.2	1.5	0.271	0.243	0.219	0.199	0.167	0.125	0.075
0.2	1.0	0.273	0.245	0.222	0.202	0.170	0.128	0.076
0.5	2.0	0.374	0.313	0.268	0.234	0.186	0.133	0.077
0.5	1.5	0.378	0.320	0.273	0.240	0.192	0.135	0.078
0.5	1.0	0.383	0.325	0.280	0.246	0.197	0.139	0.079
1.0	2.0	0.452	0.358	0.298	0.254	0.198	0.137	0.077
1.0	1.5	0.460	0.367	0.305	0.261	0.203	0.140	0.079
1.0	1.0	0.470	0.378	0.315	0.270	0.209	0.144	0.080
2.0	2.0	0.517	0.391	0.317	0.267	0.204	0.139	0.078
2.0	1.5	0.530	0.403	0.327	0.275	0.210	0.142	0.079
2.0	1.0	0.546	0.418	0.339	0.286	0.217	0.146	0.080

3.10.3 Other Exact Solutions for Planar Freezing

Besides the one- and two-region Neumann solutions, several other exact solutions for planar freezing problems are available. These include:

1. The two-region problem with different solid- and liquid-phase densities (Lunardini, 1991)
2. The two-region problem with phase change occurring over a temperature range (Cho and Sunderland, 1969)
3. The one-region problem with a mushy zone separating the pure solid and pure liquid phases (Solomon et al., 1982)
4. The two-region problem with temperature-dependent thermal conductivities k_s and k_l (Cho and Sunderland, 1974)
5. The two-region problem with arbitrary surface temperature and initial conditions (Tao, 1978)

3.10.4 Exact Solutions in Cylindrical Freezing

Carslaw and Jaeger (1959) give an exact solution for the freezing of a subcooled liquid while the solid phase remains at the freezing temperature. The latent heat released is used to bring the subcooled liquid to its freezing temperature. The process is described by the differential equation

$$\frac{1}{r} \frac{\partial}{\partial r} \left(r \frac{\partial T}{\partial r} \right) = \frac{1}{\alpha} \frac{\partial T}{\partial t} \quad (r < r_f) \quad (3.358)$$

and the initial boundary conditions

$$T(r_f, t) = T_f \quad (3.359a)$$

$$\lim_{r \rightarrow \infty} T(r, t) = T_0 \quad (3.359b)$$

$$T(r, 0) = T_0 \quad (3.359c)$$

where r_f represents the radial growth of the solid phase and $T_0 < T_f$ is the subcooled liquid temperature.

The solution of eq. (3.358) satisfying the conditions of eqs. (3.359) is

$$T = T_0 + (T_f - T_0) \frac{\text{Ei}(-r^2/4\alpha t)}{\text{Ei}(-r_f^2/4\alpha t)} \quad (3.360)$$

where $\lambda = r_f^2/4\alpha t$ is given by

$$\lambda^2 \cdot \text{Ei}(-\lambda^2) e^{\lambda^2} + \text{St} = 0 \quad (3.361)$$

In eqs. (3.360) and (3.361), Ei is the exponential integral function discussed in Section 3.3.4, and in eq. (3.361), St is the Stefan number. Table 3.16 provides the solution of eq. (3.361).

Another situation for which an exact solution is available is shown in Fig. 3.41. A line heat sink of strength Q_s (W/m) located at $r = 0$ and activated at time $t = 0$ causes the infinite extent of liquid at a uniform temperature T_i ($T_i > T_f$) to freeze. The interface grows radially outward. The mathematical formulation for the solid and liquid phases leads to

$$\frac{1}{r} \frac{\partial}{\partial r} \left(r \frac{\partial T_s}{\partial r} \right) = \frac{1}{\alpha_s} \frac{\partial T_s}{\partial t} \quad (0 < r < r_f) \quad (3.362)$$

$$\frac{1}{r} \frac{\partial}{\partial r} \left(r \frac{\partial T_l}{\partial r} \right) = \frac{1}{\alpha_l} \frac{\partial T_l}{\partial t} \quad (r_f < r < \infty) \quad (3.363)$$

with initial and boundary conditions

$$T_l(\infty, t) = T_i \quad (3.364a)$$

$$T_l(r, 0) = T_i \quad (3.364b)$$

$$T_s(r_f, t) = T_l(r_f, t) = T_f \quad (3.364c)$$

$$\left(k_s \frac{\partial T_s}{\partial r} - k_l \frac{\partial T_l}{\partial r} \right)_{r=r_f} = \rho L \frac{dr_f}{dt} \quad (3.364d)$$

TABLE 3.16 Stefan Number and Interface Location Parameter

St	λ
0.1	0.1846
0.2	0.3143
0.3	0.4491
0.4	0.6006
0.5	0.7811
0.6	1.0095
0.7	1.3237
0.8	1.8180

Ozisik (1993) gives the solution as

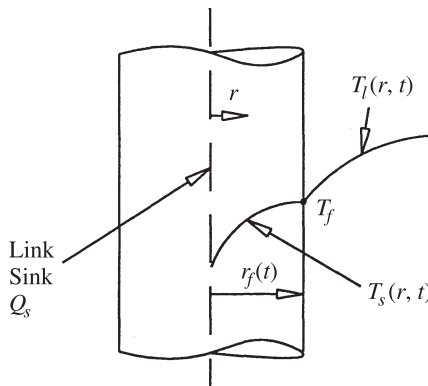
$$T_s = T_f + \frac{Q_s}{4\pi k_s} \left[\text{Ei} \left(-\frac{r^2}{4\alpha_s t} \right) - \text{Ei} \left(-\frac{r_f^2}{4\alpha_s t} \right) \right] \quad (0 < r < r_f) \quad (3.365)$$

$$T_l = T_i - \frac{T_i - T_f}{\text{Ei} \left(-\frac{r_f^2}{4\alpha_l t} \right)} \text{Ei} \left(-\frac{r^2}{4\alpha_l t} \right) \quad (r_f < r < \infty) \quad (3.366)$$

where $\lambda = r_f/2\sqrt{\alpha_s t}$ is obtained from the transcendental equation

$$\frac{Q_s}{4\pi} e^{-\lambda^2} + \frac{k_l(T_i - T_f)}{\text{Ei}(-\lambda^2\alpha_s/\alpha_l)} e^{-\lambda^2\alpha_s/\alpha_l} = \lambda^2\alpha_s\rho L \quad (3.367)$$

The solution presented by eqs. (3.365) through (3.367) has been extended by Ozisik and Uzzell (1979) for a liquid with an extended freezing temperature.

**Figure 3.41** Cylindrical freezing due to a line strength of fixed strength.

3.10.5 Approximate Analytical Solutions

Because of the mathematical complexity and the restrictive nature of exact analytical solutions, several approaches have been employed to generate approximate analytical solutions that provide rapid results in a number of practical situations. The methods used are the quasi-steady solution, the heat balance integral approach of Goodman (1958) and Lunardini (1991), and the perturbation method of Aziz and Na (1984), Aziz and Lunardini (1993), and others. A collection of such solutions is provided next.

One-Region Neumann Problem The quasi-steady-state solution where $St = 0$ for this problem is

$$T = T_0 + (T_f - T_0) \frac{x}{x_f} \quad (3.368)$$

$$x_f^2 = \frac{2k(T_0 - T_f)}{\rho L} t \quad (3.369)$$

One-Region Neumann Problem with Surface Convection With convective cooling, the boundary condition of eq. (3.347a) is replaced by

$$k \frac{\partial T}{\partial x} \bigg|_{x=0} = h [T(0, t) - T_\infty] \quad (3.370)$$

where T_∞ is now the coolant temperature. The quasi-steady-state approach with $St = 0$ yields

$$T = T_f + \frac{h(T_f - T_\infty)(x - x_f)}{k + hx_f} \quad (3.371)$$

$$t = \frac{\rho L x_f}{h(T_f - T_\infty)} \left(1 + \frac{hx_f}{2k} \right) \quad (3.372)$$

as the results.

Outward Cylindrical Freezing Consider a saturated liquid at the freezing temperature T_f , surrounding a cylinder of radius r_0 whose outer surface is kept at a sub-freezing temperature, $T_0 < T_f$. If a quasi-steady-state assumption ($St = 0$) is used, the solution is

$$T = T_0 + \frac{T_f - T_0}{\ln(r_f/r_0)} \ln \frac{r}{r_0} \quad (3.373)$$

$$t = \frac{\rho L}{k(T_f - T_0)} \left[\frac{1}{2} r_f^2 \ln \frac{r_f}{r_0} - \frac{1}{4} (r_f^2 - r_0^2) \right] \quad (3.374)$$

An improvement on the quasi-steady-state solution can be achieved with the regular perturbation analysis provided by Aziz and Na (1984). The improved version of eq. (3.374) is

$$t = \frac{\rho L}{k(T_f - T_0)} \left[\frac{1}{2} r_f^2 \ln \frac{r_f}{r_0} - \frac{1}{4} (r_f^2 - r_0^2) - \frac{1}{4} \text{St} (r_f^2 - r_0^2) \left(1 + \frac{1}{\ln(r_f/r_0)} \right) \right] \quad (3.375)$$

If the surface of the cylinder is convectively cooled, the boundary condition is

$$k \frac{\partial T}{\partial r} \bigg|_{r=r_0} = h [T(r_0, t) - T_\infty] \quad (3.376)$$

and the quasi-steady-state solutions for $\text{St} = 0$ in this case is

$$T = \frac{T_f - T_\infty}{(k/hr_0) + \ln(r_f/r_0)} \ln \frac{r}{r_f} + T_f \quad (3.377)$$

$$t = \frac{\rho L}{k(T_f - T_\infty)} \left[\frac{1}{2} r_f^2 \ln \frac{r_f}{r_0} - \frac{1}{4} (r_f^2 - r_0^2) \left(1 - \frac{2k}{hr_0} \right) \right] \quad (3.378)$$

Noting that the quasi-steady-state solutions such as eqs. (3.377) and (3.378) strictly apply only when $\text{St} = 0$, Huang and Shih (1975) used them as zero-order solutions in a regular perturbation series in St and generated two additional terms. The three-term perturbation solution provides an improvement on eqs. (3.377) and (3.378).

Inward Cylindrical Freezing Consider a saturated liquid at the freezing temperature contained in a cylinder of inside radius r_i . If the surface temperature is suddenly reduced to and kept at T_0 such that $T_0 < T_f$, the liquid freezes inward. The governing equation is

$$\frac{1}{r} \frac{\partial}{\partial r} \left(r \frac{\partial T}{\partial r} \right) = \frac{1}{\alpha} \frac{\partial T}{\partial t} \quad (3.379)$$

with initial and boundary conditions

$$T(r_i, t) = T_0 \quad (3.380a)$$

$$T(r_f, 0) = T_f \quad (3.380b)$$

$$k \frac{\partial T}{\partial r} \bigg|_{r=r_f} = \rho L \frac{dr_f}{dt} \quad (3.380c)$$

Equations (3.373) and (3.374) also give the quasi-steady-state solutions in this case except that r_0 now becomes r_i .

If the surface cooling is due to convection from a fluid at temperature T_∞ , with heat transfer coefficient h , the quasi-steady-state solutions for T and t are

$$T = T_\infty + \left[\frac{T_f - T_\infty}{\ln(r_f/r_i) - (k/hr_i)} \right] \left(\ln \frac{r}{r_i} - \frac{k}{hr_i} \right) \quad (3.381)$$

$$t = \frac{\rho L}{k(T_f - T_\infty)} \left[\frac{1}{2} r_f^2 \ln \frac{r_f}{r_i} + \frac{1}{4} (r_i^2 - r_f^2) \left(1 + \frac{2k}{hr_i} \right) \right] \quad (3.382)$$

Outward Spherical Freezing Consider a situation where saturated liquid at the freezing temperature T_f is in contact with a sphere of radius r_0 whose surface temperature T_0 is less than T_f . The differential equation for the solid phase is

$$\frac{1}{r} \frac{\partial^2 (Tr)}{\partial r^2} = \frac{1}{\alpha} \frac{\partial T}{\partial t} \quad (3.383)$$

which is to be solved subject to the conditions of eqs. (3.380) (r_i replaced by r_0).

In this case, the quasi-steady-state solution with $St = 0$ is

$$T = T_0 + \frac{T_f - T_0}{1/r_f - 1/r_0} \left(\frac{1}{r} - \frac{1}{r_0} \right) \quad (3.384)$$

$$t = \frac{\rho L r_0^2}{k(T_f - T_0)} \left[\frac{1}{3} \left(\frac{r_f}{r_0} \right)^3 - \frac{1}{2} \left(\frac{r_f}{r_0} \right)^2 + \frac{1}{6} \right] \quad (3.385)$$

A regular perturbation analysis allows an improved version of eqs. (3.384) and (3.385) to be written as

$$\frac{T - T_0}{T_f - T_0} = \frac{1 - 1/R}{1 - 1/R_f} + St \left[\frac{R_f^2 - 3R_f + 2}{6(R_f - 1)^4} \left(1 - \frac{1}{R} \right) - \frac{R^2 - 3R + 2}{6R_f(R_f - 1)^3} \right] \quad (3.386)$$

and

$$\tau = \frac{1}{6} \left[(1 + 2R_f^3 - 3R_f^2) + St (1 + R_f^2 - 2R_f) \right] \quad (3.387)$$

where

$$R = \frac{r}{r_0} \quad R_f = \frac{r_f}{r_0} \quad St = \frac{c(T_f - T_0)}{L} \quad \tau = \frac{k(T_f - T_0)t}{\rho L r_0^2}$$

If the surface boundary condition is changed to eq. (3.376), the quasi-steady-state solutions ($St = 0$) for T and t are

$$T = T_f + \frac{(T_f - T_0)r_0}{1 - r_0/r_f + k/hr_0} \left(\frac{1}{r_f} - \frac{1}{r} \right) \quad (3.388)$$

$$t = \frac{\rho L r_0^2}{k(T_f - T_\infty)} \left\{ \frac{1}{3} \left[\left(\frac{r_f}{r_0} \right)^3 - 1 \right] \left(1 + \frac{k}{h r_0} \right) - \frac{1}{2} \left(\frac{r_f}{r_0} \right)^2 + \frac{1}{2} \right\} \quad (3.389)$$

A three-term solution to the perturbation solution which provides an improvement over eqs. (3.388) and (3.389) is provided by Huang and Shih (1975).

Other Approximate Solutions Yan and Huang (1979) have developed perturbation solutions for planar freezing (melting) when the surface cooling or heating is by simultaneous convection and radiation. A similar analysis has been reported by Seniraj and Bose (1982). Lock (1971) developed a perturbation solution for planar freezing with a sinusoidal temperature variation at the surface. Variable property planar freezing problems have been treated by Pedroso and Domato (1973) and Aziz (1978). Parang et al. (1990) provide perturbation solutions for the inward cylindrical and spherical solidification when the surface cooling involves both convection and radiation.

Alexiades and Solomon (1993) give several approximate equations for estimating the time needed to melt a simple solid body initially at its melting temperature T_m . For the situation when the surface temperature T_0 is greater than T_m , the melt time t_m can be estimated by

$$t_m = \frac{l^2}{2\alpha_l(1 + \omega)\text{St}} \left[1 + (0.25 + 0.17\omega^{0.70})\text{St} \right] \quad (0 \leq \text{St} \leq 4) \quad (3.390)$$

where

$$\omega = \frac{lA}{V} - 1 \quad \text{and} \quad \text{St} = \frac{c_l(T_l - T_m)}{L} \quad (3.391)$$

and l is the characteristic dimension of the body, A the surface area across which heat is transferred to the body, and V the volume of the body. For a plane solid heated at one end and insulated at the other, $\omega = 0$ and l is equal to the thickness. For a solid cylinder and a solid sphere, l becomes the radius and $\omega = 1$ for the cylinder and $\omega = 2$ for the sphere.

If a hot fluid at temperature T_∞ convects heat to the body with heat transfer coefficient h , the approximate melt time for $0 \leq \text{St} \leq 4$ and $\text{Bi} \geq 0.10$ is

$$t_m = \frac{l^2}{2\alpha_l(1 + \omega)\text{St}} \left[1 + \frac{2}{\text{Bi}} + (0.25 + 0.17\omega^{0.70})\text{St} \right] \quad (3.392)$$

where $\text{Bi} = hl/k$.

In this case, the surface temperature $T(0, t)$ is given by the implicit relationship

$$t = \frac{\rho c_l k_l}{2h^2 \cdot \text{St}} \left\{ 1.18\text{St} \left[\frac{T(0, t) - T_m}{T_\infty - T(0, t)} \right]^{1.83} + \left[\frac{T_\infty - T_m}{T_\infty - T(0, t)} \right]^2 - 1 \right\} \quad (3.393)$$

Equations (3.390), (3.392), and (3.393) are accurate to within 10%.

3.10.6 Multidimensional Freezing (Melting)

In Sections 3.10.1 through 3.10.5 we have discussed one-dimensional freezing and melting processes where natural convection effects were assumed to be absent and the process was controlled entirely by conduction. The conduction-controlled models described have been found to mimic experimental data for freezing and melting of water, *n*-octadecane, and some other phase-change materials used in latent heat energy storage devices.

Multidimensional freezing (melting) problems are far less amenable to exact solutions, and even approximate analytical solutions are sparse. Examples of approximate analytical solutions are those of Budhia and Kreith (1973) for freezing (melting) in a wedge, Riley and Duck (1997) for the freezing of a cuboid, and Shamshundar (1982) for freezing in square, elliptic, and polygonal containers. For the vast majority of multidimensional phase-change problems, only a numerical approach is feasible. The available numerical methods include explicit finite-difference methods, implicit finite-difference methods, moving boundary immobilization methods, the isotherm migration method, enthalpy-based methods, and finite elements. Ozisik (1994) and Alexiades and Solomon (1993) are good sources for obtaining information on the implementation of finite-difference schemes to solve phase-change problems. Papers by Comini et al. (1974) and Lynch and O'Neill (1981) discuss finite elements with reference to phase-change problems.

3.11 CONTEMPORARY TOPICS

A major topic of contemporary interest is microscale heat conduction, mentioned briefly in Section 3.1, where we cited some important references on the topic. Another area of active research is inverse conduction, which deals with estimation of the surface heat flux history at the boundary of a heat-conducting solid from a knowledge of transient temperature measurements inside the body. A pioneering book on inverse heat conduction is that of Beck et al. (1985), and the book of Ozisik and Orlande (2000) is the most recent, covering not only inverse heat conduction but inverse convection and inverse radiation as well.

Biothermal engineering, in which heat conduction appears prominently in many applications, such as cryosurgery, continues to grow steadily. In view of the increasingly important role played by thermal contact resistance in the performance of electronic components, the topic is pursued actively by a number of research groups. The development of constructal theory and its application to heat and fluid flow discussed in Bejan (2000) offers a fresh avenue for research in heat conduction. Although Green's functions have been employed in heat conduction theory for many decades, the codification by Beck et al. (1992) is likely to promote their use further. Similarly, hybrid analytic-numeric methodology incorporating the classical integral transform approach has provided an alternative route to fully numerical methods. Numerous heat conduction applications of this numerical approach are given by Cotta and Mikhailov (1997). Finally, symbolic algebra packages such as *Maple V* and

Mathematica are influencing both teaching and research in heat conduction, as shown by Aziz (2001), Cotta and Mikhailov (1997), and Beltzer (1995).

NOMENCLATURE

Roman Letter Symbols

A	cross-sectional area, m^2 area normal to heat flow path, m^2
A_p	fin profile area, m^2
A_s	surface area, m^2
a	constant, dimensions vary absorption coefficient, m^{-1}
B	frequency, dimensionless
b	constant, dimensions vary fin or spine height, m^{-1}
Bi	Biot number, dimensionless
C	constant, dimensions vary
c	specific heat, $\text{kJ/kg} \cdot \text{K}$
d	spine diameter, m
\dot{E}_g	rate of energy generation, W
$ Fo$	Fourier number, dimensionless
f	frequency, s^{-1}
H	height, m fin tip heat loss parameter, dimensionless
h	heat transfer coefficient, $\text{W/m}^2 \cdot \text{K}$
h_c	contact conductance, $\text{W/m}^2 \cdot \text{K}$
\mathbf{i}	unit vector along the x coordinate, dimensionless
\mathbf{j}	unit vector along the y coordinate, dimensionless
k	thermal conductivity, $\text{W/m} \cdot \text{K}$
\mathbf{k}	unit vector along the z coordinate, dimensionless
L	thickness, length, or width, m
l	thickness, m characteristic dimension, m
M	fin parameter, $\text{m}^{-1/2}$
m	fin parameter, m^{-1}
N_1	convection–conduction parameter, dimensionless
N_2	radiation–conduction parameter, dimensionless
n	exponent, dimensionless integer, dimensionless heat generation parameter, m^{-1} normal direction, m parameter, s^{-1}
P	fin perimeter, m
p	integer, dimensionless

Q	cumulative heat loss, J
Q_s	strength of line sink, W/m
q	rate of heat transfer, W
\dot{q}	volumetric rate of energy generation, W/m ³
q''	heat flux, W/m ²
R	radius, dimensionless
	thermal resistance, K/W
R_c''	contact resistance, m ² ·K/W
R_f	freezing interface location, dimensionless
r	cylindrical or spherical coordinate, m
S	shape factor for two-dimensional conduction, m
St	Stefan number, dimensionless
s	general coordinate, m
T	temperature, K
T^*	Kirchhoff transformed temperature, K
t	time, s
V	volume, m ³
W	depth, m
X	distance, dimensionless
x	Cartesian length coordinate, m
y	Cartesian length coordinate, m
Z	axial distance, dimensionless
z	Cartesian or cylindrical length coordinate, m

Greek Letter Symbols

α	thermal diffusivity, m ² /s
α^*	ratio of thermal diffusivities, dimensionless
β	constant, K ⁻¹
	phase angle, rad
γ	length-to-radius ratio, dimensionless
δ	fin thickness, m
ϵ	fin effectiveness, dimensionless
	surface emissivity or emittance, dimensionless
η	fin efficiency, dimensionless
θ	temperature difference, K
	temperature parameter, dimensionless
	coordinate in cylindrical or spherical coordinate system, dimensionless
θ^*	temperature, dimensionless
λ_n	n th eigenvalue, dimensionless
ν	order of Bessel function, dimensionless
ρ	density, kg/m ³
σ	Stefan–Boltzmann constant, W/m ² ·K ⁴
τ	time, dimensionless
ϕ	temperature difference, K

	indicates a function, dimensionless
	spherical coordinate, dimensionless
ω	angular frequency, rad/s
	shape parameter, dimensionless

Roman Letter Subscripts

a	fin tip
b	fin base
cond	conduction
conv	convection
f	fin
	freezing interface
	fluid
i	integer
	initial
	ideal
j	integer
l	liquid
m	mean
	melting
max	maximum
n	normal direction
opt	optimum
s	surface condition
	solid
t	fin tip
0	condition at $x = 0$ or $r = 0$

Additional Subscript and Superscript

∞	free stream condition
p	integer

REFERENCES

- Abramowitz, M., and Stegun, I. A. (1955). *Handbook of Mathematical Functions*, Dover Publications, New York.
- Adebiyi, G. A. (1995). A Single Expression for the Solution of the One-Dimensional Transient Conduction Equation for the Simple Regular Shaped Solids, *J. Heat Transfer*, 117, 158–160.
- Alexaides, V., and Solomon, A. D. (1993). *Mathematical Modeling of Melting and Freezing Processes*, Hemisphere Publishing, Washington, DC.
- Andrews, L. C. (1992). *Special Functions of Mathematics for Engineers*, McGraw-Hill, New York.
- Arpaci, V. S. (1966). *Conduction Heat Transfer*, Addison-Wesley, Reading, MA.

- Aziz, A. (1978). New Asymptotic Solutions for the Variable Property Stefan Problem, *Chem. Eng. J.*, 16, 65–68.
- Aziz, A. (1992). Optimum Dimensions of Extended Surfaces Operating in a Convecting Environment, *Appl. Mech. Rev.*, 45, 155–173.
- Aziz, A. (1997). The Critical Thickness of Insulation, *Heat Transfer Eng.*, 18, 61–91.
- Aziz, A. (2001). *Heat Conduction with Maple™*. To be published.
- Aziz, A., and Hamad, G. (1977). Regular Perturbation Expansions in Heat Transfer, *Int. J. Mech. Eng.*, 5, 167–182.
- Aziz, A., and Kraus, A. D. (1996). Optimum Design of Convecting and Convecting–Radiating Fins, *Heat Transfer Eng.*, 17, 44–78.
- Aziz, A., and Lunardini, V. J. (1993). Perturbation Techniques in Phase Change Heat Transfer, *Appl. Mech. Rev.*, 46, 29–68.
- Aziz, A., and Lunardini, V. J. (1994). Analytical and Numerical Modeling of Steady, Periodic, Heat Transfer in Extended Surfaces, *Comput. Mech.*, 14, 387–410.
- Aziz, A., and Lunardini, V. J. (1995). Multi-dimensional Steady Conduction in Convecting, Radiating and Convecting–Radiating Fins and Fin Assemblies, *Heat Transfer Eng.*, 16, 32–64.
- Aziz, A., and Na, T. Y. (1984). *Perturbation Methods in Heat Transfer*, Hemisphere Publishing, Washington, DC.
- Beck, J. V., Blackwell, B. F., and St. Clair, C. A., Jr. (1985). *Inverse Heat Conduction*, Wiley, New York.
- Beck, J. V., Cole, K. D., Haji-Sheikh, A., and Litkouhi, B. (1992). *Heat Conduction Using Green's Functions*, Hemisphere Publishing, Washington, DC.
- Bejan, A. (1993). *Heat Transfer*, Wiley, New York.
- Bejan, A. (2000). *Shape and Structure from Engineering to Nature*, Cambridge University Press, Cambridge.
- Beltzer, A. I. (1995). *Engineering Analysis with Maple™/Mathematica™*, Academic Press, San Diego, CA.
- Blackwell, B. F. (1990). Temperature Profile in Semi-infinite Body with Exponential Source and Convective Boundary Condition, *J. Heat Transfer*, 112, 567–571.
- Budhia, H., and Kreith, F. (1973). Heat Transfer with Melting or Freezing in a Corner, *Int. J. Heat Mass Transfer*, 16, 195–211.
- Carslaw, H. S., and Jaeger, J. C. (1959). *Conduction of Heat in Solids*, Oxford University Press, Oxford.
- Cheng, K. C., and Seki, N., eds. (1991). *Freezing and Melting Heat Transfer in Engineering*, Hemisphere Publishing, Washington, DC.
- Cho, S. H., and Sunderland, J. E. (1969). Heat Conduction Problems with Freezing or Melting, *J. Heat Transfer*, 91, 421–428.
- Cho, S. H., and Sunderland, J. E. (1974). Phase Change Problems with Temperature Dependent Thermal Conductivity, *J. Heat Transfer*, 96, 214–217.
- Churchill, S. W., and Evans, L. B. (1971). Calculation of Freezing in a Semi-infinite Region, *J. Heat Transfer*, 93, 234–236.
- Comini, G., Del Guidice, S., Lewis, R. W., and Zienkiewicz, O. G. (1974). Finite Element Solution of Nonlinear Heat Conduction Problems with Special Reference to Phase Change, *Int. J. Numer. Methods Eng.*, 8, 613–623.

- Comini, G., Del Guidice, S., and Nonino, C. (1994). *Finite Element Analysis in Heat Transfer*, Taylor & Francis, Washington, DC.
- Cotta, R. M., and Mikhailov, M. D. (1997). *Heat Conduction: Lumped Analysis, Integral Transforms and Symbolic Computation*, Wiley, New York.
- Duncan, A. B., and Peterson, G. P. (1994). Review of Microscale Heat Transfer, *Appl. Mech. Rev.*, 47, 397–428.
- Fletcher, L. S. (1988). Recent Developments in Contact Conductance Heat Transfer, *J. Heat Transfer*, 110, 1059–1070.
- Gebhart, B. (1993). *Heat Conduction and Mass Diffusion*, McGraw-Hill, New York.
- Goodman, T. R. (1958). The Heat Balance Integral and Its Application to Problems Involving a Change of Phase, *Trans. ASME*, 80, 335–342.
- Huang, C. L., and Shih, Y. P. (1975). A Perturbation Method for Spherical and Cylindrical Solidification, *Chem. Eng. Sci.*, 30, 897–906.
- Incropera, F., and DeWitt, D. P. (1996). *Introduction to Heat Transfer*, Wiley, New York.
- Jaluria, Y., and Torrance, K. E. (1986). *Computational Heat Transfer*, Hemisphere Publishing, Washington, DC.
- Jiji, L. M. (2000). *Heat Conduction*, Begell House, New York.
- Kern, D. Q., and Kraus, A. D. (1972). *Extended Surface Heat Transfer*, McGraw-Hill, New York.
- Kraus, A. D., Aziz, A., and Welty, J. R. (2001). *Extended Surface Heat Transfer*, Wiley, New York.
- Lock, G. H. S. (1971). On the Perturbation Solution of the Ice-Layer Problem, *Int. J. Heat Mass Transfer*, 14, 642–644.
- Lunardini, V. J. (1991). *Heat Transfer with Freezing and Thawing*, Elsevier Science, Amsterdam.
- Lynch, D. R., and O'Neill, K. (1981). Continuously Deforming Finite Elements for the Solution of Parabolic Problems with and without Phase Change, *Int. J. Numer. Methods Eng.*, 17, 81–93.
- Madhusadana, C. V. (1996). *Thermal Contact Conductance*, Springer-Verlag, New York.
- Myers, G. E. (1998). *Analytical Methods in Conduction Heat Transfer*, AMCHT Publications, Madison, WI.
- Nguyen, H., and Aziz, A. (1992). Heat Transfer from Conducting–Radiating Fins of Different Profile Shapes, *Waerme-Stoffuebertrag.*, 27, 67–72.
- Ozisik, M. N. (1993). *Heat Conduction*, Wiley, New York.
- Ozisik, M. N. (1994). *Finite Difference Methods in Heat Transfer*, CRC Press, Boca Raton, FL.
- Ozisik, M. N., and Orlande, H. R. B. (2000). *Inverse Heat Transfer*, Taylor & Francis, New York.
- Ozisik, M. N., and Uzzell, J. C., Jr. (1979). Exact Solution for Freezing in Cylindrical Symmetry with Extended Freezing Temperature Range, *J. Heat Transfer*, 101, 331–334.
- Parang, M., Crocker, D. S., and Haynes, B. D. (1990). Perturbation Solution for Spherical and Cylindrical Solidification by Combined Convective and Radiative Cooling, *Int. J. Heat Fluid Flow*, 11, 142–148.
- Pedroso, R. I., and Domato, G. A. (1973). Technical Note on Planar Solidification with Fixed Wall Temperature and Variable Thermal Properties, *J. Heat Transfer*, 93, 553–555.

- Pletcher, R. H., Minkowycz, W. J., Sparrow, E. M., and Schneider, G. E. (1988). Overview of Basic Numerical Methods, in *Handbook of Numerical Heat Transfer*, W. J. Minkowycz, E. M. Sparrow, G. E. Schneider, and R. H. Pletcher, eds., Wiley, New York, Chap. 1.
- Poulikakos, D. (1994). *Conduction Heat Transfer*, Prentice Hall, Englewood Cliffs, NJ.
- Riley, D. S., and Duck, P. W. (1977). Application of the Heat Balance Integral Method to the Freezing of a Cuboid, *Int. J. Heat Mass Transfer*, 20, 294–296.
- Rubinsky, B., and Eto, T. K. (1990). Heat Transfer during Freezing of Biological Materials, in *Annual Review of Heat Transfer*, C. L. Tien, ed., Hemisphere Publishing, Washington, DC, Chap. 1.
- Sahin, A. Z. (1992). Transient Heat Conduction in Semi-infinite Solid with Spatially Decaying Exponential Heat Generation, *Int. Commun. Heat Mass Transfer*, 19, 349–358.
- Schneider, P. J. (1955). *Conduction Heat Transfer*, Addison-Wesley, Reading, MA.
- Sen, A. K., and Trinh, S. (1986). An Exact Solution for the Rate of Heat Transfer from a Rectangular Fin Governed by Power Law Type Temperature Difference, *J. Heat Transfer*, 108, 457–459.
- Seniraj, R. V., and Bose, T. K. (1982). One-Dimensional Phase Change Problems with Radiation–Convection, *J. Heat Transfer*, 104, 811–813.
- Shamsundar, N. (1982). Approximate Calculation of Multidimensional Solidification Using Conduction Shape Factors, *J. Heat Transfer*, 104, 8–12.
- Solomon, A. D., Wilson, D. G., and Alexiades, V. (1982). A Mushy Zone Model with an Exact Solution, *Lett. Heat Mass Transfer*, 9, 319–324.
- Tao, L. N. (1978). The Stefan Problem with Arbitrary Initial and Boundary Conditions, *Q. Appl. Math.*, 36, 223–233.
- Tien, C. L., and Chen, G. (1994). Challenges in Microscale Conduction and Radiative Heat Transfer, *J. Heat Transfer*, 116, 799–807.
- Tien, C. L., Majumdar, A., and Gerner, F. M. (1998). *Microscale Energy Transport*, Taylor & Francis, Washington, DC.
- Tzou, D. Y. (1997). *Macro- to Microscale Heat Transfer*, Taylor & Francis, Washington, DC.
- Ullman, A., and Kalman, H. (1989). Efficiency and Optimized Dimensions of Annular Fins of Different Cross Sections, *Int. J. Heat Mass Transfer*, 32, 1105–1111.
- Viskanta, R. (1983). *Phase Change Heat Transfer*, in *Solar Heat Storage: Latent Heat Materials*, G. A. Lane, ed., CRC Press, Boca Raton, FL, pp. 153–222.
- Viskanta, R. (1988). Heat Transfer during Melting and Solidification of Metals, *J. Heat Transfer*, 110, 1205–1219.
- Yan, M. M., and Huang, P. N. S. (1979). Perturbation Solutions to Phase Change Problem Subject to Convection and Radiation, *J. Heat Transfer*, 101, 96–100.
- Zhuang, J. R., Werner, K., and Schlünder, E. U. (1995). Study of Analytical Solution to the Heat Transfer Problem and Surface Temperature in a Semi-infinite Body with a Constant Heat Flux at the Surface and an Initial Temperature Distribution, *Heat Mass Transfer*, 30, 183–186.